

# Engineering Journal



American Institute of Steel Construction

Second Quarter 2013 Volume 50, No. 2

- 69 Message from the Editor
- 71 Flange Bending in Single Curvature  
Bo Dowswell
- 89 Buckling Restrained Braced Frame with  
All-Bolted Gusset Connections  
Patrick S. McManus, Addison MacMahon and Jay A. Puckett
- 117 Uncertainty in Life-Cycle Assessment Induced by Life-Cycle  
Inventory Data: The Case of Structural Steel  
Iordanis Zygomalas and Charalambos Baniotopoulos
- 129 Current Steel Structures Research No. 33  
Reidar Bjorhovde



# ENGINEERING JOURNAL

AMERICAN INSTITUTE OF STEEL CONSTRUCTION

*Dedicated to the development and improvement of steel construction,  
through the interchange of ideas, experiences and data.*

## Editorial Staff

*Editor:* KEITH A. GRUBB, S.E., P.E.

*Research Editor:* REIDAR BJORHOVDE, PH.D.

*Production Editor:* ARETI CARTER

## Officers

WILLIAM B. BOURNE, III, *Chairman*  
Universal Steel, Inc., Lithonia, GA

JEFFREY E. DAVE, P.E., *Vice Chairman*  
Dave Steel Company, Inc., Asheville, NC

ROGER E. FERCH, P.E., *President*  
American Institute of Steel Construction, Chicago

DAVID B. RATTERMAN, *Secretary & General Counsel*  
American Institute of Steel Construction, Chicago

CHARLES J. CARTER, S.E., P.E., PH.D., *Vice President and  
Chief Structural Engineer*  
American Institute of Steel Construction, Chicago

JACQUES CATTAN, *Vice President*  
American Institute of Steel Construction, Chicago

JOHN P. CROSS, P.E., *Vice President*  
American Institute of Steel Construction, Chicago

SCOTT L. MELNICK, *Vice President*  
American Institute of Steel Construction, Chicago

The articles contained herein are not intended to represent official attitudes, recommendations or policies of the Institute. The Institute is not responsible for any statements made or opinions expressed by contributors to this Journal.

The opinions of the authors herein do not represent an official position of the Institute, and in every case the officially adopted publications of the Institute will control and supersede any suggestions or modifications contained in any articles herein.

The information presented herein is based on recognized engineering principles and is for general information only. While it is believed to be accurate, this information should not be applied to any specific application without competent professional examination and verification by a licensed professional engineer. Anyone making use of this information assumes all liability arising from such use.

Manuscripts are welcomed, but publication cannot be guaranteed. All manuscripts should be submitted in duplicate. Authors do not receive a remuneration. A "Guide for Authors" is printed on the inside back cover.

ENGINEERING JOURNAL (ISSN 0013-8029) is published quarterly. Subscriptions: Members: one subscription, \$40 per year, included in dues; Additional Member Subscriptions: \$40 per year. Non-Members U.S.: \$160 per year. Foreign (Canada and Mexico): Members \$80 per year. Non-Members \$160 per year. Published by the American Institute of Steel Construction at One East Wacker Drive, Suite 700, Chicago, IL 60601.

Periodicals postage paid at Chicago, IL and additional mailing offices. **Postmaster:** Send address changes to ENGINEERING JOURNAL in care of the American Institute of Steel Construction, One East Wacker Drive, Suite 700, Chicago, IL 60601.

Copyright 2013 by the American Institute of Steel Construction. All rights reserved. No part of this publication may be reproduced without written permission. The AISC logo is a registered trademark of AISC.

Subscribe to *Engineering Journal* by visiting our website [www.aisc.org/ej](http://www.aisc.org/ej) or by calling 312.670.5444.

Copies of current and past *Engineering Journal* articles are available free to members online at [www.aisc.org/ej](http://www.aisc.org/ej).

Non-members may purchase *Engineering Journal* article downloads at the AISC Bookstore at [www.aisc.org/ej](http://www.aisc.org/ej) for \$10 each.

# Message from the Editor

The American Institute of Steel Construction was based in New York City in 1963. AISC's chief engineer at the time was Robert O. Disque, a graduate of Northwestern University and Drexel University who had joined AISC in 1959.

Now, you may not know Bob—as he is known to his friends—but you are probably familiar with his work: he supervised the production of the 9th (green) edition *ASD Manual* and the 1st (blue) and 2nd (silver) editions of the *LRFD Manual*. Bob is a member of the Research Council on Structural Connections and was instrumental in the introduction of the “snug-tight” bolt concept. You may also have run across him via one of his textbooks or papers, by taking one of his classes at the University of Maine in the 1980s, or through his consulting at GNCB Engineers in Connecticut. Bob retired from AISC in 1991 and in 2000 received AISC's Lifetime Achievement Award for his outstanding service to AISC and the structural steel design, construction and education community.

One little known fact is that it was Bob and his colleagues who developed the idea for *Engineering Journal*. He was kind enough to share the memory, below. Many thanks, Bob!



Keith A. Grubb, P.E., S.E.  
Editor

*In 1963 the only periodical AISC published was “Steel Construction Digest,” a thin quarterly magazine consisting mainly of articles reproduced—with permission—from other periodicals, such as Engineering News Record.*

*There were several of us on the AISC headquarters staff who thought we needed something additional—and more technical. There was a lot of discussion among us and with interested engineers from member companies. Finally, it was agreed that there should be a quarterly publication. Interestingly, there was quite a debate on what it should be named.*

*Most of the staff thought the title should contain the word “steel.” However, I differed and modestly offered the title “Engineering Journal,” which prevailed. We started publication in 1964.*

*At first, most of the papers were written by staff or solicited from the steel community. There were no reviewers and only the staff decided what would be printed. We did a lot of editing and rewriting. After several years, and not without some internal controversy, we decided to use outside reviewers. Engineering Journal continued to grow to become the great publication that it is today.*

*Robert O. Disque*



# Flange Bending in Single Curvature

BO DOWSWELL

---

## ABSTRACT

Local bending of beam and column flanges is a common design consideration in steel structures. In most cases, the flange bends in double curvature due to the restraining effect of the connecting element. When a restraining force is not present, the flange will deform in single curvature. Common cases of single-curvature bending occur at the bottom flange of monorail beams and at hanger rod connections. In this paper, the equivalent-width method was explored in an effort to determine design procedures for elastic and plastic strength of flanges in single-curvature bending.

This paper compares the available procedures for designing flanges bent in single curvature. New finite element models and yield line analyses are used to verify, expand and improve the existing design methods. Design recommendations are made for both elastic and ultimate strength approaches. Recommendations are also made for interaction of the local bending strength with longitudinal stresses in the flange. The effects of closely spaced loads and loads acting near the ends of members are also addressed.

**Keywords:** flange bending, design recommendations.

---

## INTRODUCTION

Local bending of beam and column flanges is a common design consideration in steel structures. Flange bending usually occurs when a tension member is bolted to the flange as shown in Figure 1a. In this case, the flange bends in double curvature due to the restraining effect of the connecting element. When a restraining force is not present, the flange will deform in single curvature as shown in Figure 1b. Common cases of single-curvature bending occur at the bottom flange of monorail beams and at hanger connections as shown in Figures 2a and 2b, respectively.

Geometry is the dominant factor in the behavior of bolted flange connections. Another major factor is the amount of inelastic deformation that can be tolerated before serviceability requirements are exceeded. The monorail beam flange in Figure 2a must remain essentially elastic under service loads. Conversely, the strength of the hanger connection in Figure 2b can normally be calculated on the basis of a fully plastic yield line solution. Additionally, it may be practical to use an ultimate strength approach when calculating the strength of a monorail flange to ensure safety at overload conditions.

Figure 3 shows a generic load versus deformation curve for flanges bent in single curvature. The curve is linear up to the elastic load,  $P_e$ . After yielding, the curve is nonlinear over a large increment of the total load, and then the curve flattens out and becomes essentially linear until collapse.

The inelastic load,  $P_i$ , is at the intersection of the elastic loading line and the plastic loading line. Tests and inelastic finite element results summarized by Dowswell (2011) indicate that  $P_i$  is generally 60 to 70% greater than the initial yield load,  $P_e$ . The plastic collapse load,  $P_c$ , can be more than four times the initial yield load; however, Dowswell also showed that the deformation will be approximately  $\frac{1}{4}$  in. at the nominal load calculated with the yield line method.

When a concentrated load is applied to the flange, bending stresses develop in two directions. Because the stresses in the longitudinal direction (Z-axis in Figure 2a) are much smaller than those in the transverse direction (X-axis in Figure 2a), the stresses in the longitudinal direction are often neglected in design. A simple method to calculate the stresses in the transverse direction is the equivalent-width method. In the equivalent-width method, the flange is treated as a rectangular cantilever beam of width,  $b_e$ , based on an assumed load distribution angle,  $\theta$ , as shown in Figure 4. Goldman (1990) recommended a load distribution angle of  $45^\circ$ , which results in an equivalent width of  $2b$ . Although the  $45^\circ$  angle is common for design use, this paper shows that the equivalent width is dependent on the  $b/c$  ratio and the level of inelasticity.

The equivalent-width method will be explored in an effort to determine procedures for elastic and plastic design of flanges in single-curvature bending. The effects of closely spaced loads and loads acting near the ends of the member will also be addressed.

Using the equivalent-width approach, the required moment is

$$M_r = Pb \quad (1)$$

For design of flanges that must remain elastic, the nominal yield moment is

$$M_n = S_e F_y \quad (2)$$

$$S_e = \frac{b_e t_f^2}{6} \quad (3)$$

When the plastic strength is used, the nominal moment is

$$M_n = Z_e F_y \quad (4)$$

$$Z_e = \frac{b_e t_f^2}{4} \quad (5)$$

where

$F_y$  = specified minimum yield stress, ksi

$P$  = concentrated force, kips

$S_e$  = section modulus of the equivalent beam, in.<sup>3</sup>

$Z_e$  = plastic modulus of the equivalent beam, in.<sup>3</sup>

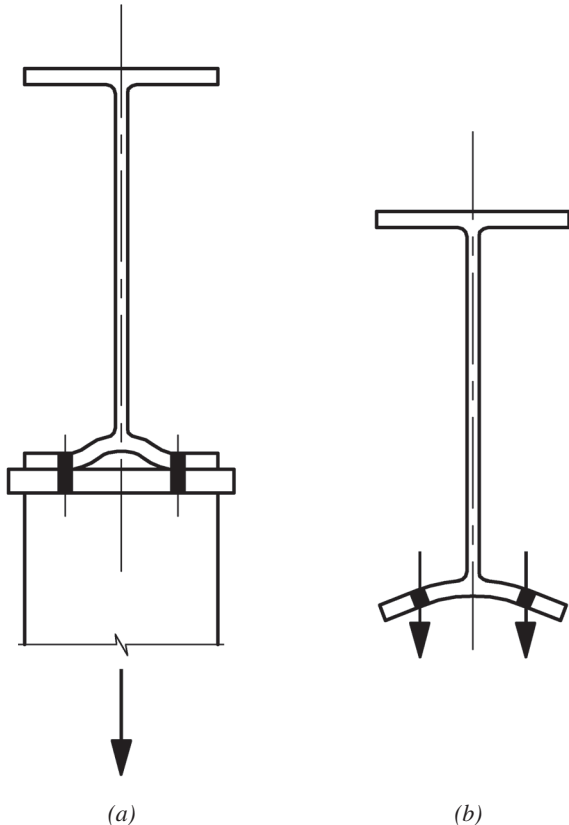


Fig. 1. Effect of restraint on flange bending:  
(a) double curvature; (b) single curvature.

$b$  = distance from the concentrated load to the fixed end of the equivalent beam, in.

$b_e$  = equivalent width, in.

$t_f$  = flange thickness, in.

### ELASTIC STRESSES

In this section, the previous research on elastic bending stresses in flanges will be summarized. The equivalent-width equations discussed are for use with the section modulus, and the nominal strength is calculated with Equation 2.

#### Jaramillo (1950)

The first research was published by Jaramillo (1950), who transformed the exact solution into series form and solved for the moments in an infinitely long plate with one edge fixed and the other edge free. The results were presented in the form of a table, which was reproduced in Young (1989). The equivalent width is calculated using Equation 6 with the values for  $K_m$  listed in Table 1.

$$b_e = \frac{b}{K_m} \quad (6)$$

Timoshenko and Woinowsky-Krieger (1959) published the solution for an infinitely long plate fixed at one edge and free at the other edge with a concentrated load at the free edge. The unit moment causing bending stress perpendicular to the length of the beam is

$$m_z = 0.509P \quad (7)$$

The unit moment causing bending stress parallel to the length of the beam is

$$m_x = \nu m_z = 0.153P \quad (8)$$

The equivalent width can be determined by combining Equations 1 and 7.

$$b_e = \frac{M_r}{m_z} = \frac{Pb}{m_z} \approx 2b \quad (9)$$

This results in a load distribution angle of 45°, which is the same as Jaramillo (1950) when  $b/c = 1$ .

$b/c$	$K_m$
0.25	0.332
0.50	0.370
0.75	0.428
1.00	0.509

**Ballio and Mazzolani (1983)**

Ballio and Mazzolani (1983) presented the results of a finite element study aimed at generalizing the solution of Timoshenko and Woinowsky-Krieger (1959). They published Equation 10 for calculating the equivalent width.

$$b_e = b \left( 3.5 - 1.5 \frac{b}{c} \right) \tag{10}$$

where

$c$  = horizontal distance from the face of the web to the tip of the flange, in.

**Current Study**

To supplement the previous research, the problem was modeled by the author using elastic finite element models with rectangular plate elements. The plate was fixed at one boundary and free at the remaining three edges. It was determined that a length of five times the width was adequate to model an infinitely long plate in the elastic range. The mesh size was chosen to provide a convenient number of equally spaced load points. However, a mesh study revealed that the element size provided convergence within 2%.

The results are presented in the same form as Jaramillo (1950), and the equivalent width can be calculated using Equation 6 with the values for  $K_m$  listed in Table 2. The results agree well with those of Jaramillo (1950), Timoshenko and Woinowsky-Krieger (1959) and Ballio and Mazzolani (1983).

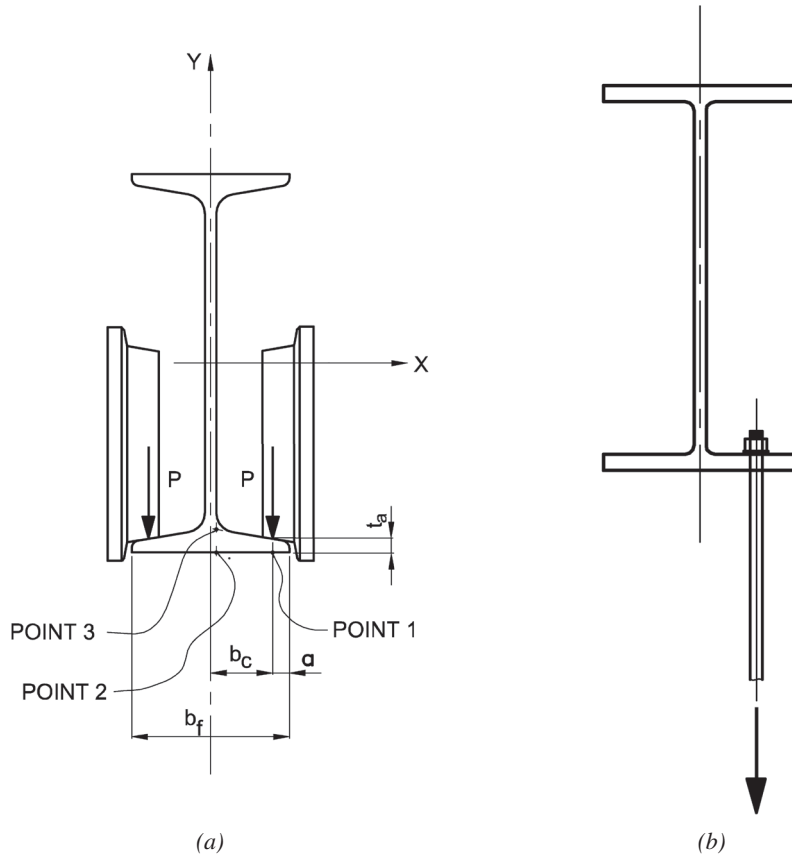


Fig. 2. Common cases of flange bending in single curvature: (a) monorail; (b) hanger.

$b/c$	$K_m$
0.125	0.252
0.250	0.312
0.375	0.337
0.500	0.363
0.625	0.392
0.750	0.426
0.875	0.464
1.00	0.508

### INELASTIC STRENGTH

In this section, the research on inelastic bending strength of flanges are summarized. The equivalent-width equations discussed are for use with the plastic modulus, and the nominal strength is calculated with Equation 4.

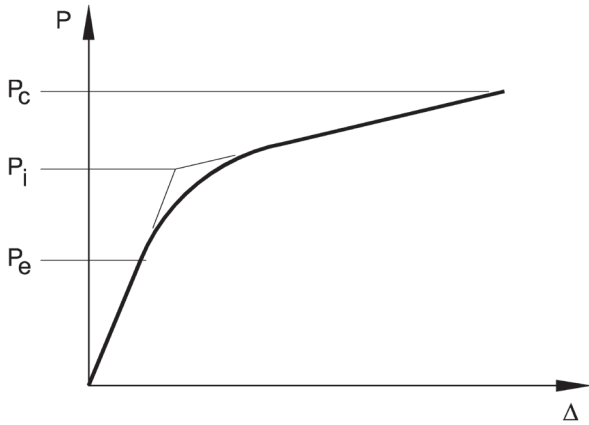


Fig. 3. Load versus deformation curve.

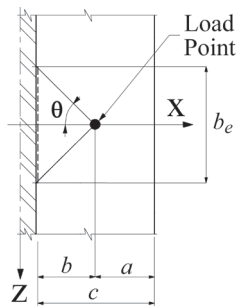


Fig. 4. Equivalent-width approach.

### Ballio, Poggi and Zanon (1981)

Ballio, Poggi and Zanon (1981) used experimental tests on monorail beams and inelastic finite element models of long plates with one edge fixed and three edges free. The suggested design equations contain variables for the load application width, assuming a uniform load over a finite-width patch. For a concentrated load, the width of the load is zero, and the equivalent width is calculated with Equation 11.

$$b_e = b \left( 9 - 6 \frac{b}{c} \right) \quad (11)$$

Equation 11 was derived to provide a target nominal strength at the intersection of the elastic loading line and the plastic loading line as labeled  $P_i$  in Figure 3 when used with the plastic modulus.

### PLASTIC STRENGTH

In this section, the available yield line patterns for single-curvature bending of flanges are summarized. The equivalent-width equations discussed are for use with the plastic modulus, and the nominal strength is calculated with Equation 4.

#### Triangular Yield Line Pattern (Dranger, 1977)

Dranger (1977) derived an equation for the flange strength using the yield line pattern of Figure 5. The nominal load is

$$P_n = F_y t_f^2 \sqrt{2} \left( \frac{c}{b} \right) \quad (12)$$

Combining Equations 1, 4 and 12, the equivalent width is

$$b_e = 4c\sqrt{2} \quad (13)$$

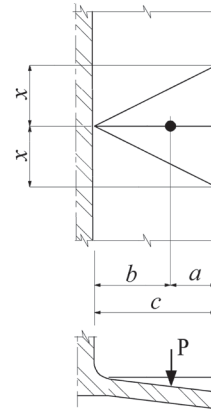


Fig. 5. Triangular yield line pattern.

### Parabolic Yield Line Pattern (Otegui, 1996)

Based on earlier work on curved yield line patterns by Packer and Morris (1977) and Mann and Morris (1979), Otegui (1996) derived the flange bending strength of a tee stub with bolts near the end, as shown in Figure 6. Otegui used a parabolic pattern with an experimentally located distance from the focal point to the vertex of  $2.17b$ . He showed that the internal work is independent of the radius of the yield line pattern; therefore, the radius can vary around the arc of the curve, but the internal work is dependent on the total angle of the parabola. Another important concept in Otegui's derivation is that the work done along the curved yield lines is equal to that of the straight yield lines projecting from the center of the load point.

The strength of the yield line pattern in Figure 7 can be derived based on the principles developed by Otegui. The external work is

$$W_e = P\delta \quad (14)$$

where

$\delta$  = virtual displacement of the load

The internal work is

$$W_i = 4m_p \alpha \delta \quad (15)$$

where

$m_p$  = plastic moment capacity per unit length, kips

$\alpha$  = half angle around the parabola (Figure 7), radians

The plastic capacity per unit length of yield line is

$$m_p = \frac{F_y t_f^2}{4} \quad (16)$$

The half angle around the parabola is

$$\alpha = \frac{\pi}{2} + \beta \quad (17)$$

where

$$\tan \beta = \frac{a}{x} \quad (18)$$

Dimensions  $a$  and  $x$  are shown in Figure 7.

From Otegui (1996),

$$x = 3\sqrt{bc} \quad (19)$$

Set  $W_e = W_i$  and substitute  $m_p$  from Equation 16 to get the nominal load

$$P_n = F_y t_f^2 \alpha \quad (20)$$

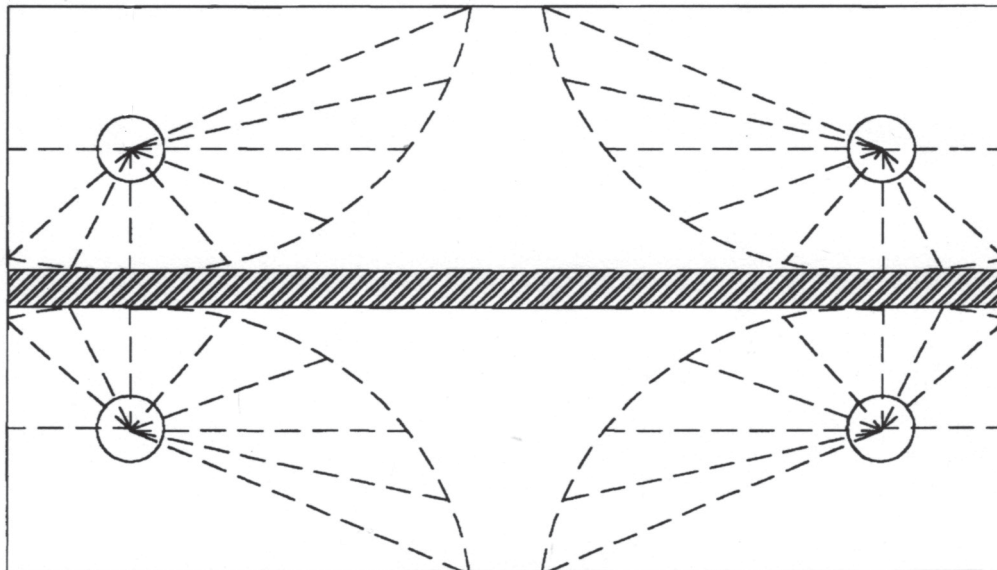


Fig. 6. Yield line pattern of Otegui (1996).

Equation 17 is substituted into Equation 20 to get the final design equation

$$P_n = F_y t_f^2 \left[ \frac{\pi}{2} + \beta \right] \quad (21)$$

Equation 19 can be substituted into Equation 18 to get

$$\tan \beta = \frac{a}{3\sqrt{bc}} \quad (22)$$

Combining Equations 1, 4 and 21, the equivalent width is

$$b_e = 4b \left( \frac{\pi}{2} + \beta \right) \quad (23)$$

### REVIEW OF MONORAIL DESIGN SPECIFICATIONS

In this section, the available monorail design specifications will be summarized. Because the beam flange must remain essentially elastic, the equivalent-width equations discussed are for use with the section modulus and the nominal strength is calculated with Equation 2.

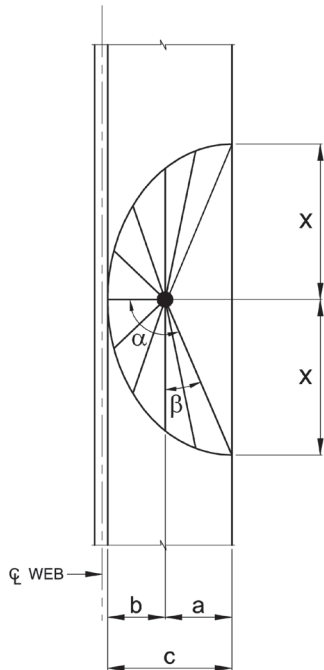


Fig. 7. Parabolic yield line pattern.

### CMAA Specification

CMAA *Specification* (CMAA, 2008) Section 3.3.2.4 contains detailed design provisions for calculation of flexural normal stresses in directions parallel and perpendicular to the longitudinal axis of the beam. The rules were taken from FEM (1983), with the development and background research by Hannover and Reichwand (1982). Hannover and Reichwand developed the equations by curve-fitting data from experimental tests, finite element models, and theoretical calculations using Kirchoff's plate theory. The notation in the design equations reproduced here is shown in Figure 2a.

Stresses at point 1

$$\sigma_{x1} = C_{x1} \left( \frac{P}{t_a^2} \right) \quad (24)$$

$$\sigma_{z1} = C_{z1} \left( \frac{P}{t_a^2} \right) \quad (25)$$

Stresses at point 2

$$\sigma_{x2} = C_{x2} \left( \frac{P}{t_a^2} \right) \quad (26)$$

$$\sigma_{z2} = C_{z2} \left( \frac{P}{t_a^2} \right) \quad (27)$$

Stresses at point 3

$$\sigma_{x3} = -\sigma_{x2} \quad (28)$$

$$\sigma_{z3} = -\sigma_{z2} \quad (29)$$

For tapered flange sections

$$t_a = t_f - \frac{b_f}{24} + \frac{a}{6} \quad (30)$$

$$C_{x1} = 3.97 - 4.84\lambda - 3.97e^{-2.68\lambda} \quad (31)$$

$$C_{x2} = -1.10 + 1.10\lambda + 0.192e^{-6.00\lambda} \quad (32)$$

$$C_{z1} = 1.81 - 1.15\lambda - 1.06e^{-7.70\lambda} \quad (33)$$

$$C_{z2} = -0.981 - 1.48\lambda + 1.12e^{1.32\lambda} \quad (34)$$

For parallel flanged sections

$$t_a = t_f \quad (35)$$

$$C_{x1} = 10.1 - 7.41\lambda - 10.1e^{-1.36\lambda} \quad (36)$$

$$C_{x2} = -2.11 + 1.98\lambda + 0.0076e^{6.53\lambda} \quad (37)$$

$$C_{z1} = 2.23 - 1.49\lambda - 1.39e^{-18.3\lambda} \quad (38)$$

$$C_{z2} = 0.050 - 0.580\lambda + 0.148e^{3.02\lambda} \quad (39)$$

where

$$\begin{aligned} \lambda &= \frac{2a}{b_f - t_w} \\ &= \frac{a}{c} \end{aligned} \quad (40)$$

$t_a$  = beam flange thickness at the point of load application, in.

=  $t_f$  for parallel flange sections

$t_w$  = web thickness, in.

$b_f$  = flange width, in.

$a$  = distance from the edge of the flange to the point of load application, in.

For parallel flanged sections, the equivalent width can be determined by substituting  $\sigma_{x2}$  from Equation 26 for  $F_y$  in Equation 2, and combining with Equations 1 and 3, which results in Equation 41.

$$b_e = \frac{6b}{C_{x2}} \quad (41)$$

### Australian Standard AS 1418.18-2001

Australian Standard AS 1418.18-2001 (AS, 2001) Section 5.12.3.1 specifies Equation 42 to calculate the allowable wheel load for the limit state of local flange bending. In order to use consistent terminology and units throughout this paper, some of the constants and variable names were changed from the original equation.

$$P_a = K_L t_f^2 \left( \frac{\alpha F_y}{1 + 8b_c/b_f} \right) \quad (42)$$

where

$P_a$  = allowable wheel load, kips

$K_L$  = load position factor

= 1.7 where the distance from the end of the beam to the wheel load is at least  $b_f + d$

= 1.0 where the distance from the end of the beam to the wheel load is less than  $b_f + d$

$b_c$  = horizontal distance from the center of the beam to the wheel load, in.

$b_f$  = beam flange width, in.

$d$  = beam depth, in.

$\alpha$  = reduction factor to account for longitudinal stress in the bottom flange due to global bending of the beam

For comparison with the other design equations,  $K_L = 1.7$  and  $\alpha = 1.0$  are substituted into Equation 42, which then reduces to Equation 43.

$$P_a = \frac{1.7F_y t_f^2}{1 + 8b_c/b_f} \quad (43)$$

Combining Equations 1, 2 and 43, assuming a safety factor of 1.67, and neglecting the web thickness, the equivalent width is

$$b_e = \frac{17b}{1 + 4b/c} \quad (44)$$

### Eurocode 1993-6

For design at service loads, Eurocode (1999) specifies the same equations as CMAA *Specification* (CMAA, 2008) Section 3.3.2.4. For ultimate strength design, Eurocode specifies the equations developed by Dranger (1977), except that the critical section for bending is assumed to be at the tangent point of the fillet radius instead of the face of the web. For wheel loads remote from the end of the member and at large enough spacings to preclude interaction between any adjacent yield lines, the available load for strength design is

$$P_a = \frac{b_e t_f^2 \alpha F_y}{4b'\gamma} \quad (45)$$

where

$$b_e = 4c'\sqrt{2} \quad (46)$$

$b'$  = horizontal distance from the tangent point of the fillet radius to the concentrated load, in.

=  $b - r$

$c'$  = horizontal distance from the tangent point of the fillet radius to the tip of the flange, in.

=  $c - r$

$r$  = fillet radius, in.  
 $\gamma$  = partial safety factor for LRFD design  
= 1.1

## SUMMARY AND CONCLUSIONS FOR EQUIVALENT-WIDTH EQUATIONS

### Comparison of Equivalent-Width Equations

Figure 8 shows a plot of the normalized equivalent width,  $b_e/b$ , versus the normalized load location,  $a/c$ , for each of the equivalent-width equations discussed in this paper. All of the equivalent-width equations are for parallel flanged sections; therefore, the CMAA (2008) curve used Equation 37 to calculate  $C_{x2}$ .

The equivalent-width equations are separated into three groups: elastic (green line), inelastic (red lines) and plastic (blue lines). Figure 8 shows that the curves are bunched accordingly, with the smallest equivalent width in the elastic group. The largest equivalent widths are in the plastic group, and the inelastic group falls between the elastic group and the plastic group. This behavior is expected because stress redistribution allows the equivalent width to increase with the amount of plastic material. As discussed previously, the equivalent widths of Dranger (1977), Otegui (1996) and Ballio et al. (1981) were derived for use with the plastic modulus, and the equivalent widths of AS 1418 (AS, 2001), CMAA (2008) and Ballio and Mazzolani (1983) were derived for use with the section modulus.

Because the equation developed by Ballio and Mazzolani (1983) is in very close agreement with the work of Jaramillo (1950), Timoshenko and Woinowsky-Krieger (1959)

and the current finite element results in this paper, it will be regarded as the correct elastic curve. Therefore, all of the elastic research is represented with Equation 10.

The equivalent widths implicit in the monorail design specifications (CMAA, AS 1418) are somewhat higher than the elastic values; it can be concluded then, that some inelastic deformation is required to reach the nominal strength. Although the equation of Ballio et al. (1981) was developed for use with the plastic modulus, it provides a reasonable linear approximation of the implied equivalent widths in the monorail design specifications, which use the section modulus.

For strength design, the equivalent width according Dranger (1977) is less than that of Otegui (1996) for small values of  $a/c$ . However, the difference between the two values is small, and Otegui's equation controls the design over most of the  $a/c$  range.

### Design Recommendations for Equivalent-Width Equations

The design of flanges bent in single curvature can be separated into two groups: serviceability design and strength design. Serviceability design should be used where the flange must remain essentially elastic to prevent localized distortion, such as for monorail beams. Selection of the proper design philosophy is important because the plastic strength is more than four times the initial yield load. However, when the flange strength is calculated on the basis of a fully plastic yield line pattern, a deformation of approximately  $\frac{1}{4}$  in. can be expected at the nominal load level (Dowswell, 2011).

In most cases of serviceability design, a limited amount of yielding can be allowed to accommodate some minor stress redistribution. The available equivalent-width equations in this inelastic group are from the design methods of Ballio et al. (1981), AS 1418 and CMAA. Because the three design methods in this group result in similar equivalent widths and the equation developed by Ballio et al. is the least complex, it is recommended for design. Therefore, Equation 11 is recommended for calculation of the nominal yield moment according to Equations 2 and 3. In rare cases, where even a small amount of inelastic deformation would be detrimental, Equation 10 can be used to calculate the equivalent width.

For strength design, both of the available equivalent-width equations were developed with the yield line method. Figure 8 shows that Otegui's (1996) yield line pattern controls the design over the practical range of  $a/c$ , and the equivalent width using Dranger's (1977) pattern is smaller only at very low  $a/c$  ratios. Therefore, Equation 23 is proposed for equivalent-width calculations using strength design. The nominal plastic moment is calculated with Equations 4 and 5.

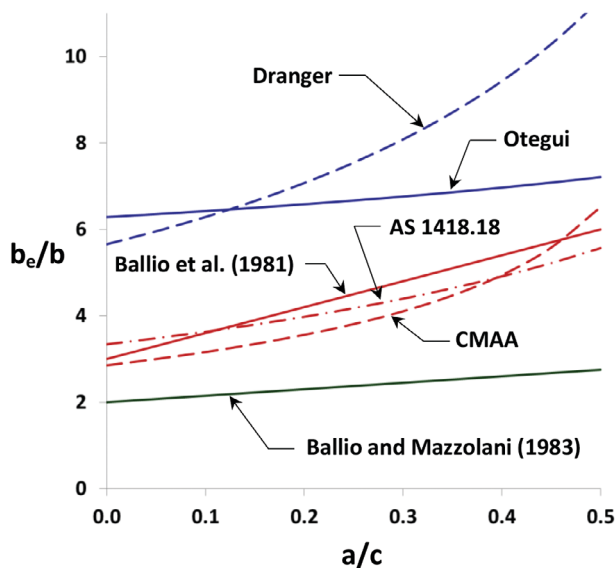


Fig. 8. Comparison of equivalent widths.

## STRESS INTERACTION

When the flange is subjected to longitudinal stress in addition to local bending stress, interaction of the stresses can reduce the local bending strength. Longitudinal stresses are typically caused by global strong-axis bending of the beam but can also be caused by axial loading and global bending about the weak axis of the beam. The quantification of this effect is complex due to the two-way local bending of the flange and the stress redistribution that occurs with increased load. The interaction of stresses has been the subject of several research projects, and it is addressed by the monorail design specifications.

### Elastic Stress

Von Mises' criterion is accurate for predicting the initiation of yield in ductile metals when loaded by various combinations of normal stress and shear stress. For plane stress, von Mises' equation reduces to

$$\sigma_{ev} = \sqrt{\sigma_x^2 + \sigma_z^2 - \sigma_x \sigma_z + 3\tau^2} \quad (47)$$

where

- $\sigma_{ev}$  = effective uniaxial yield stress, ksi
- $\sigma_x$  = applied stress in the  $x$ -direction, ksi (tension positive)
- $\sigma_z$  = applied stress in the  $z$ -direction, ksi (tension positive)
- $\tau$  = applied shear stress, ksi

If the shear stress is neglected, von Mises' equation can be expressed in the form of a reduction factor,  $\alpha$ .

$$\alpha = \sqrt{1 - \frac{3n^2}{4} - \frac{n}{2}} \quad (48)$$

where

$$n = \frac{f_b}{F_y} \quad (49)$$

- $F_y$  = specified minimum yield stress of beam, ksi
- $f_b$  = longitudinal stress in the bottom flange of the beam, ksi

### Inelastic Strength

For use with Equation 11, Ballio et al. (1981) suggested an elliptical interaction of the local bending strength of the flange and the longitudinal tension stress in the flange.

$$\left(\frac{f_b}{F_y}\right)^2 + \left(\frac{P}{P_n}\right)^2 \leq 1.0 \quad (50)$$

where

- $P_n$  = nominal load calculated with Equations 1, 4 and 5, kips

Equation 50 can be expressed in the form of a reduction factor as

$$\alpha = \sqrt{1 - n^2} \quad (51)$$

### Plastic Strength

When the main member carries axial compression, the plastic local bending strength is reduced. Cao, Packer and Yang (1998) reviewed the previous work on the reduction in strength due to normal stresses acting on the yield line pattern. They found that the reduction factor was dependent not only on the axial stress in the element containing the yield line pattern, but also on the geometry of the yield line pattern. In addition to developing a new equation, Cao et al. showed that Equation 52, originally developed by Kurobane (1981) for circular hollow sections, provides a conservative estimate of the strength reduction for elements with rectangular yield line patterns.

$$\alpha = 1 - 0.3n_c(1 + n_c) \quad (52)$$

where

$$n_c = \frac{f_c}{F_y} \quad (53)$$

- $f_c$  = longitudinal compression stress in the element (compression positive), ksi

When the element carries axial tension, Cao et al. (1998) showed that the yield line strength is not reduced.

### Monorail Design Specifications

Von Mises' criterion is specified in CMAA (2008) and for serviceability design in Eurocode (1999). For ultimate strength design, Eurocode specifies a reduction factor of

$$\alpha = 1 - \left(\frac{\gamma f_b}{F_y}\right)^2 \quad (54)$$

which can be simplified with the substitution of Equation 49.

$$\alpha = 1 - (\gamma n)^2 \quad (55)$$

To get a nominal reduction factor, set  $\gamma = 1.0$ , which gives

$$\alpha = 1 - n^2 \quad (56)$$

Australian Standard AS 1418 (AS, 2001) Section 5.12.3.1 specifies Equation 57.

$$\alpha F_y = F_y - 1.1 f_b \quad (57)$$

Equation 57 can be expressed in the form of a reduction factor and simplified with the substitution of Equation 49 to get Equation 58.

$$\alpha = 1 - 1.1n \quad (58)$$

If the 1.1 multiplier on  $n$  is assumed to be a partial safety factor, the nominal reduction factor is

$$\alpha = 1 - n \quad (59)$$

### Summary and Conclusions for Stress Interaction

Figure 9 shows a plot of the reduction factor,  $\alpha$ , versus the normalized longitudinal stress,  $n$ , for each of the reduction factor equations discussed in this paper. Von Mises' equation and the AS 1418 reduction factor are intended to ensure the material remains elastic. The remaining curves are for

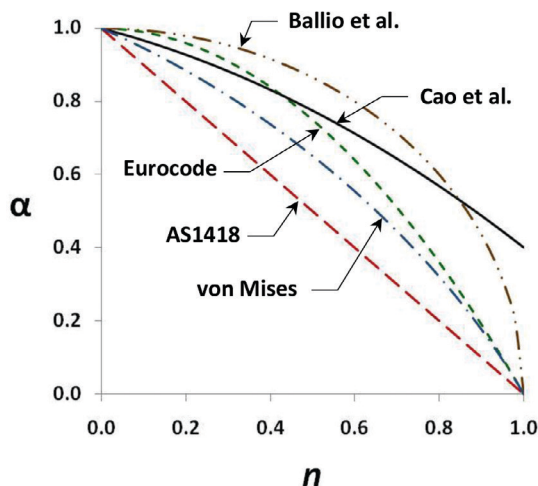


Fig. 9. Reduction factors for longitudinal stress in the bottom flange.

reductions in the inelastic and plastic strength. The curves show that the effect of longitudinal stress is more pronounced for elastic design than for plastic design.

### Design Recommendations for Stress Interaction

Reduction factors for stress interaction in serviceability design are intended to prevent large-scale yielding that would cause unacceptable deformations. The two reduction factors available for serviceability design were developed from AS 1418 and von Mises' criterion. It is well known that von Mises' criterion provides accurate results, and Figure 9 shows that the linear equation in AS 1418 provides conservative results compared to von Mises' criterion. Although von Mises' criterion is slightly more complex than the linear interaction in AS 1418, it provides a significant increase in strength for most values of  $n$ . Therefore, the additional complexity appears to be justified to obtain a more accurate solution. Equation 48 is proposed to estimate the strength reduction in the presence of longitudinal stress for serviceability design.

Reduction factors for stress interaction in strength design were presented by Cao et al. (1998), Ballio et al. (1981) and Eurocode. The equation by Cao et al. is the only method that has been proven accurate compared to tests and finite element models. The recommendations of Cao et al., which reduces the strength according to Equation 52, can be used to estimate the effect of longitudinal compression stress for strength design.

### CLOSELY SPACED LOADS

Closely spaced loads are common at beam flanges supporting four-wheel monorail trolleys. This loading condition can also occur when two hanger rods are located close together. If the spacing between the loads is large enough, two separate failure patterns will form as shown in Figure 10a. In this case the strength is independent of the spacing. If the spacing is less than the critical spacing, a single failure pattern will form as shown in Figure 10b, which will cause a reduction in strength.

### Monorail Design Specifications

CMAA (2008) and AS 1418 (AS, 2001) provide no specific guidance for closely spaced loads. However, Section 3.3.2.4.5 of CMAA requires that "consideration should be given to lower flange stresses which are not calculable by the formulae presented in section 3.3.2.4."

For design at service loads, Eurocode (1999) Section 5.5.2 (6) addresses closely spaced loads, where the spacing is less than  $1.5b_f$ : "Unless special measures are adopted to determine the local stresses, a conservative approach should be adopted by superposing the stresses calculated for each wheel acting separately." Eurocode strength design

provisions for closely spaced loads are based on Dranger's (1977) triangular yield line pattern.

### Elastic Stresses

In addition to the maximum stresses in Table 1, Jaramillo (1950) also provided coefficients for stresses at intermediate locations in the  $z$ -direction along the flange. These coefficients were superimposed in a staggered pattern to calculate the maximum total stress at a point when two loads are applied. The results are expressed as a maximum stress ratio

$$k_s = \frac{\sigma_2}{\sigma_1} \tag{60}$$

where

- $\sigma_1$  = stress caused by a single load, ksi
- $\sigma_2$  = stress caused by two closely spaced loads, ksi

The  $k_s$  values for various combinations of  $s/c$  and  $b/c$  are listed in Table 3, where  $s$  is the spacing between loads.

In Figure 11,  $k_s$  is plotted versus  $z/c$  for  $s/c = 1$ , where  $z$  is the distance from the first load along the length of the beam. The shape of the curve is dependent on the  $s/c$  and  $b/c$  ratios. In some cases, the maximum stress occurs between the loads, as shown in Figure 11 for  $b/c = 1$ . In other cases, the maximum stresses occur at the same location as the loads, as shown in Figure 11 for  $b/c = 0.75$  and less.

Figure 12 shows the stress ratio,  $k_s$ , versus the spacing ratio,  $s/c$ . At a spacing ratio of two, the stress ratio is negligible for the practical range of  $b/c$ . Therefore, the spacing effect can be neglected if the distance between adjacent wheel loads is less than the flange width. This leads to a critical spacing of

$$s_{ce} = 2c \approx b_f \tag{61}$$

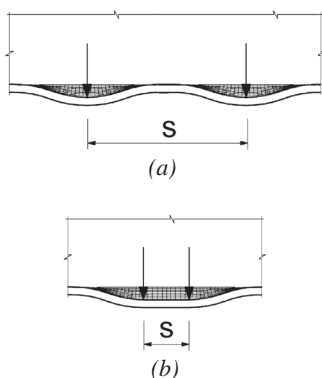


Fig. 10. Closely spaced loads: (a) actual spacing greater than critical spacing; (b) actual spacing less than critical spacing.

Relative to Equation 61, the critical end distance requirement in Eurocode (1999) is 50% conservative. For design of monorail beams, the geometry of most trolley/beam combinations will allow the spacing effect to be neglected.

When the actual spacing is less than the critical spacing, the reduction in strength can be accounted for by dividing the equivalent width for a single load by  $k_s$  from Table 3. The modified equivalent width for closely spaced loads is

$$b_{es} = \frac{b_e}{k_s} \tag{62}$$

For design, Equation 62 should be used to calculate the equivalent width if the actual spacing is less than the critical spacing. Otherwise, the spacing effect can be neglected.

### Plastic Strength

For closely spaced loads, the plastic strength can be calculated using two half yield line patterns separated by the spacing between the loads as shown in Figure 13. The total equivalent width is calculated as the sum of the equivalent

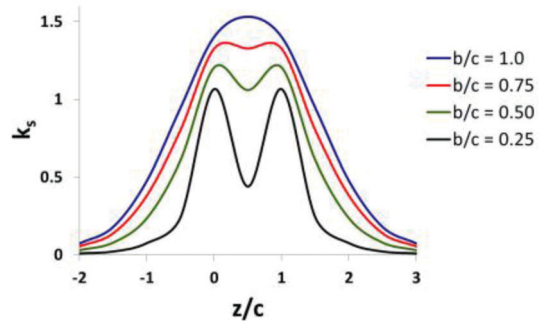


Fig. 11.  $k_s$  versus  $z/c$  for  $s/c = 1$ .

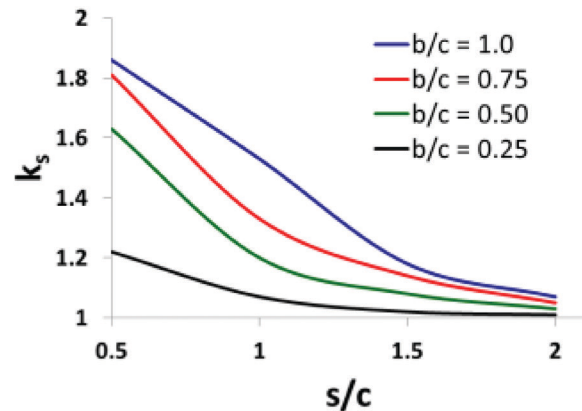


Fig. 12.  $k_s$  versus  $s/c$ .

Table 3. Values of $k_s$ for Closely Spaced Loads				
$s/c$	$b/c$			
	1.0	0.75	0.50	0.25
0.50	1.86	1.81	1.63	1.22
1.0	1.53	1.33	1.20	1.07
1.5	1.18	1.14	1.08	1.02
2.0	1.07	1.05	1.03	1.01

width of the parabolic yield line pattern plus the distance between the loads,  $s$ . Adding  $s$  to  $b_e$  from Equation 23 and dividing by 2 to get the equivalent width per load, the plastic equivalent width is

$$b_{es} = 2b \left( \frac{\pi}{2} + \beta \right) + \frac{s}{2} \quad (63)$$

Because of the stress redistribution required to obtain the plastic strength, the critical spacing for strength design is larger than for serviceability design. The critical spacing is determined by setting Equation 63 equal to Equation 23 and solving for  $s$ , which results in Equation 64.

$$s_{cp} = 4b \left( \frac{\pi}{2} + \beta \right) \quad (64)$$

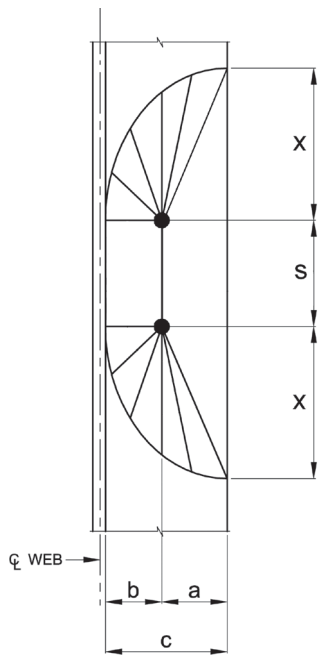


Fig. 13. Yield line pattern for closely spaced loads.

For design, Equation 63 should be used to calculate the equivalent width if the actual spacing is less than the critical spacing. Otherwise, Equation 23 should be used.

### END LOADS

Although monorail beams typically have end stops (which keep the trolley away from the end of the beam), sometimes nonwelded splices are used (which creates a condition where the load acts at the beam end when the wheel rolls over the splice). Also, there are cases where hangers and other loads are applied near the end of the member. If the load is located beyond a critical distance from the end of the member, the strength will not be affected. However, the strength can be reduced substantially when the load is close to the member end.

### Monorail Design Specifications

CMAA (2008) provides no specific guidance for loads near the end of monorail beams. However, Section 3.3.2.4.5 requires that “consideration should be given to lower flange stresses which are not calculable by the formulae presented in section 3.3.2.4.”

For flanges that are free to displace at the end of the beam, AS 1418 (AS, 2001) Section 5.12.3.1 requires the flange thickness to be increased by 30% if the load is within  $b_f + d$  of the end of the beam. This is an equivalent stress multiplier of  $(1.3)^2 = 1.7$ .

For serviceability design, Eurocode (1999) Section 5.5.2 (4) provides Equation 65 to calculate the flange bending stress when the load is at the end of the member.

$$\sigma = \left( \frac{P}{I_f^2} \right) \left[ 5.6 - 3.2 \left( \frac{a}{c} \right) - 2.8 \left( \frac{a}{c} \right)^3 \right] \quad (65)$$

Equation 65 neglects the effect of the distance from the load to the end of the member. Presumably, it was developed with the load at the end of the flange ( $e = 0$ ), which is the worst case. Strength design provisions in Eurocode (1999) are based on the triangular yield line pattern derived by Dranger (1977).

**Table 4. Values of  $k_e$  for Loads Near Member Ends**

$e/c$	$b/c$			
	1.0	0.75*	0.50*	0.25*
0	2.60	2.84	3.09	3.11
0.125	2.28	2.35	2.26	1.79
0.250	1.97	1.92	1.81	1.30
0.375	1.74	1.67	1.46	1.15
0.500	1.55	1.45	1.26	1.09
0.625	1.38	1.29	1.16	1.05
0.750	1.26	1.19	1.11	1.04
0.875	1.19	1.13	1.08	1.03
1.000	1.13	1.09	1.06	—
1.125	1.09	1.07	1.04	—
1.250	1.06	1.05	1.03	—
1.375	1.04	1.03	—	—
1.5	1.03	—	—	—

\* Only values of 1.03 and greater are listed

### Elastic Stresses

According to Equation 65, the stress due to end loads can be much higher than for intermediate loads. To determine the effect of the distance from the load to the end of the member, 44 finite element models were built using the modeling procedure described earlier. The models were proven accurate by comparison with the theoretical solutions of Jaramillo (1950) and Timoshenko and Woinowsky-Krieger (1959) and the finite element models of Ballio and Mazzolani (1983).

The  $e/c$  ratio varied from 0 to 1.5, where  $e$  is the distance from the load to the end of the member. Four  $b/c$  ratios were used: 0.25, 0.50, 0.75 and 1.0. The results are presented in Table 4 as a stress ratio,  $k_e$ .

$$k_e = \frac{\sigma_e}{\sigma_d} \quad (66)$$

where

$\sigma_d$  = stress caused by a load not at a member end, ksi

$\sigma_e$  = stress caused by a load near a member end, ksi

With the finite element results as a basis, it can be observed that the critical end distance in AS 1418 (AS, 2001) is extremely conservative. Conversely, the 1.3 factor for end-loaded flanges can be very nonconservative for  $e/c < 0.375$ .

Equation 65 from Eurocode (1999) agrees reasonably well (17% conservative on average) with Table 4 values at  $e/c = 0$  and  $b/c \geq 0.5$ . Therefore, the equation can be used for end loaded monorail beams ( $e = 0$ ). The most common case with  $e = 0$  is nonwelded splices, where the wheel passes from one

beam to the next. For monorail beams with angle end stops, where  $e > 0$ , Equation 65 can be extremely conservative.

The  $k_e$  values are plotted versus  $e/c$  in Figure 14. It may seem intuitive for design engineers to simply assume the equivalent width is reduced by 50% at the end of the beam (where  $e = 0$ ). Figure 14 clearly shows that this is nonconservative because the stress increases by more than 200% when  $b/c \geq 0.5$ . The reason for  $k_e$  values  $> 2$  can be better understood by observing the deformed shape of the flange. Figure 15a shows the deformed shape of a flange with an intermediate load and Figure 15b shows the deformed shape of an end-loaded flange. It can be seen that the end-loaded flange is in single curvature and the flange with the intermediate load is in double curvature. The flexural stiffness provided by the double-curvature bending spreads the equivalent width farther along the length of the flange, providing more strength.

For  $e/c \leq 1.375$  and  $b/c \geq 0.5$ , which covers the most common cases,  $k_e$  can be calculated with Equation 67. This equation was developed by curve-fitting the data and adjusting the curve-fit equation upward to eliminate excessive nonconservatism. In the worst cases within the range of applicability, Equation 67 is conservative by 17% and non-conservative by 3%.

$$k_e = -1.85 \left( \frac{e}{c} \right)^3 - 5.23 \left( \frac{e}{c} \right)^2 - 5.24 \left( \frac{e}{c} \right) + 3.03 \quad (67)$$

From observation of Table 4, the end distance effect can be neglected for all values of  $b/c$  if  $e/c$  is less than 1.375. This

leads to a critical end distance of

$$e_{ce} = 1.38c \approx 0.7b_f \quad (68)$$

For most monorail beams with angle end stops, the end stop leg width plus the wheel radius will be greater than  $0.7b_f$ . Therefore, in this case, the end-load effect is negligible.

When the actual end distance is less than the critical end distance, the reduction in strength can be accounted for by dividing the equivalent width for a single load by  $k_e$ . The modified equivalent width for serviceability design is

$$b_{ee} = \frac{b_e}{k_e} \quad (69)$$

### Plastic Strength

The plastic strength of end-loaded flanges can be calculated using the yield line pattern in Figure 16. The equivalent width is half of the equivalent width of the parabolic yield line pattern plus the distance from the load to the end of the member. Adding  $e$  to  $b_e/2$ , where  $b_e$  is taken from Equation 23, the equivalent width is

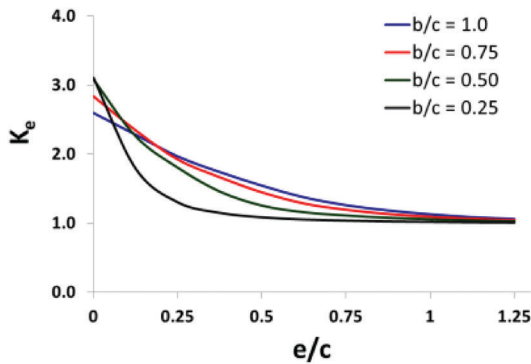


Fig. 14.  $k_e$  versus  $e/c$ .

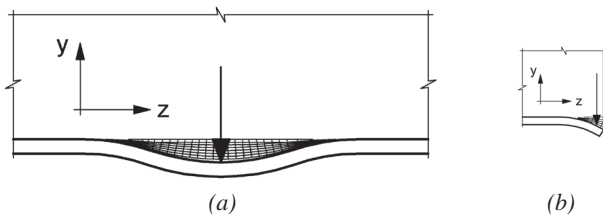


Fig. 15. Deformed shapes for double- and single-curvature bending: (a) double-curvature bending; (b) single-curvature bending.

$$b_e = 2b \left( \frac{\pi}{2} + \beta \right) + e \quad (70)$$

The critical end distance is determined by setting Equation 70 equal to Equation 23 and solving for  $e$ , which results in Equation 71.

$$e_{cp} = 2b \left( \frac{\pi}{2} + \beta \right) \quad (71)$$

For design, Equation 70 should be used to calculate the equivalent width if the actual end distance is less than the critical end distance. Otherwise, Equation 23 should be used.

For loads at the end of the member ( $e = 0$ ), Eurocode (1999) specifies  $b_e = 2c'$ , which is much less than the equivalent width calculated with Equation 70. Because the other Eurocode provisions are based on a triangular yield line pattern, the equivalent width for a triangular pattern at the end of a beam will be derived. A yield line cannot develop along the free edge at the end of the beam; therefore, the triangular yield line pattern consists of a single skewed yield line as shown in Figure 17. This pattern can potentially control the design over the parabolic pattern due to the availability of only one of the three yield lines that are available for the full yield line pattern (Figure 5).

The external work is

$$W_e = P\delta \quad (72)$$

The internal work is

$$W_i = m_p \left( \frac{\delta}{b} \right) \left( x + \frac{2c^2}{x} \right) \quad (73)$$

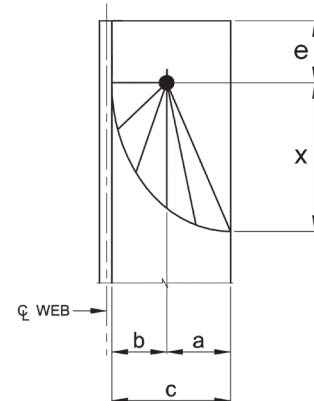


Fig. 16. Yield line pattern for loads near member ends.

where

$x$  = width of the yield line pattern in the direction parallel to the beam length

Set internal work equal to external work and solve for  $P$ .

$$P = \left( \frac{m_p}{b} \right) \left( x + \frac{2c^2}{x} \right) \quad (74)$$

Determine the derivative of  $P$  with respect to  $x$ .

$$\frac{dP}{dx} = \frac{m_p}{b} \left( 1 - \frac{2c^2}{x^2} \right) \quad (75)$$

Set  $\frac{dP}{dx} = 0$  and solve for  $x$ .

$$x = c\sqrt{2} \quad (76)$$

Substitute  $x$  into Equation 74 to get the nominal load.

$$P_n = \frac{F_y t_f^2}{\sqrt{2}} \left( \frac{c}{b} \right) \quad (77)$$

Combining Equations 1, 4 and 77, the equivalent width is

$$b_e = 2c\sqrt{2} \quad (78)$$

This is half of the equivalent width of the full triangular pattern given by Equation 13, and the strength at the beam end is reduced by only 50% despite the loss of two of the three yield lines. This can be explained by noting that dimension  $x$  at the beam end is only half that of the full yield line, which provides a much smaller effective lever arm.

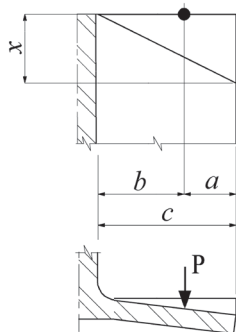


Fig. 17. Triangular yield line pattern at member end.

In conclusion, the plastic strength of a flange with a load at the end ( $e = 0$ ) is equal to half of the strength of the full yield line pattern. This applies to the triangular pattern and the parabolic pattern in Figures 5 and 7, respectively. The conclusions from Figure 8 are valid at beam ends, and the parabolic pattern controls the design over most of the  $a/c$  range. Therefore, Equation 70 is recommended for strength design in all cases of end loading.

## CONCLUSIONS

The equivalent-width method was explored in an effort to determine design procedures for elastic and plastic strength of flanges in single-curvature bending. The available procedures for designing flanges bent in single curvature were reviewed. New finite element models and yield line analyses were used to verify, expand and improve the existing design methods. Design recommendations were made for both the elastic and ultimate strength approaches. Recommendations were also made for interaction of the local bending strength with longitudinal stresses in the flange. The effects of closely spaced loads and loads acting near the ends of members were also addressed.

## ACKNOWLEDGMENT

Thanks to Ed Marshall of Southern Company, who provided the interpretation of Hannover and Reichwald (1982).

## SYMBOLS

$F_y$	Specified minimum yield stress, ksi
$K_L$	Load position factor
$K_m$	Equivalent width factor
$P$	Concentrated force, kips
$P_a$	Available wheel load, kips
$P_n$	Nominal load, kips
$S_e$	Section modulus of the equivalent beam, in. <sup>3</sup>
$W_e$	External work, kip-in.
$W_i$	Internal work, kip-in.
$Z_e$	Plastic modulus of the equivalent beam, in. <sup>3</sup>
$a$	Distance from the edge of the flange to the point of load application, in.
$b$	Horizontal distance from the face of the web to the concentrated load, in.
$b'$	Horizontal distance from the tangent point of the fillet radius to the concentrated load, in.

$b_c$	Horizontal distance from the center of the beam to the wheel load, in.	$\alpha$	Reduction factor to account for longitudinal stress in the bottom flange due to global bending of the beam
$b_e$	Equivalent width, in.	$\alpha$	Half angle around the parabolic yield line pattern (Figure 7), radians
$b_{ee}$	Equivalent width for end loads, in.	$\delta$	Virtual displacement of the load
$b_{es}$	Equivalent width per load for closely spaced loads, in.	$\gamma$	Partial safety factor for LRFD design
$b_f$	Flange width, in.	$\theta$	Load distribution angle
$c$	Horizontal distance from the face of the web to the tip of the flange, in.	$\sigma_1$	Stress caused by a single load, ksi
$c'$	Horizontal distance from the tangent point of the fillet radius to the tip of the flange, in.	$\sigma_2$	Stress caused by two closely spaced loads, ksi
$d$	Beam depth, in.	$\sigma_d$	Stress caused by a load not at a member end, ksi
$e$	Distance from the load to the end of the member, in.	$\sigma_e$	Stress caused by a load near a member end, ksi
$e_{ce}$	Critical end distance for elastic design, in.	$\sigma_{ev}$	Effective uniaxial stress, ksi
$e_{cp}$	Critical end distance for plastic design, in.	$\sigma_x$	Applied stress in the $x$ -direction, ksi
$f_b$	Longitudinal stress in the bottom flange of the beam, ksi	$\sigma_z$	Applied stress in the $y$ -direction, ksi
$f_c$	Longitudinal compressive stress in the element in question, ksi	$\tau$	Applied shear stress, ksi
$k_e$	Stress ratio for end-loaded flanges		
$k_s$	Maximum stress ratio for flanges with closely spaced loads		
$m_p$	Plastic capacity per unit length of yield line, kips		
$m_z$	Unit moment causing bending stress perpendicular to the length of the beam, kips		
$m_x$	Unit moment causing bending stress parallel to the length of the beam, kips		
$r$	Fillet radius, in.		
$t_a$	Flange thickness at the point of load application (for tapered flanges), in.		
$t_f$	Flange thickness, in.		
$t_w$	Web thickness, in.		
$s$	Spacing between loads, in.		
$s_{ce}$	Critical spacing for serviceability design, in.		
$s_{cp}$	Critical spacing for strength design, in.		
$x$	Width of the yield line pattern in the direction parallel to the beam length, in.		
$z$	Distance along the length of the beam, in.		

## REFERENCES

- AS (2001), *Cranes, Hoists and Winches, Part 18: Crane Runways and Monorails*, Australian Standard, AS 1418.18-2001.
- Ballio, G. and Mazzolani, F.M. (1983), *Theory and Design of Steel Structures*, Chapman and Hall.
- Ballio, G., Poggi, C. and Zanon, P. (1981), "Elastic Plastic Bending of Plates Subjected to Concentrated Loads," *Joints in Structural Steelwork*, Proceedings of the International Conference held at Teeside Polytechnic, April 6–9, John Wiley and Sons
- Cao, J.J., Packer, J.A. and Yang, G.J. (1998), "Yield Line Analysis of RHS Connections with Axial Loads," *Journal of Constructional Steel Research*, Vol. 48, pp. 1–25.
- CMAA (2008), "Specifications for Top Running & Under Running Single Girder Electric Traveling Cranes Utilizing Under Running Trolley Hoist," Publication No. 74, Crane Manufacturers Association of America.
- Dowswell, B. (2011), "A Yield Line Component Method for Bolted Flange Connections," *Engineering Journal*, AISC, Second Quarter, Vol. 48, No. 2.
- Dranger, T.S. (1977), "Yield Line Analysis of Bolted Hanging Connections," *Engineering Journal*, AISC, Third Quarter, Vol. 14, No. 3.
- Eurocode (1999), *Eurocode 3: Design of Steel Structures—Part 6: Crane Supporting Structures*, European Committee for Standardization.

- FEM (1983), *Local Girder Stresses*, Federation Europeenne de la Manutention, FEM 9.341, First Edition, Section IX, Series Lifting Equipment.
- Goldman, C. (1990), "Design of Crane Runway Girders for Top Running and Underrunning Cranes and Monorails," *Canadian Journal of Civil Engineering*, Vol. 17, pp. 987–1004.
- Hannover, H. and Reichwald, R. (1982), "Local Flexural Stressing of Girder Lower Flanges, Part 1," *F&H*, No. 6, pp. 455–460 (in German).
- Jaramillo, T.J. (1950), "Deflections and Moments Due to a Concentrated Load on a Cantilever Plate of Infinite Length," *Journal of Applied Mechanics*, ASME, Vol. 17, No. 1, March, pp. 67–72.
- Kurobane, Y. (1981), *New Developments and Practices in Tubular Joint Design*, IIW Document XV-488-81, International Institute of Welding.
- Mann, A.P. and Morris, L.J. (1979), "Limit Design of Extended End-Plate Connections," *Journal of the Structural Division*, ASCE, Vol. 105, No. ST3, March, pp. 511–526.
- Otegui, M.A. (1996), *Simplified Method for Design of Stiffened and Unstiffened Structural Tee Hangers*, Master's Thesis, Virginia Polytechnic Institute, Blacksburg, VA.
- Packer, J.A. and Morris, L.J. (1977), "A Limit State Design Method for the Tension Region of Bolted Beam-Column Connections," *The Structural Engineer*, Vol. 55, No. 10, October.
- Timoshenko, S. and Woinowsky-Krieger, S. (1959), *Theory of Plates and Shells*, 2nd ed., McGraw-Hill, New York, NY.
- Young, W.C. (1989), *Roark's Formulas for Stress and Strain*, 6th ed., McGraw-Hill, New York, NY.



# Buckling Restrained Braced Frame with All-Bolted Gusset Connections

PATRICK S. MCMANUS, ADDISON MACMAHON and JAY A. PUCKETT

---

## ABSTRACT

A braced-frame, lateral-load-resisting system was developed in which inelastic deformations due to seismic loading were intended to be isolated to easily replaceable buckling restrained braces (BRB). Bolted brace-to-gusset and gusset-to-beam and column connections were utilized to facilitate simple brace and gusset plate installation and replacement. Full-scale testing using two BRBs was executed to assess performance. Analytical frame models were developed using the nonlinear load-deformation characteristics of the braces. The experimental and analytical results were compared to validate reasonable nonlinear parameters for industry use.

All-bolted brace connections designed per AISC requirements provided adequate capacity to develop the BRBs. With proper detailing, inelastic deformations can be isolated substantially to the BRBs such that a repairable system is achieved. Load-deformation data for individual braces as provided by the supplier can be used to create reasonable analytical models for frames designed with all-bolted connections.

**Keywords:** buckling restrained braced frames, bolted brace connections, nonlinear analysis, performance-based seismic design.

---

## INTRODUCTION

According to the Hazards U.S. Multi-Hazard (HAZUS) analysis performed by the Federal Emergency Management Agency (FEMA), the costs associated with a catastrophic seismic event are significant (2008). However, it can be argued that the many indirect long-term costs—which are difficult to measure and admittedly neglected by FEMA—may have even greater impact. The long-term societal effects a catastrophic event can have on an area can necessitate years and perhaps decades of recovery. This is evidenced in the United States by the aftermath of Hurricane Katrina and, more recently, the 2011 Virginia earthquake. Several seismic events worldwide in recent years, such as the 2011 Christchurch, New Zealand, earthquake, further illustrate the point. By mitigating the initial impact of a significant seismic event and, more importantly, by reducing the direct costs and duration of repair and recovery for the building inventory in a given area, indirect long-term costs can be dramatically reduced.

Seismic-load-resisting systems for structural steel buildings have undergone considerable evolution over the past two decades. The seismic design criteria adopted by reference in

the 2009 International Building Code (IBC) are based upon the performance objective of collapse prevention, assuming a maximum considered earthquake (MCE) with a return period of 2,475 years (2% probability of exceedance in 50 years) (FEMA, 2003). The collapse prevention (S-5) performance objective, as described within ASCE 41-06, “Seismic Rehabilitation of Existing Buildings,” allows for considerable inelastic deformations within primary members such that a structure subject to the MCE likely has little residual lateral-load-carrying capacity and cannot be economically repaired (ASCE, 2007). ASCE 41-06 defines higher discrete performance objectives as life safety (S-3) and immediate occupancy (S-1), as well as intermediate objectives damage control range (S-2) and limited safety range (S-4). These higher performance objectives are typically evaluated in consideration of an earthquake of lesser magnitude than the MCE, such as the design basis earthquake (DBE). In the context of ASCE 41-06, the DBE represents an event with return period of 474 years (10% probability of exceedance in 50 years). While some structures designed in accordance with the IBC 2006 or IBC 2009 may inherently achieve higher performance levels for the DBE, ASCE 41-06 indicates that a structure meeting the life safety performance objective may still be beyond economical repair. The resulting expense to the owner or insurer from a seismic event of similar significance could be economically devastating.

As can be seen by various systems described in the 2005 AISC *Seismic Provisions for Structural Steel Buildings* (AISC, 2005a), achieving the design objectives of current building codes in steel-framed buildings is primarily accomplished by proportioning elements such that specific major components experience inelastic deformations. The 2005 *Seismic Provisions* were current at the time of this research

---

Patrick S. McManus, Structural Technical Director, Martin/Martin, Inc., Lakewood, CO (corresponding). E-mail: pmcmanus@martinmartin.com

Addison MacMahon, Design Engineer, Martin/Martin, Inc., Lakewood, CO. E-mail: amacmahon@martinmartin.com

Jay A. Puckett, Associate Dean and V.O. Smith Professor, Department of Civil & Architectural Engineering, University of Wyoming, Laramie, WY. E-mail: puckett@uwyo.edu

---

and are referenced in this paper. Components that connect major lateral-load-resisting elements, as well as components that are not intended to resist lateral loads, are anticipated to remain substantially elastic and undergo minimal damage. While the idea of isolating large deformations to anticipated components and locations has considerable merit, the current design methods by which this concept is applied pose some possible inefficiencies, including potentially detracting from the reparability of the structural system.

The controlled and predictable yield of major components has resulted in considerable limitations on global and local member geometry. To achieve desired compactness requirements and slenderness ratios, often beam, brace and column sections gravitate to sectional areas well in excess of those required to resist loads derived from the load combinations of the applicable building code. This places considerable force demands on connections, which in seismic applications are typically required to develop the expected yield strength of the primary member. The results are increased material and connection costs.

To develop the expected yield strength of members such as beams or braces, welded connections are typically required. The reason is the area reduction due to holes for bolted connections typically results in inadequate available tensile strength at the net section to develop the required expected yield strength of the member. Usually, some magnitude of welding must occur in the field, which is arguably the most expensive process in steel construction. This may increase the relative cost of the steel frame, making it less competitive with other lateral-load-resisting systems.

Primary structural components such as beams and columns are extremely expensive by structural standards and difficult to adequately repair or replace, particularly when equipped with fully welded connections. Typically, these components, by design, are fully integrated with the overall structural scheme and, in most cases, are relied upon to carry gravity loads in addition to lateral loads. Therefore, as noted previously in relation to ASCE 41-06, replacement of such components once significantly damaged is often unrealistic, leaving complete demolition and replacement of the building as the only viable option. New innovations in seismic-load-resisting systems have recognized that the approach of isolating inelastic deformations to primary, permanently attached components may be flawed when reparability is a primary objective. By instead isolating inelastic deformations to easily accessible, bolted components that can be relatively inexpensively removed and replaced, a repairable seismic-load-resisting system can be achieved.

Herein, a *repairable system* is defined as a frame where inelastic deformation has been accommodated in such a way that the damaged element can be reasonably removed from the frame after a seismic event and replaced with a similar element, e.g., a buckling restrained brace (BRB).

Connections and/or other members are designed to remain substantially elastic and can therefore be reused.

Repairable seismic-load-resisting systems pose several advantages. Components that are relatively easily replaced characteristically exhibit easy initial installation. Therefore, the field labor associated with initial installation of a repairable system may be reduced over the current labor-intensive installation processes described previously. Reduction in field labor typically translates to reduction in overall cost and schedule. Additionally, structures with enhanced potential to be viably salvageable after a significant seismic event are likely marketable to owners and insurers. It is recognized that a repairable structure does not reduce the deformations and associated damage of nonstructural components nor does it address the repair of those components. Enhanced detailing of nonstructural components may be required to ensure a building with a repairable structural system is salvageable.

To adequately address a wide spectrum of building program needs, proposed repairable connections and components have been developed for moment frame (McManus and Puckett, 2011) and braced frame systems. Only the braced frame system—referred to as fully bolted, buckling restrained braced frames (BRBF)—is addressed herein. Two full-scale BRBF one-bay, one-story frames were tested. The brace-to-gusset, gusset-to-member and member-to-member frame connections were fully bolted. The BRB could be replaced by unbolting the damaged brace and replacing it with a new one. In the present test series, a Star Seismic BRB (WC250, implying a core yield strength of 250 kips) was initially installed in the test frame. The translation/drift regimen of Appendix T of the 2005 AISC *Seismic Provisions* was used based on a maximum drift of 2%. The BRB and connections performed well, and the system illustrated robust and stable hysteric behavior.

The frame was re-plumbed and another brace (WC200) was installed. Testing of the second brace again employed the regimen prescribed in the AISC *Seismic Provisions* with a 2% maximum drift. The frame was examined for damage and then tested again under the AISC regimen adjusted for 3% maximum drift. The brace and the connections performed well. The hysteric behavior again was stable for all cycles. Because 3% was the limit of the test configuration, the test series was ended.

The test regimen of Appendix T of the 2005 AISC *Seismic Provisions* is intended to achieve a maximum story drift equal to twice the design story drift. The proportioning of structural elements to achieve the design story drift can vary considerably as the result of many factors, such as analysis methodology and building classification within the applicable building code. Consequently, it is beyond the scope of this paper to identify a specific magnitude of earthquake for which a structural system utilizing the BRBF connections

described herein is economically repairable. Rather, the intent is to demonstrate adequate performance in accordance with requirements of the AISC *Seismic Provisions* and enhanced reparability compared with other structural systems or BRBF systems with welded gusset-to-beam/column connections.

This article contains the test description and results for global behavior for the frame and local strains in areas of interest. The information from these tests was used to develop recommendations for proportioning and configuring the members and connections. In summary, the concept of designing a structural frame with enhanced reparability appears to be viable. Connection details can accommodate the significant drift requirements. The replacement of the brace was demonstrated.

## BACKGROUND

### Buckling Restrained Braced Frames—Overview

In high-seismic regions, it is probable that structures designed in accordance with IBC 2009 will experience inelastic deformations from a seismic event during the

course of its service life (McManus and Puckett, 2011). The inelastic deformations can occur in several ways, depending on the goals and type of system being designed. The BRBF system uses diagonal-brace elements, which are designed to yield in a predictable and favorable manner. Figure 1 illustrates a typical BRBF and the BRB application in the two-story X-bracing configuration. These gusset plates are welded to the columns and beams.

Figure 2 illustrates a schematic of a BRB made of three distinct sections: the core that is design to yield, the transition zone and the extension plate. The steel core and transition are encased in a grouted tube that restrains the core from buckling under compressive loads. Typical cross-section details are illustrated in Figure 3. The details for the tested BRBs are changed to accommodate bolting. The BRB details are provided in McManus, Puckett and MacMahon (2011).

### Repairable BRBF Seismic Systems

Because the core of the brace need only be proportioned to provide sufficient stiffness to meet story drift requirements



Fig. 1. BRBF Example: Lawrence Berkeley National Lab (Star Seismic).

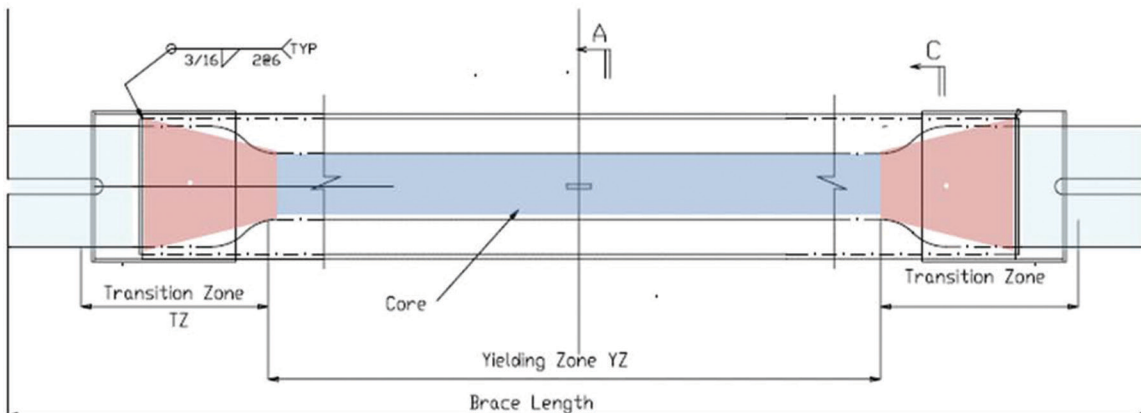


Fig. 2. Schematic of a BRB.

or to carry the loads from the applicable building code without consideration of buckling, the required strength of the connections to develop the expected yield of these braces is typically less than that of other types of seismic braced frames. Forces to the connections can therefore be adequately addressed with bolted connections. However, tests of BRBF assemblies to date have consisted primarily of welded connections between the gusset and column and almost entirely of welded connections between the gusset and beam [refer to Lopez et al. (2004) and Thornton and Muir (2009) for examples with associated references]. Test results in

braced frame systems often result in significant damage at the interface between the gusset and beam or column due to the large rotations induced at the connection under the large story drifts simulated in seismic testing (Thornton and Muir, 2009). Therefore, even if the BRBF were bolted to the gusset but welded to the primary members, a repairable system would not be achieved should damage to the gusset occur during a seismic event. By bolting the gusset to the brace as well as the beam and column as shown in Figure 4, a repairable system can be produced.

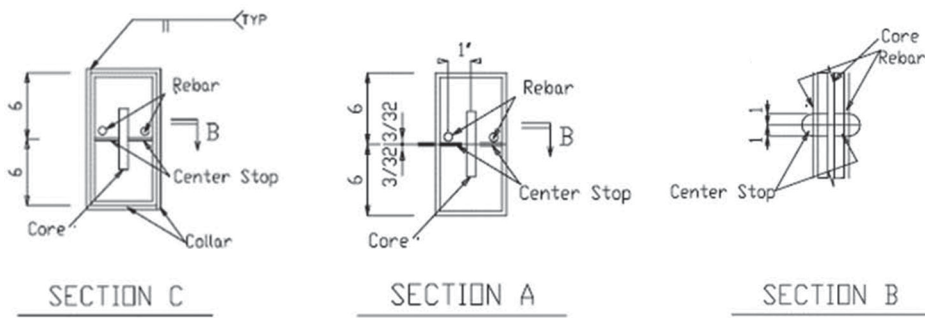


Fig. 3. Typical BRB section details.

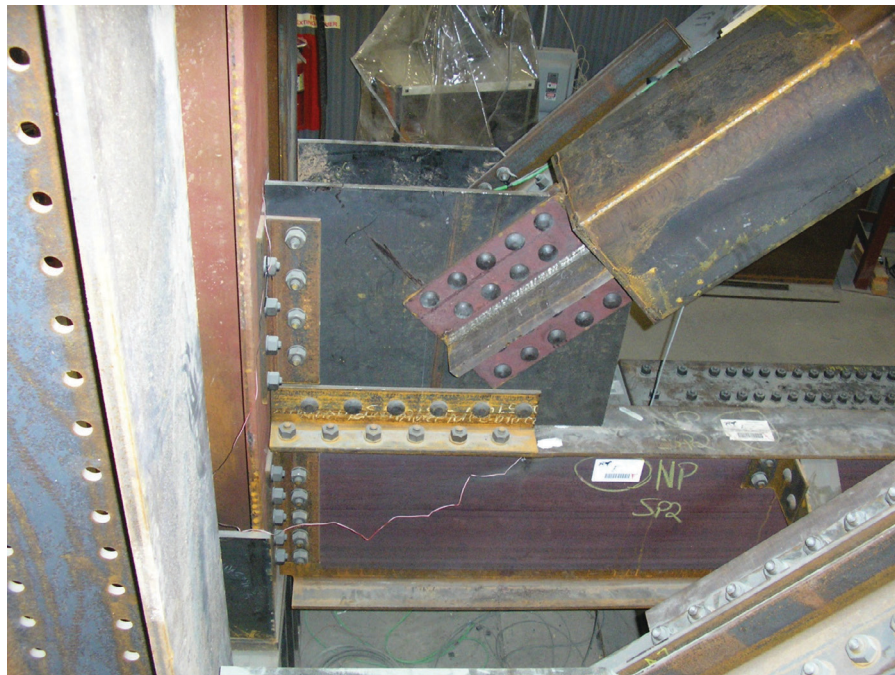


Fig. 4. Fully bolted buckling restrained brace connection prior to test.

## RESEARCH OBJECTIVES

The primary goal of this research was to evaluate fully bolted BRBFs as repairable seismic-load-resisting systems through experimental testing. A second goal was to verify that fully bolted connections designed using then-current AISC provisions adequately developed the BRB at code-required story drifts. Finally, the third goal was the development of linear and nonlinear analysis procedures that adequately represent the behavior. Recommendations for design as well as linear and nonlinear modeling were developed.

## BRACE AND FRAME DESIGN

### Beam and Column Design

Primary framing members for the test frame and reaction frame were intended to remain elastic during the tests. Initial design was consistent with simple hand methods that are common in professional practice. The adjusted brace strength of the WC250 in compression was assumed to develop in the brace. The adjusted brace strength in compression is defined within the 2005 AISC *Seismic Provisions* as  $\beta\omega R_y P_{ysc}$ , where  $\beta$  is the compression strength factor,  $\omega$  is the strain hardening factor,  $R_y$  is the ratio of expected yield stress to minimum specified yield stress, and  $P_{ysc}$  is the axial yield strength of the core (AISC, 2005a). The ratio of compression strength to tension strength,  $\beta$ , was assumed to be 1.14 based on test data from the University of Utah (Romero et al., 2007). From the same data, the hardening factor,  $\omega$ , was assumed to be 1.58. The  $\beta$  and  $\omega$  factors were calculated based on the anticipated strains in the steel core at twice the design story drift in accordance with the 2005 AISC *Seismic Provisions*. Because Star Seismic performed tensile coupon

tests on the braces provided for the testing herein,  $R_y$  was taken as 1.0. The forces in the primary framing members associated with the assumed adjusted brace strength were calculated using statics, and the strength was checked using standard AISC LRFD procedures. Members were assumed to have pinned ends with an effective length factor,  $K$ , of 1.0. All wide-flange sections were ASTM A992 steel. Coupon tests of connection, beam and column material were not performed.

Seismic compactness criteria and available sections from the fabricator assisting with the project were also considered in the design. The lightest seismically compact nominal 14 in. by 14 in. (356 mm by 356 mm) wide-flange shapes (W14×132) were used for the columns in the test frame (see Figure 5). The high and low ends of the BRB (diagonal orientation) were initially configured such that the actuator force would be delivered to the brace through the upper beam of the test frame. Consequently, the upper beam (W21×62) was initially sized to carry this force. It was also sized based on availability from Puma Steel, flange geometry to adequately receive bolted connections, and flange and web compactness ratios within the maximums allowed by the 2005 AISC *Seismic Provisions*. However, the brace direction was switched later in design such that the actuator and brace would be in compression at the same time. This was done to ensure that the strength of the brace was developed recognizing the strength of the brace and capacity of the actuator were both greater in compression than in tension. With the new configuration, the upper beam of the test frame theoretically became a zero force member.

The lower beam of the test frame (W24×55) transferred the horizontal component of the brace force through a

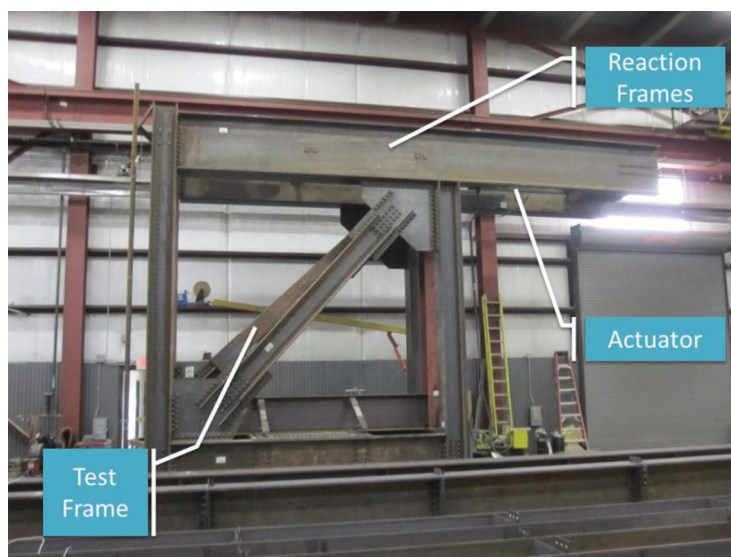


Fig. 5. North view of frame.

diaphragm plate to the reaction frame. This beam was designed assuming strong-axis brace points at the member ends and weak-axis brace points at the ends and at third points. Strong-axis eccentricity was not considered in the initial design because eccentric forces were assumed to be easily resolved through the frequent bottom-flange connections to cross beams within the reaction frame. The lower beam was sized using similar considerations to the upper beam, except that the web compactness ratio was slightly above the AISC maximum seismic compactness limit. Exceeding the web seismic compactness ratio was intentional to challenge the beam capacity and ensure, through successful performance, that all compact sections could be assumed to perform adequately. Additionally, the web of the lower beam was slender for shear strength calculations per the 2005 AISC *Specification for Structural Steel Buildings* (AISC, 2005b).

Primary members within in the reaction frame were also chosen based on material availability but were primarily intended to provide elastic stiffness several times that of the test frame. Consequently, demand-to-capacity ratios in the members were relatively small, and seismic compactness was not considered. Adequate capacity of all members was verified in later analytical modeling.

### Design of BRB-to-Frame Connections

In general, for any bolted joint in the seismic-load-resisting system (SLRS), the joint can be designed as a bearing-type connection if standard holes are used in all plies, but it must be constructed as slip-critical. Thus, the bolts must be pretensioned, and the faying surface must meet at least class A requirements (class B and C faying surface requirements would also be acceptable). This requirement is intended to limit deformations within the joint during an earthquake. An exception to this requirement is for bolted joints at diagonal brace connections. In this case, oversized holes are permitted in one ply of connected interfaces provided the connection is designed as slip-critical. This exception was added to the 2005 AISC *Seismic Provisions* based on feedback from erectors, who indicated that fit-up of bolted brace connections was very difficult with standard holes.

Finally, for any bolted joint in the SLRS, the nominal bearing strength cannot be taken greater than  $2.4dtF_u$ , where  $d$  is bolt diameter and  $t$  and  $F_u$  are the thickness and rupture strength of the material being connected, respectively. Chapter J of the AISC *Specification* permits the nominal bearing strength to be taken as high as  $3.0dtF_u$ . However, at this level, significant hole elongation occurs. Consequently, in order to again limit movement at bolted joints during an earthquake, the AISC *Seismic Provisions* limit the nominal bearing strength.

The uniform force method was used to determine the force distribution in the brace connections. The uniform

force method determines force distribution to connection components and primary members based on the geometric extents of the primary members being connected. Further description of this method can be found in the 13th edition of the AISC *Steel Construction Manual* (AISC, 2005c). Special case 2, as defined by AISC, was used at the upper brace connection to theoretically eliminate shear to the beam. This addresses multiple force distribution approaches through the testing. The gusset plate at the upper connection was attached to the column web, whereas the gusset was connected to the column flange at the lower connection to incorporate multiple framing conditions into the testing as well. Figures 6 and 7 depict the connections at the lower and upper end of the brace, respectively.

All plate and angle material was ASTM A36. All bolts were  $\frac{7}{8}$ -in. (22-mm) diameter. ASTM A325 bearing bolts with threads excluded from the faying surfaces were used to connect angles to gusset plates and primary members. ASTM A490 bolts were used to connect the BRB to the gusset plates using slip-critical connections. A class A faying surface preparation was provided with standard holes in the gusset plates and oversized holes in the connection plates on the BRB.

The probable brace forces used for connection design were developed in accordance with the 2005 AISC *Seismic Provisions* using  $\beta$  and  $\omega$  factors recommended from tests of Star Seismic braces at the University of Utah (Romero et al., 2007), discussed previously regarding member design. Star Seismic uses these factors in practice, and the intent was to be consistent with its typical design approach. Standard Load and Resistance Design (LRFD)  $\phi$  factors were applied in designing for each of the connection limit states.

Governing design limit states of the gusset-to-beam/column connections were bolt shear, prying action and bolt bearing on the gusset. Slip-critical joints with ASTM A490 bolts in oversized holes were used to connect the braces to the gussets. Thus, slip-critical shear values governed the brace-to-gusset connections. Demand/capacity ratios varied between roughly 0.9 and 1.1 for these governing limit states. The 10% overstresses were typically on prying action checks in the connection angles. The overstress was intentional to challenge the design, recognizing weak-axis bending of the angles often governs strength and stiffness in all bolted connections.

## EXPERIMENTAL TEST SETUP

### Test Procedure, Arrangement and Equipment

Full-scale testing of the braces first involved one trial run on the test specimen without any brace installed. The intent of the trial run was to verify that the data acquisition software would work properly with the instrumentation. Testing of the two buckling restrained braces was performed per the provisions of Appendix T of the 2005 AISC *Seismic*

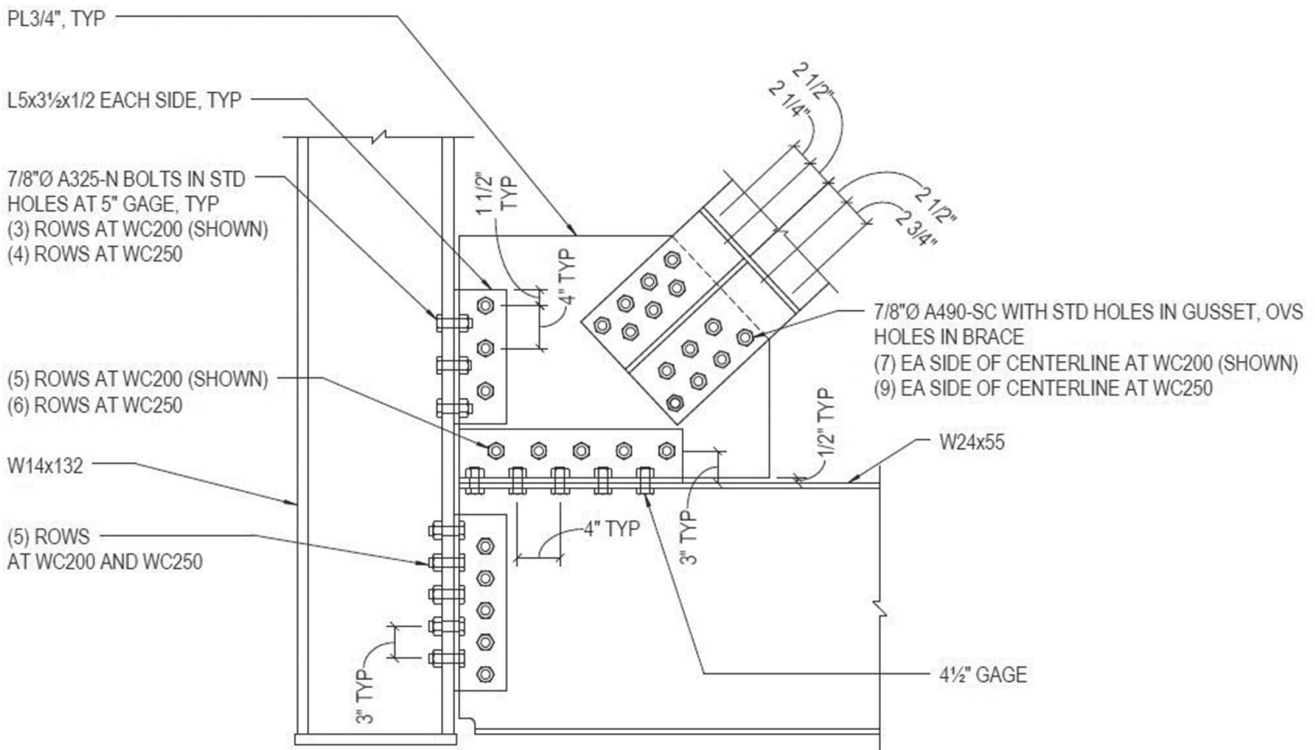


Fig. 6. Brace connection detail at lower brace end.

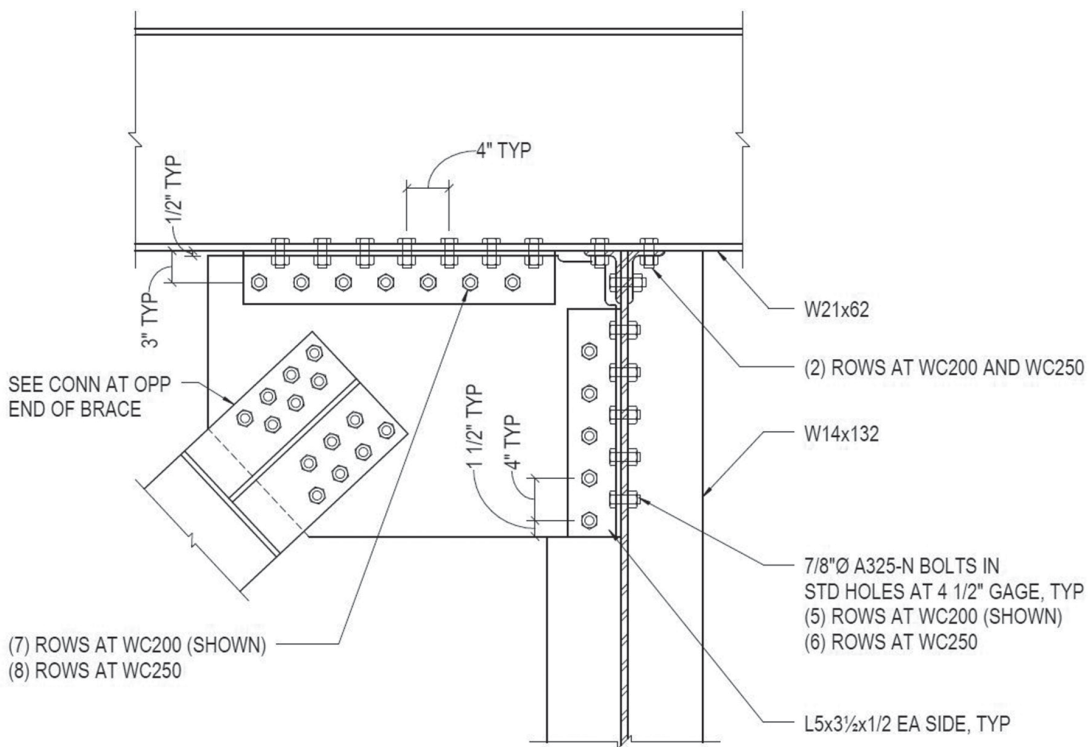


Fig. 7. Brace connection detail at upper brace end.



potentiometer was mounted along the BRB long axis with mounting points near the ends of the reduced yield zone section to measure total axial deformation of the steel core (see designation C in Figure 8).

The strain gauge orientation for the first test on the WC250 was primarily located around the bottom gusset plate connecting the brace to the beam and column. Strain gauge 1 (SG1) was mounted vertically on the gusset plate. SG2 was mounted on the gusset plate aligned with the brace. SG3 was mounted horizontally near the same location as SG1 and SG2 with the intent of capturing the in-plane state of stress in the gusset (see Figure 9).

SG4 was located on the angle connecting the gusset plate to the bottom beam and was placed near the outermost bolt hole. SG5 was placed under the top flange of the bottom beam directly below SG4 (see Figure 10). SG6 was placed on the outstanding leg of the angle connecting the gusset plate to the column next to the outermost bolt hole, similar to SG4 (see Figure 11).

For the WC200 test, SG1 through SG5 were in the same locations as in the WC250 test. However, SG6 was placed on the web of the bottom beam, see Figure 12.

The initial trial run of the data acquisition software, with gusset plates in place but no brace, provided information to adjust the software, but also unintentionally resulted in pulling the test frame to a drift of nearly 3%, which caused local web yielding and web crippling in the bottom beam in the test frame. Note the beam was intentionally slightly outside

the limits for seismic web compactness, and the web was slender for shear. The proportions were selected to suggest any compact section would perform adequately under similar loading. However, the mishap now leaves a question as to whether web yielding and crippling would have occurred if a compact section had been used. The excessive deformation was the result of an error in the software that pushed the frame past the target deformation and continued until the program was shut down manually. Also, it was determined that the original automated software could not function properly due to high load spikes produced when joints at the gusset plate-to-beam and column connections that were designed with bearing bolts—but constructed as slip-critical in accordance with the *AISC Seismic Provisions*—slipped into and out of bearing. The pressure gauges in the actuator were not designed for dynamic loading and thus would read pressures beyond the recordable limits of the sensors when small, sudden movements in the frame occurred. Based on these limitations, it was decided to conduct the test manually, with one computer operator controlling the actuator until the desired test frame displacement was reached. This approach proved to be adequate and was used for all subsequent tests.

The data acquisition software used to collect translation, pressure and strain data was National Instruments' LabView 2010, version 10.0.0. All strain gauges used were Vishay Micro-Measurements and SR-4 general-purpose strain gauges. The digital string pot used on the braces was

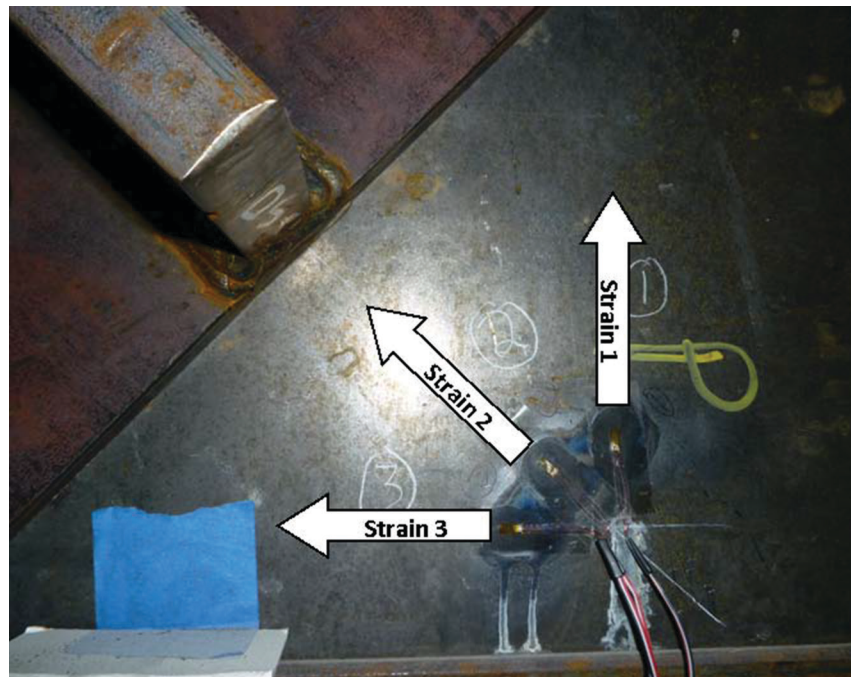


Fig. 9. WC250 strain gauges.



Fig. 10. WC250 strain gauges.



Fig. 11. WC250 strain gauges.

Celesco model SR1E, with an incremental encoder output signal and a stroke range of 125 in. (3180 mm.) The smaller string pot mounted at the top of the column with a 10-in. (254-mm) stroke was UniMeasure model JX-EP-10. The linear potentiometer used at the base of the outer column was ETI Systems model LCP12S-100. Details are provided in the associated manuals (see McManus et al., 2011).

## EXPERIMENTAL RESULTS

### Test 1 Results: WC250 Brace

Due to “banging” from built-up load and subsequent slip in the joints, much of the information was simply filtered to remove transients. Only data corresponding to the system in motion were filtered. There was negligible translation at the base of the test specimen, as expected. The applied load versus displacement history exhibited stable and repetitive behavior with positive incremental stiffness (see Figure 13).

Visual inspection of the connection material after the test suggested slip only occurred at connections between the gusset plate and connection angles that attached the beams and columns, which were designed as bearing connections with standard holes. The gusset plate at the connection of the brace, as well as the connection plates on the brace, did not show any of the scarring due to slip noticed at the bearing connections, nor any signs of hole

elongation. Consequently, the brace-to-gusset connections that were designed slip-critical appeared to resist the load without slip, as intended.

The test regimen was designed such that the frame cumulative translation would reach 131.6 in. (3343 mm). Actual accumulated frame translation was measured to be 134.5 in. (3416 mm). Because steel-core elongation was not properly measured during this test, the ratio of inelastic deformation to frame translation from the WC200 test was used to approximate the cumulative inelastic deformation for the WC250 test. This is reasonable because steel-core length and yield stress are similar between the two braces. Using the ratio from the WC200 test, the cumulative inelastic deformation for the WC250 was approximately 64.7 in. (1642 mm), which is nearly 400 times the calculated yield deformation and approximately twice the AISC minimum requirement of 33.2 in. (843 mm).

Strain data are shown in Figures 14 through 20. SG1 measures strain on the gusset in the vertical direction. The strain shows an asymmetrical response to load. At an assumed steel modulus of 29,000 ksi (200,000 MPa), the max stress in the vertical direction was 7.2 ksi (50 MPa) at a strain of  $\epsilon = 247 \mu$ . Hereafter, similar data are paired [e.g., (247  $\mu$ , 7.2 ksi)], and the results are discussed in terms of stress.

SG2 is consistent with the axial forces from the brace into the gusset plate and matches the hysteresis of the system (symmetric with loading). The max strain and stress are (1300  $\mu$ , 39 ksi) at SG2. SG3 measures the strain in

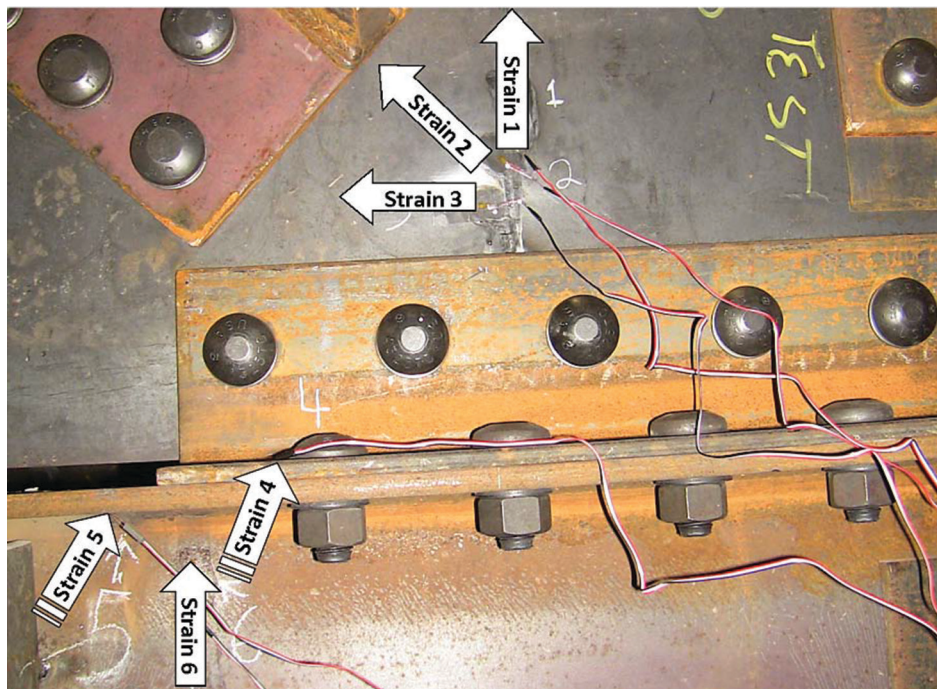


Fig. 12. WC200 strain gauges.

the horizontal direction on the gusset plate along the beam connection. SG3 exhibited behavior similar to SG1 with an asymmetric response to loading, (231  $\mu$ , 6.7 ksi). This asymmetric response is to be expected because the load transferred from the brace to the gusset is 43° from horizontal in relation to SG1 and SG3. With this orientation of the brace, the vertical component of strain (SG1) is affected more by tension forces from the brace and less by compression when the gusset is bearing on the bottom beam. The horizontal

strain (SG3) is more affected by compression forces from the braces.

SG4 was located along the bottom angle connecting the gusset plate to the bottom beam, positioned perpendicular to the longitudinal beam axis. The gauge was positioned next to a bolt and reported a maximum value of 2100  $\mu$  when the brace was in tension and the angles resist forces through bending. This value was largely in excess of the strain corresponding to minimum specified yield stress of 36 ksi

### WC 250 Hysteresis at 2% Drift

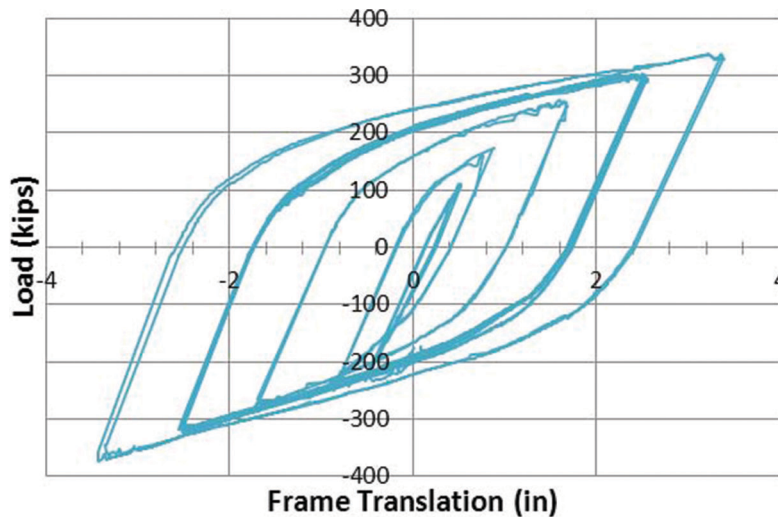


Fig. 13. Test 1 WC250 hysteresis.

### Strain 1 - WC250 2% Drift

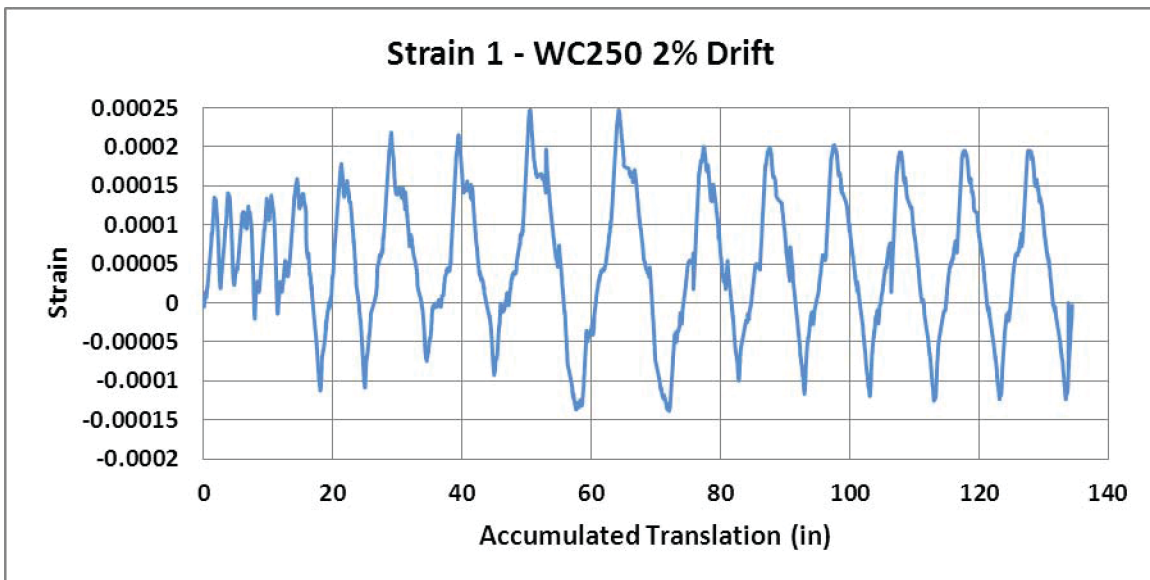


Fig. 14. Test 1, WC250 SGI.

(1200  $\mu$ ). Much lower values were present when the brace was in compression and the angles were bearing on the beam flange. At the maximum strain recorded in compression, the approximate stress was calculated to be (718  $\mu$ , 20.8 ksi). Stress in excess of theoretical yield, or even actual yield if it were known, is not surprising at this location because the stresses vary considerably across the outstanding leg of the angle, and concentrations are likely present near bolts.

SG5 measured strain perpendicular to the length of the bottom beam on the underside of the beam's top flange. The stress does spike close to yield during the two largest displacement cycles at approximately 1840  $\mu$ , which is reasonable given the higher rotations of the frame at this point and thus more tension near the bolt holes in the top flange. Similar to SG4, concentrations likely are present near the bolts.

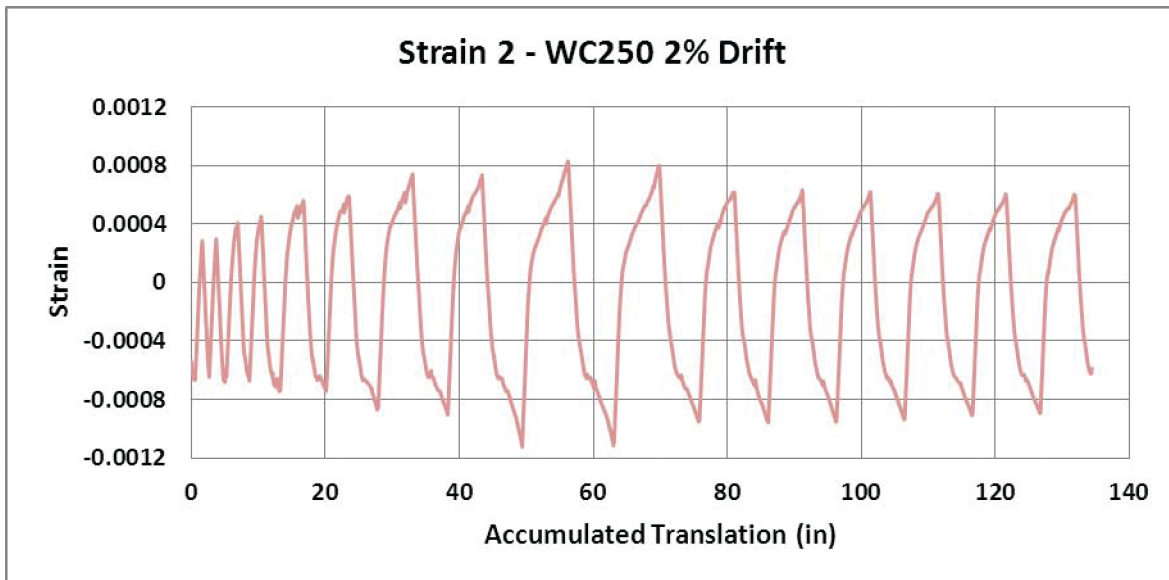


Fig. 15. Test 1, WC250 SG2.

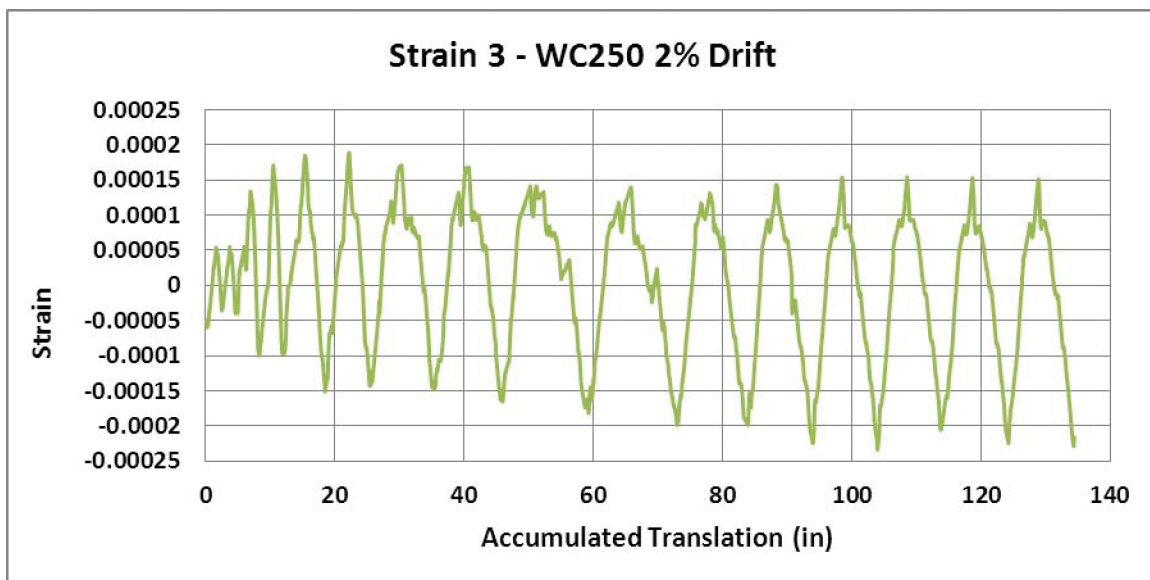


Fig. 16. Test 1, WC250 SG3.

SG6 measures strain in the angle connecting the gusset plate to the column near the outermost bolt in the horizontal direction. This connection shows similar behavior to SG4, with higher strain when the brace is in tension and lower strain in compression (bearing on the flange). The approximate stress measured was (1220  $\mu$ , 35.4 ksi), which indicates lower stress in this element than in the angles connected to the beam or in the beam flange.

SG7 was only recorded in the WC250 test and was measured roughly at the work point of the upper beam where the actuator load was applied to the test specimen. Stresses at this point were low, reaching a maximum of near (76  $\mu$ , 2.2 ksi). This value suggests approximately 40 kip (178 kN), or 12% of the load in the actuator, was transferred to the beam. Thus, 88% was resisted by the brace. The 40-kip load calculated from the strain data was relatively consistent with

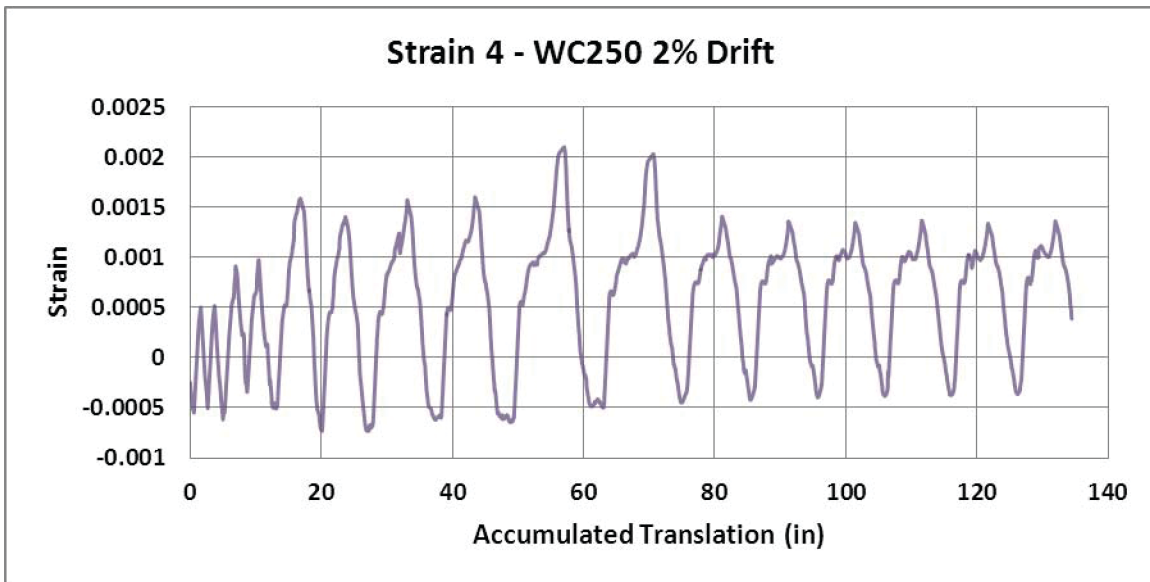


Fig. 17. Test 1, WC250 SG4.

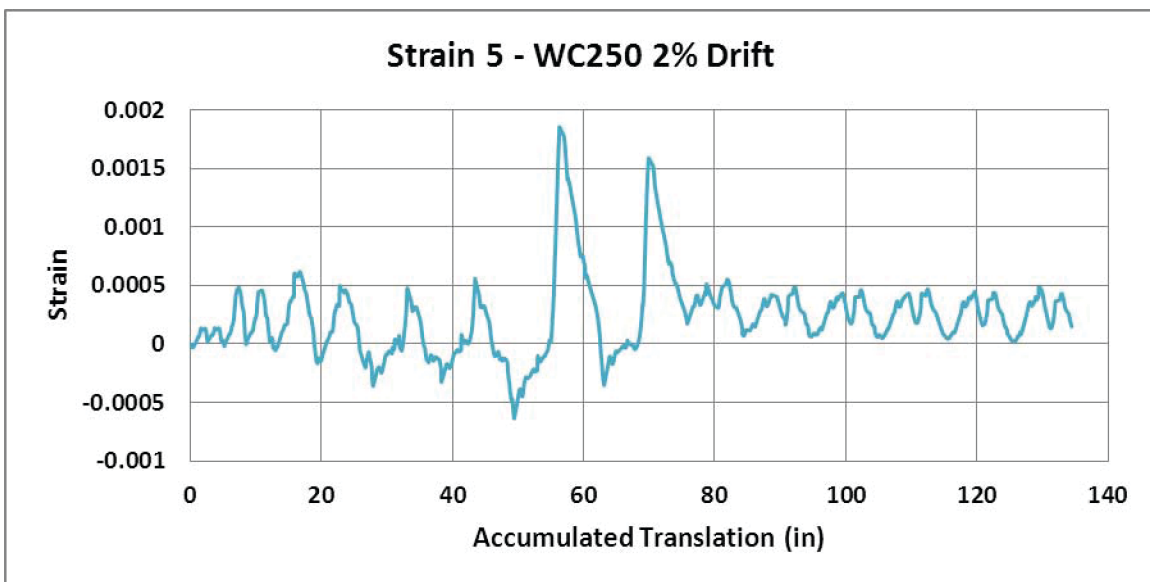


Fig. 18. Test 1, WC250 SG5.

the maximum force recorded during the calibration test with gusset plates installed, but no brace present, under similar translation.

The University of Utah (Romero et al., 2007) reported a maximum force in the WC250 during testing to be 404 kips (1797 kN) in tension and 474 kips (2108 kN) in compression. This project used a connection design axial force in the brace of 435 kips (1935 kN) in tension and 496 kips (2006 kN) in compression. During testing of the WC250,

the maximum axial force achieved in the brace was 404 kips (1797 kN) in tension (equal to the University of Utah max under similar strain) and 451 kips (2006 kN) in compression (95% of University of Utah max under similar strain). Brace force was calculated geometrically based on the force in the actuator and adjusted for the aforementioned assumption that 88% of the actuator force was resisted by the brace due to the 12% contribution of frame action.

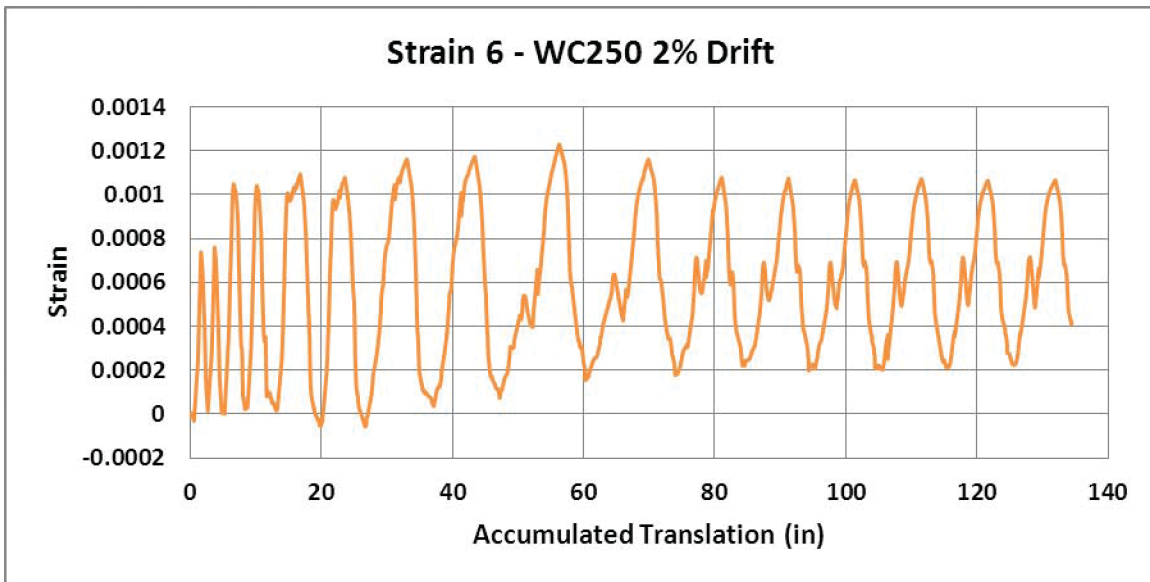


Fig. 19. Test 1, WC250 SG6.

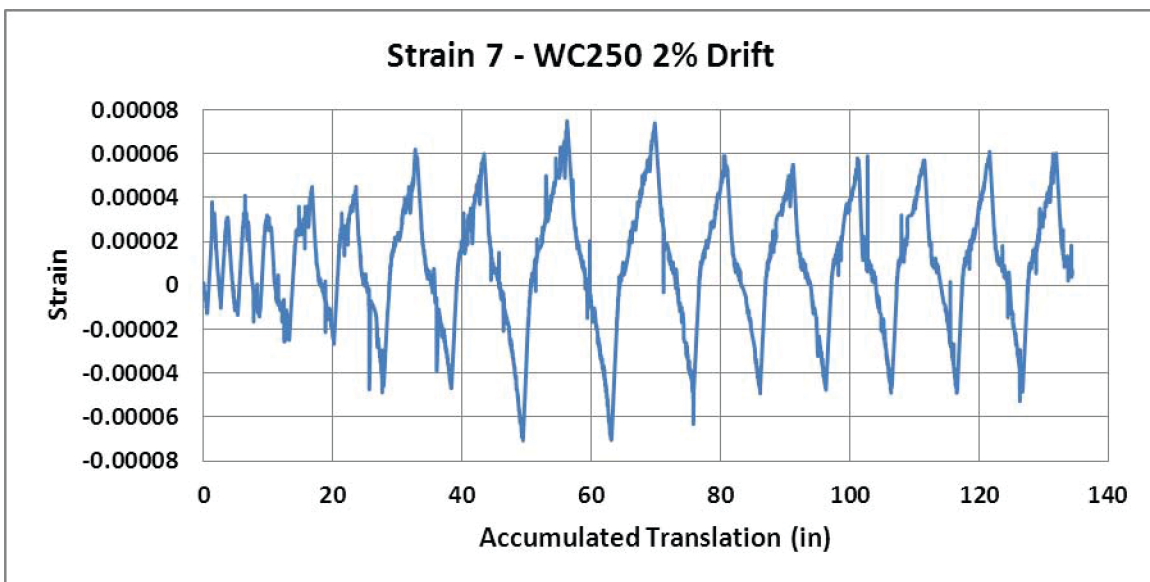


Fig. 20. Test 1, WC250 SG7.

SG1, SG2 and SG3 can be used to determine the state of strain (or stress) in the gusset plate along the brace located at the point of coincidence of the gages. (See Figure 9 and, for the WC 200, Figure 12.) Given the three normal strains at the peak load of 451 kips (2006 kN), the shear strain can be determined to be (229  $\mu$ , 6.6 ksi). This corresponds to the maximum principle shear stress of 25.0 ksi and principle normal stresses of 24.9 and 25.1 ksi. The von Mises yield criterion would predict yield at approximately  $0.57 \times F_y = 20.8$  ksi. Therefore, the max shear stress in the gusset exceeded the theoretical yield stress at the maximum load during the test.

While the upper connection of the test specimen was not instrumented with strain gauges, visual inspection of the primary members and connection components after the test indicated no noticeable damage. In connecting the gusset plate to the web of the column, the relatively high out-of-plane flexibility of the column web appeared to accommodate frame rotation without distress to connection components or primary members. Primer paint on the column, except where removed to facilitate a Class A faying surface, showed no signs of distress at the connection to the column web. Consequently, in consideration of a repairable system, this configuration was demonstrated to be significantly more desirable than connecting to the column flange.

### Test 2 Results: WC200 Brace

The WC200 test resulted in similar behavior to the WC250 test. Filtering similar to the previous test was used. Translation along the length of the brace was properly measured

in this test and produced usable hysteretic information. The frame translation versus applied load also exhibited stable and repetitive behavior with positive incremental stiffness (see Figure 21).

The total brace elongation is illustrated in Figure 22. The second regimen of cycles for 3% drift begins at scan 6000. Translation along the brace shows a slightly asymmetric response to loading, with larger displacements in tension than in compression during the 2% test and larger displacements in compression than in tension during peak loads in the 3% test. The maximum elongation during the 2% drift test is 2.1 in. (53 mm) in tension and 1.9 in. (48 mm) in compression. The maximum elongation during the 3% drift test is 2.8 in. (71 mm) in tension and 2.9 in. (74 mm) in compression equal to 2.5 and 2.6% average strain, respectively.

Similar to the test of the WC250, visual inspection of the connection material after testing the WC200 suggested slip only occurred at connections that were designed assuming bolts in bearing. The brace-to-gusset connections that were designed slip-critical appeared to resist the load without slip as intended. Further, there was also no noticeable discontinuity between the brace translation and frame translation data, which also suggests slip did not occur at the brace-to-gusset connection where oversized holes were present.

Strain data for the WC200 test shown in Figures 23 through 28 display the two consecutive tests done with 2% drift first, followed by 3% drift. The second test at 3% drift begins at approximately scan 6000 (see Figure 22). The testing regimen reached an accumulated frame translation of 133.3 in. (3386 mm) during the 2% drift test and reached a total of 265.9 in. (6754 mm) by the end of the 3% test. The

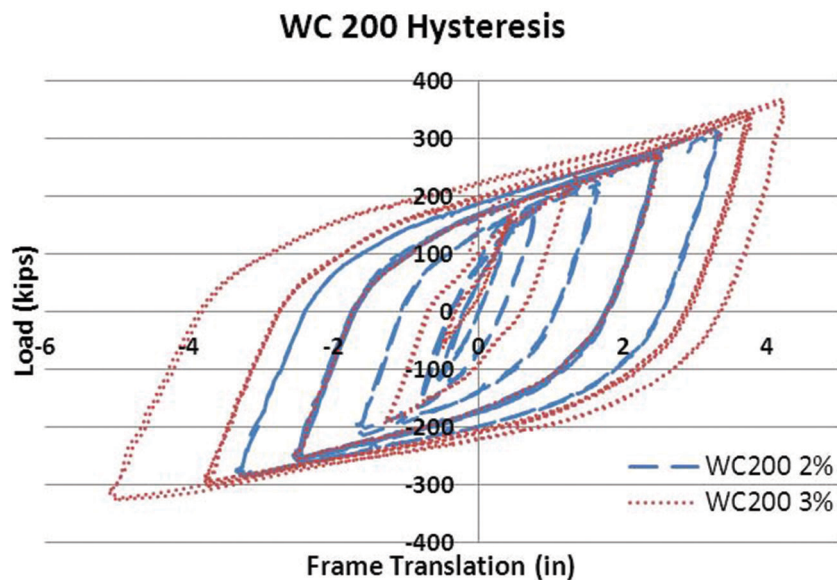


Fig. 21. Test 2, WC 200 load-translation.

cumulative inelastic axial brace deformation, as measured by the string pot on the exterior of the brace, was 64.1 in. (1628 mm) for the 2% drift test and 68.4 in. (1737 mm) for the 3% test. Thus, the total cumulative inelastic deformation was 132.5 in. (3366 mm), which corresponds to almost 800 times the calculated yield deformation or approximately four times the AISC minimum requirement.

SG7 at the top of the test frame was not measured in this test because of broken wiring. SG1 through SG5 showed

behavior similar to that in the WC250 test. SG6 was at a different location in the WC200 test and measured the stresses in the beam web perpendicular to the long axis of the beam. It was observed by strain at SG4 that once the connection angle yielded, it performed at approximately the same strains during the 2% drift test as when subjected to 3% drift. The “upward ratcheting” of SG4 is due to yielding. Note that the downward shift is consistent with the yield strain of strain-hardened steel.

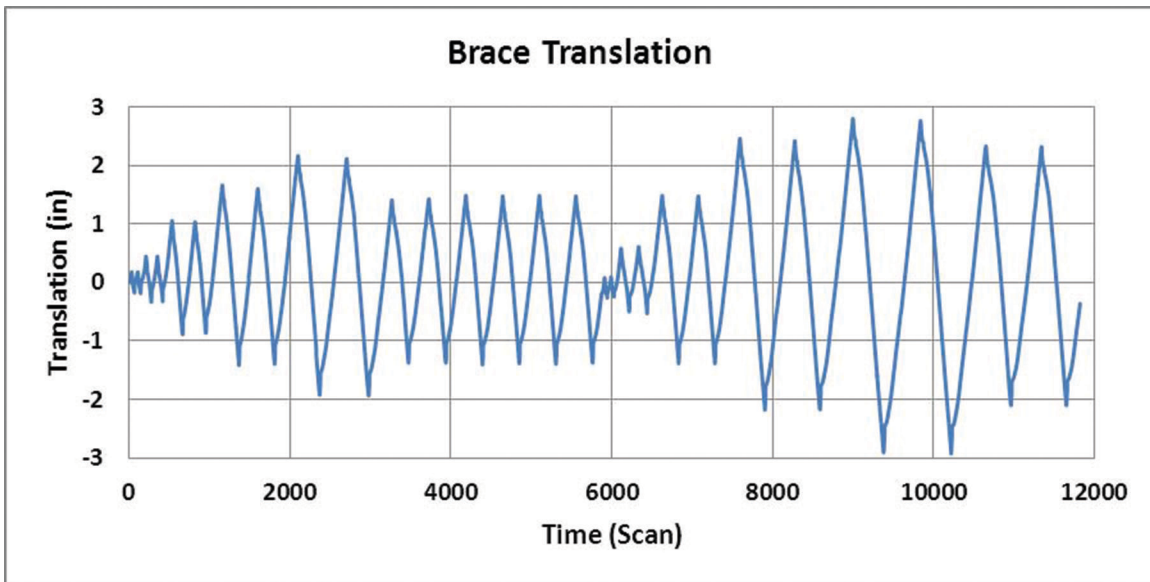


Fig. 22. WC200 brace translation.

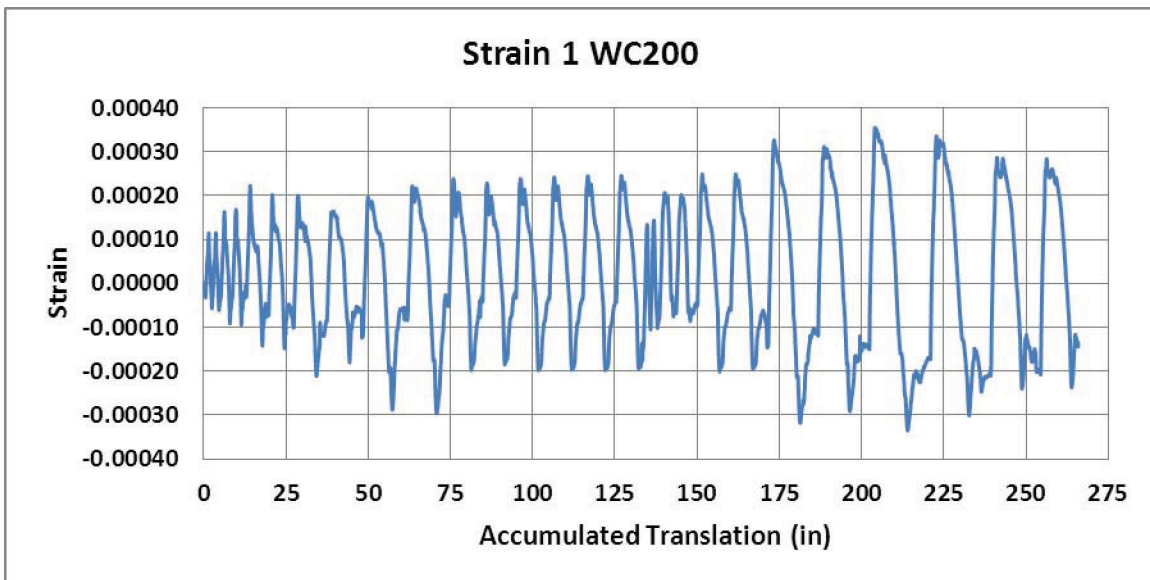


Fig. 23. Test 2, WC200 SG1.

SG5 and SG6 showed interesting behavior in the beam once they were subjected to the 3% drift cycles. It is observed that after an accumulated translation of 175 in. (4445 mm), SG5 shows the flange close to yield at a stress of 38.6 ksi (268 MPa); at the same time, SG6 shows that the web is yielding and reaching a strain of  $<6000 \mu$ . At this cycle, the brace was in tension; however, because of the frame rotation, the angle between the column and beam closes and tends to “pinch” the gusset. This results in compression in the beam

web. The web continued to exhibit some nonlinear behavior as it buckled slightly out of plane; thus, Figure 28 shows total strain (compression and bending) due to buckling.

Similar to the WC250, post-test visual inspection of the primary members and connection components at the upper connection indicated no noticeable damage. This again suggested that connecting one side of the gusset plate to a relatively flexible web of a primary member is desirable in consideration of a repairable system.

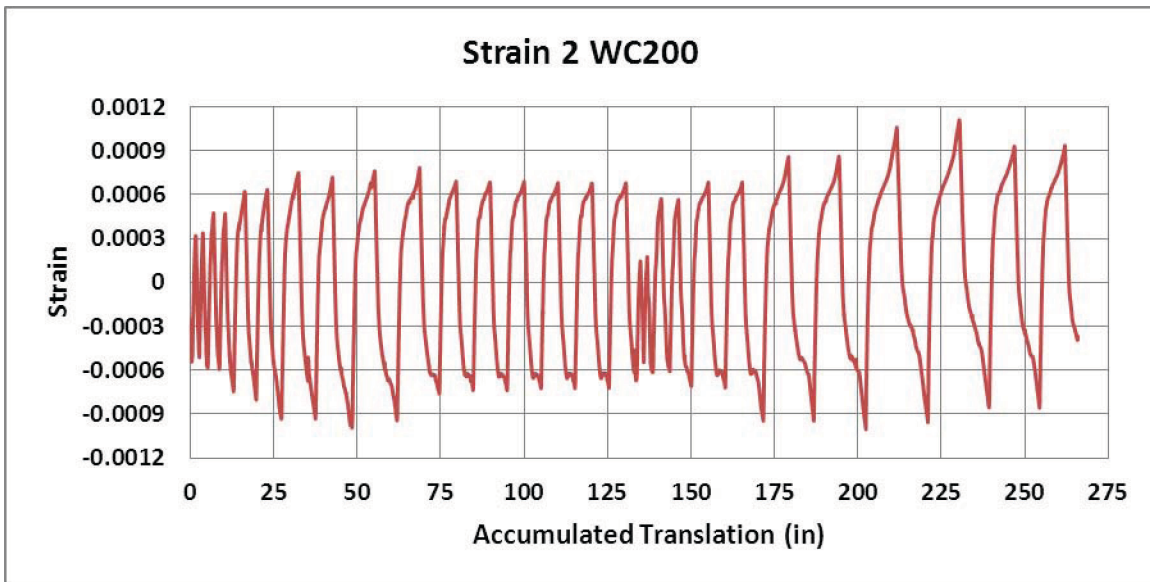


Fig. 24. Test 2, WC200 SG2.

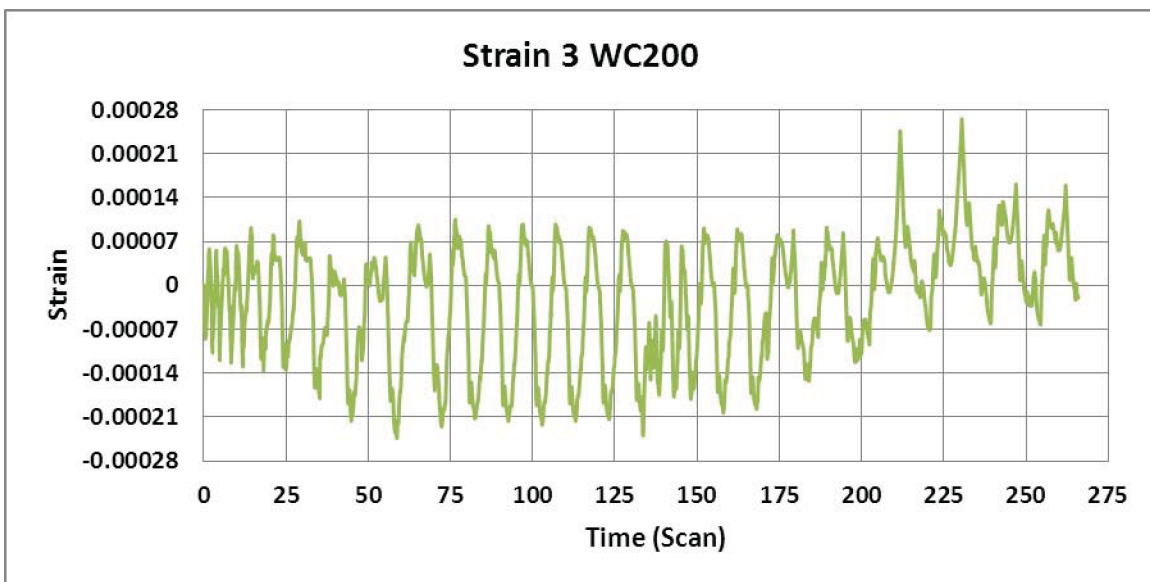


Fig. 25. Test 2, WC200 SG3.

## NUMERICAL MODELING

The objective of analytical numerical modeling is twofold:

1. Use the available BRB design parameters to verify the design of the test frame and reaction frame.
2. Compare the numerical model to the observed test results with no “tuning” of the numerical model or BRB backbone curves.

## Independent BRB Testing at University of Utah

With testing of the computer-simulated model, the linear and nonlinear behavior for the brace and test frame can be verified. Thus, methods for both linear and nonlinear frame analysis can be developed based on the test results. With this information, accomplishing the second objective provides valuable modeling parameters for use in designing and evaluating future frame and/or building models. Correct

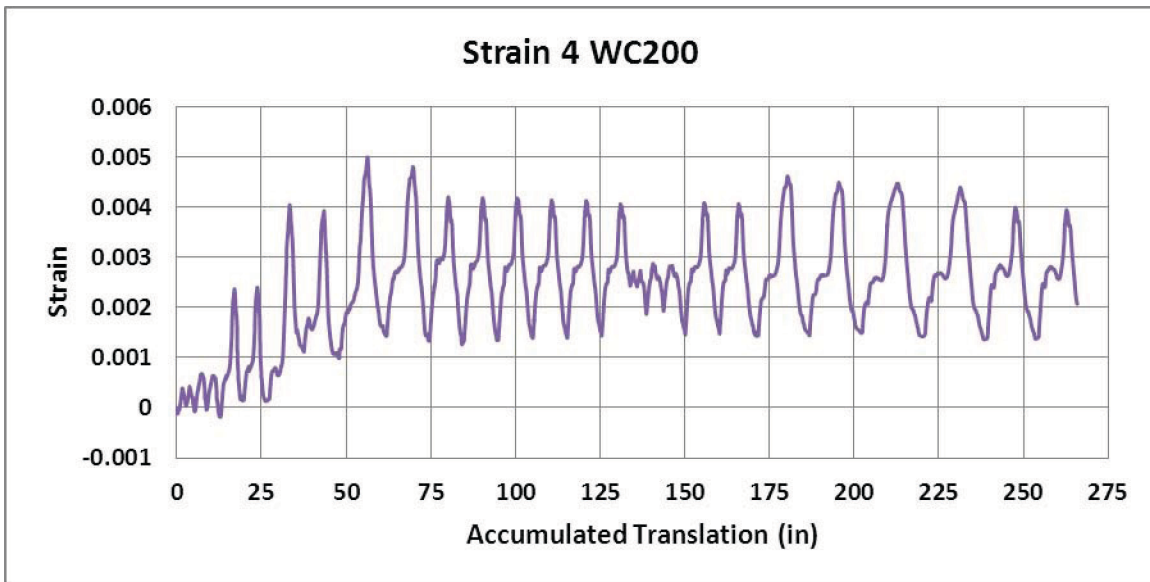


Fig. 26. Test 2, WC200 SG4.

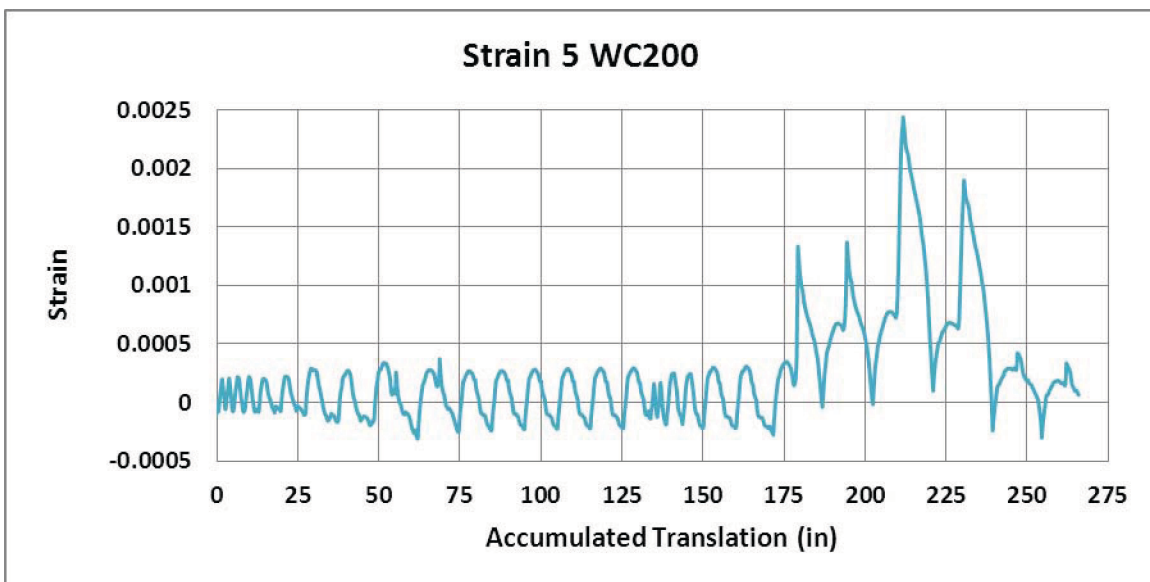


Fig. 27. Test 2, WC200 SG5.

stiffness, yield points, and BRB behavior can be determined for future use. Material and brace properties used are from previous research and testing performed outside of this project. Tensile strength for the brace cores were reported by MSI Testing and referenced by Star Seismic, which was also used in the numerical modeling [see McManus et al. (2011) for MSI results]. The tensile testing results are further discussed in the following section.

Research on the Star Seismic braces was referenced and reviewed prior to initial modeling of the braces and the test frame to verify the given Star Seismic parameters. Full-scale testing of the braces completed by Romero et al. (2007) provided regression equations to model the backbone

curves that were normalized by yield strength. The results from axial tests performed on seven BRBs were compiled into a single plot to develop the tension and compression strain versus hardening curves (see Figure 29). Figure 30 illustrates typical results for a BRB, in this case a WC250. Note that a WC250 was used in one of the present tests.

The linear regression equations from the resulting curves were established; see Equations 1 and 2:

$$\omega = 26.90\epsilon + 1.033 \tag{1}$$

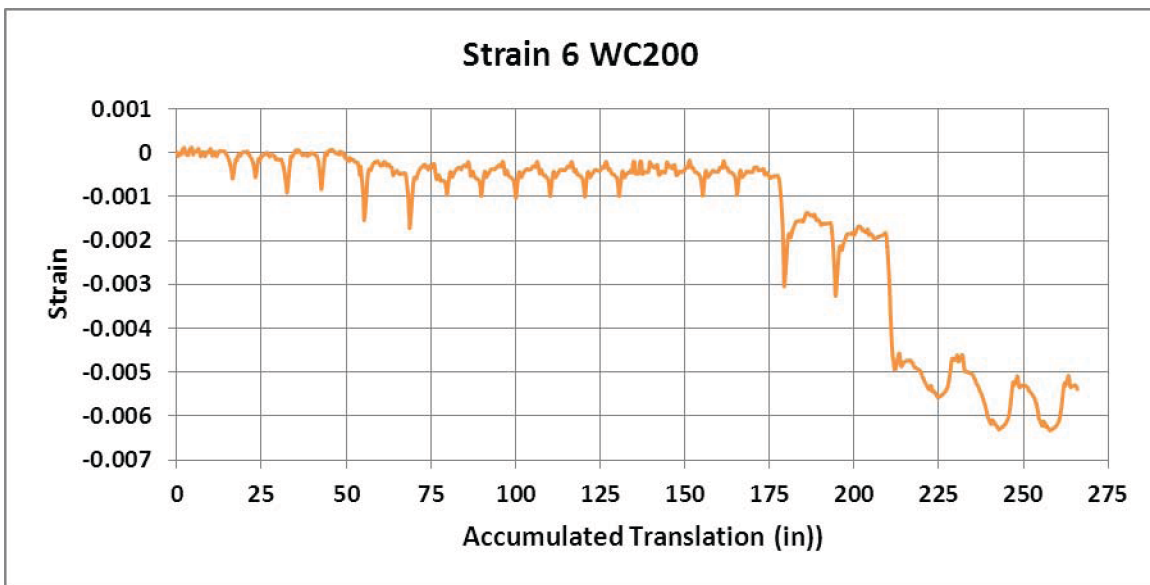


Fig. 28. Test 2, WC200 SG6.

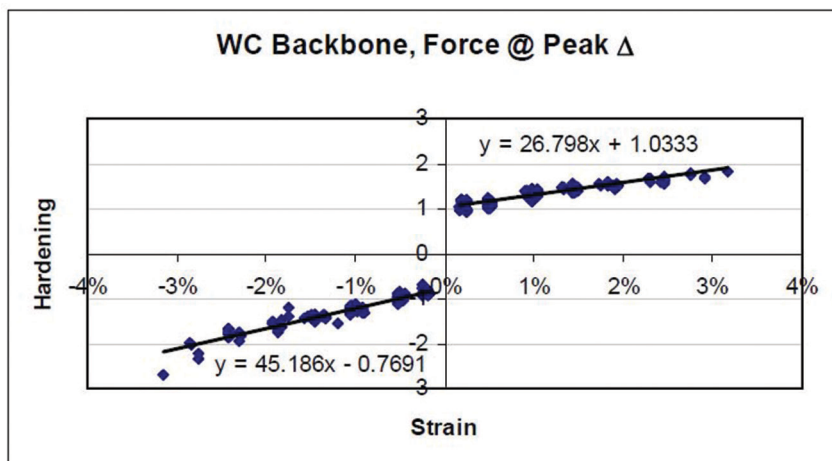


Fig. 29. WC backbone curve (Romero et al. 2007).

$$\omega\beta = 45.19\varepsilon - 0.77 \quad (2)$$

Equation 1 is the tension regression equation, and  $\omega$  is the tension hardening (the load at maximum deformation normalized to yield stress). Equation 2 is the compression regression equation, and  $\omega\beta$  is the compression hardening.

The dashed line illustrated in Figure 30 approximates the backbone with a bi-linear function. The normalized version of this function is provided in Equations 1 and 2.

Star Seismic provided the University of Utah (Romero et al., 2007) a table with the dimension of the steel core for the braces, which was used to check the accuracy of a spreadsheet developed for the research herein, see Table 1.

For the WC200 and WC250 braces provided in this project, the dimensions were calculated from the shop drawings for input into the developed spreadsheet. See McManus et al. (2011) for the shop drawing.

### Brace Modeling

In order to verify strength, results from tensile testing on the brace steel cores were provided by MSI Testing Inc. from Salt Lake City, Utah (test method ASTM 370). The report was referenced with the Nucor Mill Group of Jewett, Texas, report for the material properties of the core utilized in the Star Seismic braces. In the case of the steel used for the WC250, MSI Testing concluded that the average yield

strength was 43.1 ksi (297.2 MPa), which was greater than that stated by the mill test report of 39.2 ksi (270.3 MPa). Star Seismic noted that the average from the MSI Testing report was used in the design of the braces; thus, the same value was used in this project. The same was not observed of the WC200 with an average test value of 43.2 ksi (297.9 MPa) and a mill reported yield strength of 43.5 ksi (300 MPa). Star Seismic used an average of the MSI Testing and the mill report for the WC200 with a value of 43.3 ksi (298.5 MPa).

The brace was first modeled based on the geometric information provided by Star Seismic, and using the brace backbone model (Romero et al., 2007), developed from the University of Utah's full-scale testing of WC series buckling restrained braces.

A backbone curve was developed from the University of Utah test data, based on the load at maximum deformation normalized to the yield load for each test specimen. Regression equations were developed to model the force versus translation relationship, including the elastic and inelastic behavior.

The areas and dimensions of the BRB steel-core extension plate, transition zone, core plate, and yielding zone were assumed to be proportional to the University of Utah (UT) test specimens. An individual stiffness value for the different zones within the steel core was calculated based on area multiplied by the modulus of elasticity divided by the length. The effective stiffness was then calculated by assuming the individual sections would act as springs in series as

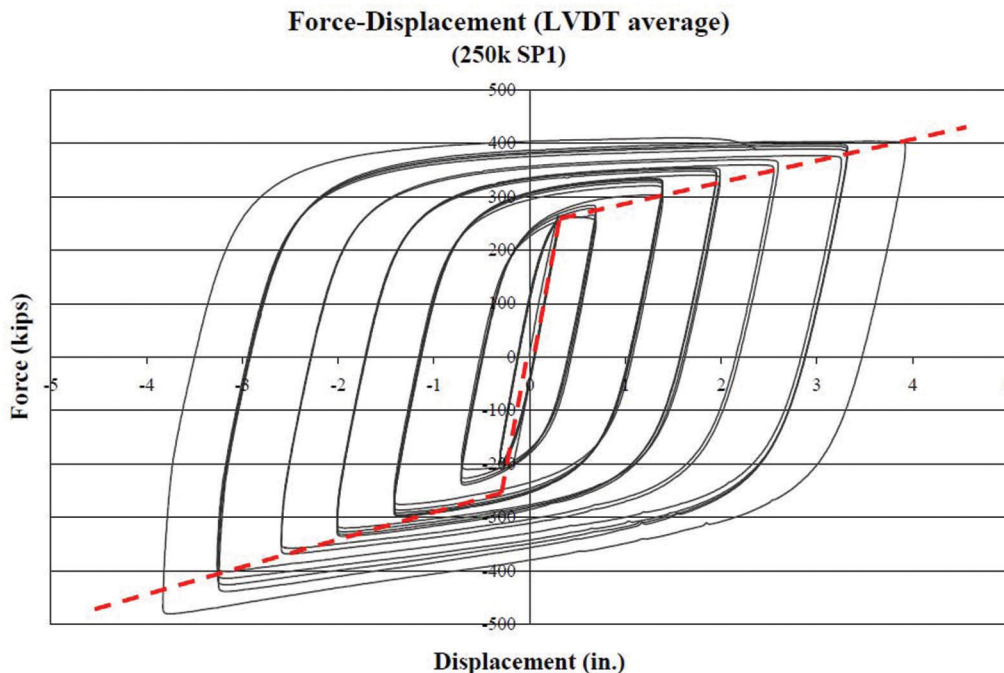


Fig. 30. Typical load translation test result (WC250) (Romero et al., 2007).

Table 1. Dimensions of Steel Core for the Braces (Romero et al., 2007)						
			Brace Designation			
			WC150	WC250	WC500	WC780
Specified Yield Strength, $F_y$ , ksi			41.4	39.9	39.9	39.9
Extension Plate (KP)		Thickness, $t_{KP}$ , in.	0.75	2	2	4
		Width, $b_{KP}$ , in.	9	9	9	18.5
		Length, $L_{KP}$ , in.	13	19	23	23
		Stiffness, $K_{KP}$ , kip/in.	15,058	27,474	22,696	93,304
Core Plate	Number of Plates		1	1	2	4
		Thickness, $t_p$ , in.	0.75	1	1	1
		Total Thickness, $t_T$ , in.	0.75	1	2	4
	Transition Zone (TZ)	Width, $b_{TZ}$ , in.	10	10	10	10
		Length, $L_{TZ}$ , in.	14	14	14	14
		Stiffness, $K_{TZ}$ , kip/in.	15,536	20,714	41,429	82,857
	Yielding Zone (YZ)	Width, $b_{YZ}$ , in.	4.90	5.75	5.75	4.88
		Length, $L_{YZ}$ , in.	152.7	134.7	134.7	132.6
		Stiffness, $K_{YZ}$ , kip/in.	698	1,238	2,476	4,269

illustrated in Figure 31. The springs represent the transition, core, and extension plates. The equivalent elastic stiffness is computed from:

$$K_{equivalent} = \left[ \frac{1}{k_1} + \frac{1}{k_2} + \frac{1}{k_3} \right]^{-1}$$

Given the shop drawings and information, the effective stiffness for the WC200 and WC250 was determined using the assumptions previously stated. The calculated effective stiffness values were used in SAP2000 v12, hereafter referred to as SAP2000, with multilinear links to model the response of each BRB. A multilinear link and a Wen model were created to ensure that the multilinear response was accurate when compared with the UT data for validation (SAP2000 v12).

Again, the inelastic behavior was modeled using the UT backbone curves. Figures 32 and 33 illustrate the SAP2000 models of a single BRB using the multilinear plastic model, the Wen model and data from one of the University of Utah WC250 tests.

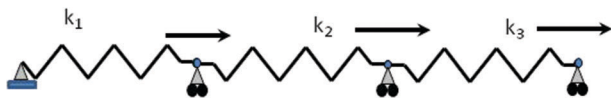


Fig. 31. Springs in series.

By comparison, the SAP2000 modeling of single BRBs is more of a coarse approximation of the actual behavior as demonstrated by the University of Utah testing results. Also, it is shown that the numerical model does not develop any asymmetrical pattern as does the actual brace when loading compression versus tension. Additionally, the SAP2000 model is based upon a kinematic strain-hardening model, while the exhibited behavior is more isotropic. Although the backbone curve is modeled reasonably well, the total energy absorbed within the model is not as large as the exhibited behavior because part of the hysteric area is missing. The model would be adequate in developing a push-over curve, but would perhaps be overly conservative in modeling a time-history event.

### Full-Frame Modeling

Due to the complexity of modeling the entire testing apparatus in SAP2000, the frame was modeled in multiple steps. First, the geometry of the frame was modeled with undefined shapes and stiffness to determine which frame members would be necessary for the full analytical model (see Figure 34). Based on a nominal 100-kip (445-kN) load applied to the top of the frame, each member was analyzed for axial and shear forces to determine its influence on the system during testing. Initial modeling of the angles bracing the test specimen from movement out-of-plane of the load direction were removed due to an undesirable transfer of shear forces to the test frame in the SAP2000 model. These angles were connected with single-bolt pinned ends in the actual test assemblage and did not resist any shear forces as they

slipped and rotated under frame translations. Constraints were imposed on the nodes where the angles connected to the test specimen as a more effective means of modeling the system. When modeling the large rigid plate connecting the test reaction frames to the test frame, it was determined that deformations in the plate were small enough that the connection could be assumed rigid, the expected result.

More load-tracking review was done in SAP2000. By observation, and as expected, it was determined that the

majority of the deformation was occurring in the test specimen due to the much greater stiffness of the reaction frames (see Figure 35).

The next step was to model the test frame alone with constraints on the nodes that would normally be attached to the reaction frame. A few assumptions were made to simplify the model. Connections were assumed to be either rigid or fully pinned because the actual stiffness of the connections was not fully known. The previously developed links were

**Single BRB Link Model in SAP 2000**

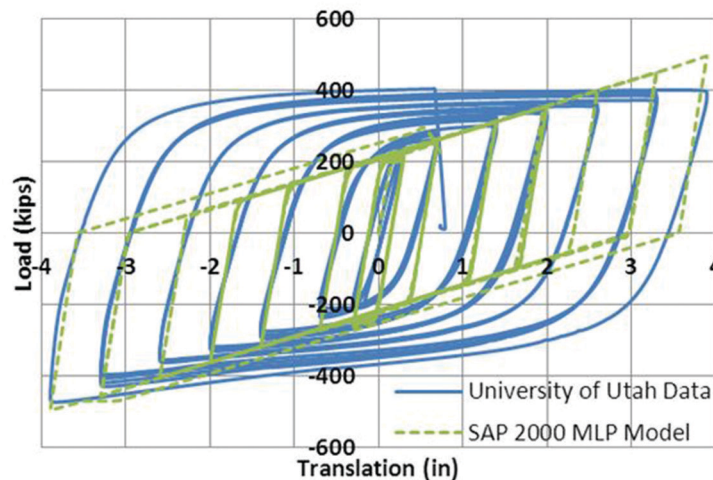


Fig. 32. Single BRB link multilinear plastic model vs. University of Utah test data.

**Single BRB Link Model in SAP 2000**

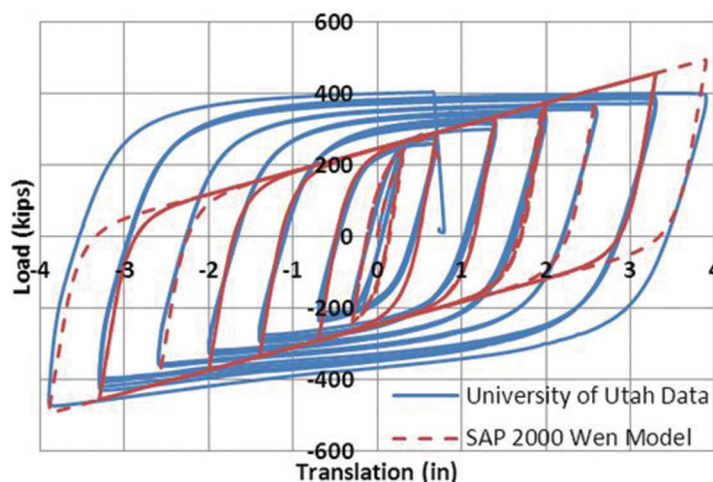


Fig. 33. Single BRB link Wen model vs. University of Utah test data.

imported into the test specimen model and placed appropriately (see Figure 36). With the 100-kip (445-kN) load applied to the test specimen, it was determined that the link was working properly when compared with hand computations.

### COMPARISON OF NUMERICAL MODELING AND EXPERIMENTAL RESULTS

By using the link developed in SAP2000, it was possible to run the same time-history test on the analytical model

as was done on the physical test frame. The target translations for the experimental testing were input into SAP2000, and a displacement controlled loading cycle was run. The results from the multilinear model of the brace were then plotted against the experimental data for comparison (see Figures 37 and 38). In order to produce a more accurate comparison, the output from the SAP2000 model was link force, column shear and axial force in the top beam, which is equivalent to the pressure gauges in the actuator measuring

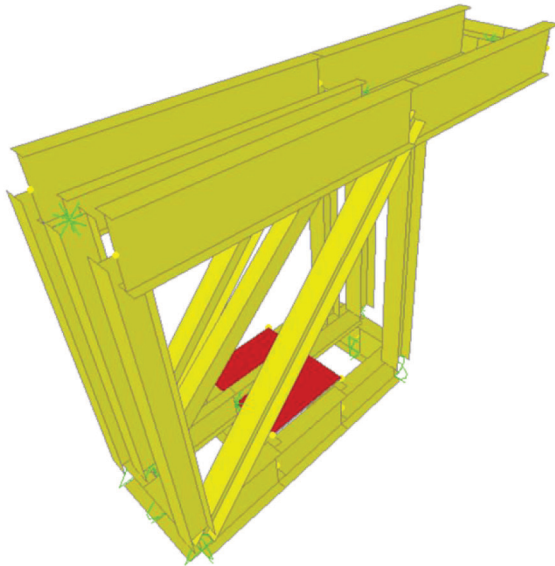


Fig. 34. Initial full frame model in SAP2000.

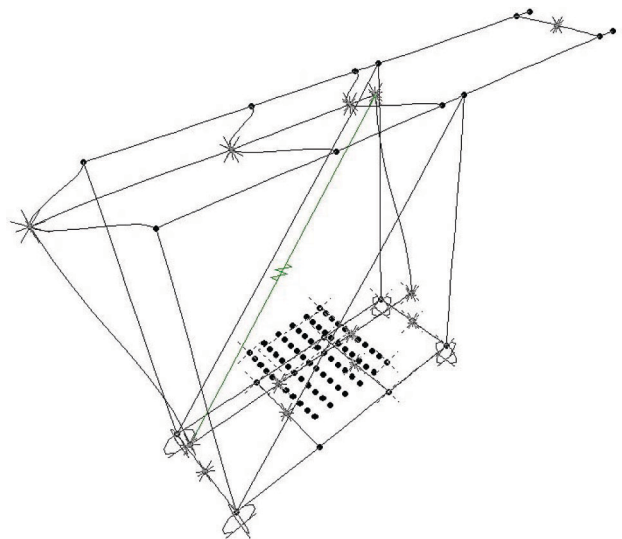


Fig. 35. Full-frame deformed shape with 100-kip load (SAP2000).

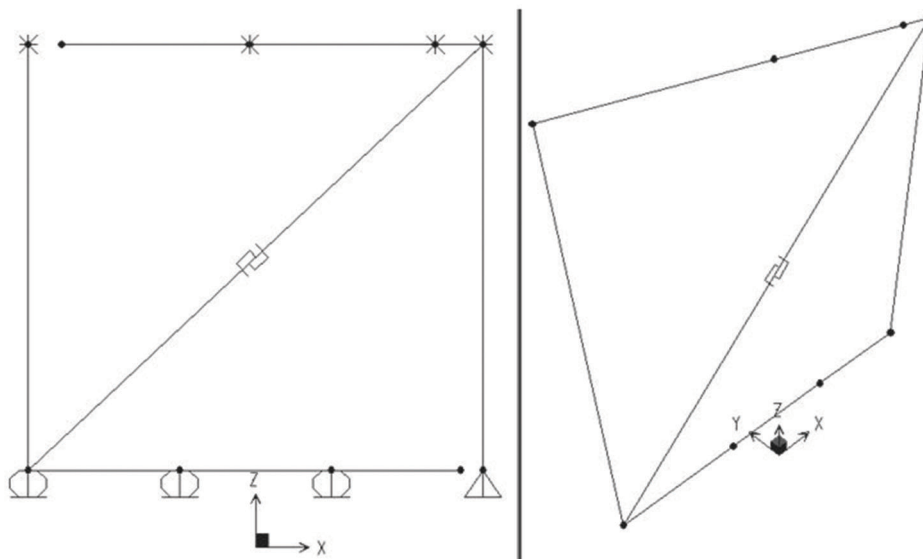


Fig. 36. Simplified analytical model (SAP2000).

forces on all these elements during the test. Notably, the multilinear model behaved similarly to the experimental model. The WC200 model did predict a slightly higher peak load at maximum positive translation, but at the maximum negative translation, the model and experimental data are almost identical. The WC250 model is much more in line with the experimental data and is even slightly conservative at maximum negative translation, having a peak load slightly lower than the experimental data.

Utilizing Wen modeling of the two braces produced a more accurate hysteresis of the frame behavior than the multilinear plastic models. The hysteretic loops match more closely with the test data, as shown in Figures 39 and 40, and had a slightly higher value at the maximum displacement, similar to the multilinear plastic model. These similarities suggest that the backbone curve developed from the University of Utah test gives proper values for modeling.

### WC200 Testing and Modeling Results

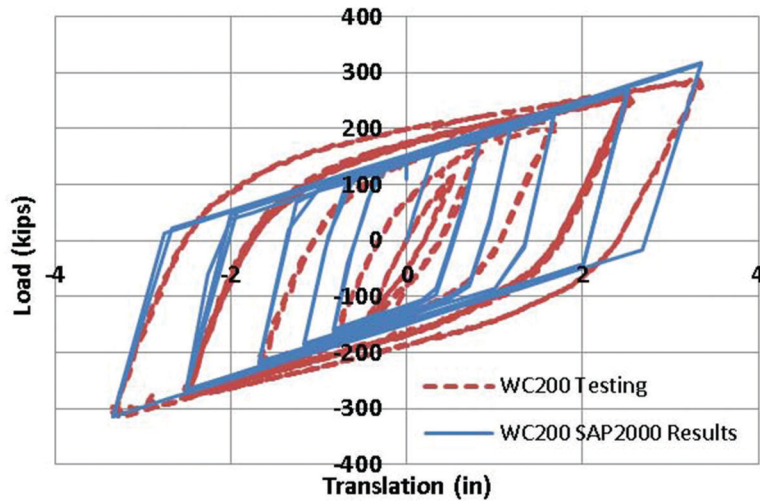


Fig. 37. WC200 testing and multilinear plastic modeling results.

### WC250 Testing and Model Results

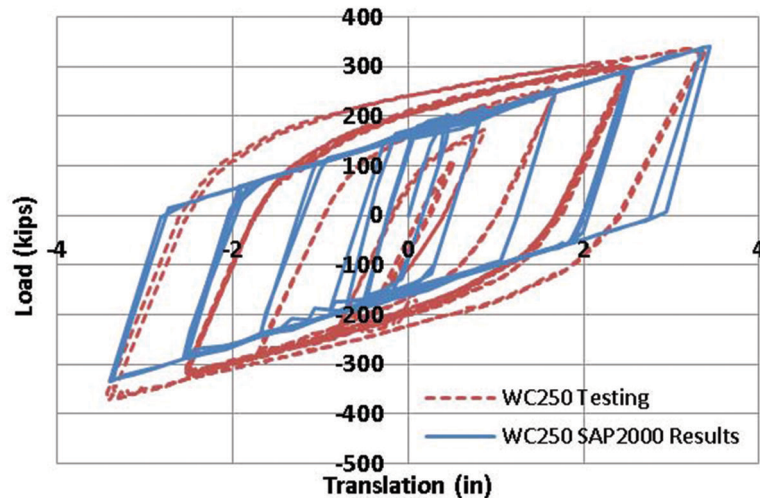


Fig. 38. WC250 testing and multilinear plastic modeling results.

It should be noted that both the multilinear and the Wen models are fully symmetrical in their response to loads in tension and compression. This explains the minor offset when comparing the testing results to the SAP2000 modeling because the BRB does perform somewhat different in tension versus compression.

### DESIGN RECOMMENDATIONS

The research herein has shown that with proper compression strength and strain-hardening adjustment factors for the buckling restrained brace, the connection design provisions of the AISC *Specification* and AISC *Seismic Provisions* result in desirable braced frame behavior using fully

#### WC200 Testing and Modeling Results

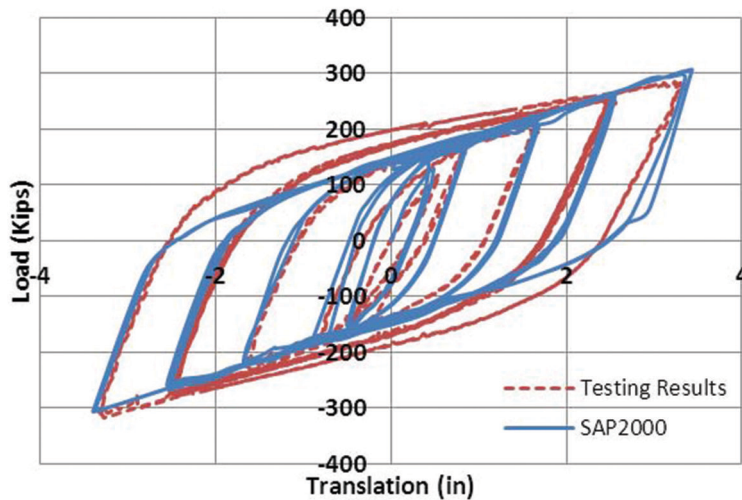


Fig. 39. WC200 testing and Wen modeling results.

#### WC250 Testing and Modeling Results

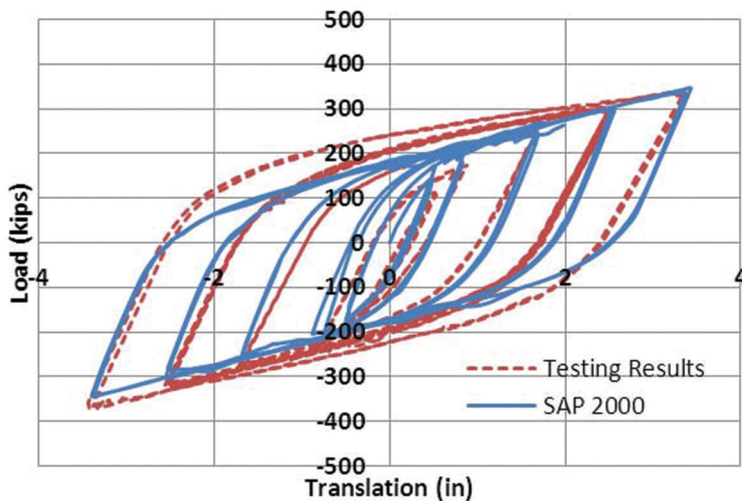


Fig. 40. WC250 testing and Wen modeling results.

bolted connections. In addition to the provisions of these documents, the following general recommendations are made to facilitate constructability and maximize connection strength. Furthermore, the following serviceability recommendations are made to promote an easily repairable system in which inelastic damage to the primary beams and columns are minimized.

### General Recommendations

1. Bearing bolts in standard holes or slip-critical bolts with oversized holes in one ply of connecting interfaces may be used to connect the ends of buckling restrained braces to gusset plates.
2. Bearing bolts in standard holes should be used to connect gusset plates to double-angle connection assemblies and double-angle connection assemblies to primary beams and columns.
3. Bolt rows in the connection-angle assemblies may be aligned or staggered. Staggered assemblies are recommended to allow for reduced bolt gauges on the flanges of the primary members.

### Repairable Recommendations

1. Beam and column flange thickness should exceed connection-angle thickness to limit bolt-bearing deformations in the primary members.
2. To reduce the possibility of inducing yield in the beam or column flange, the bending capacity of the primary member flange—including the effects of prying action—should exceed that of the outstanding legs of the connection angles. Primary members should be oriented such that at least one side of the gusset plate is connected to the web of either the beam or the column.

Orienting primary members such that the gusset plate is connected to the flange of both the beam and the column results in “pinching” forces between the gusset plate and primary members, which can result in local damage to the primary members. These forces are alleviated by connecting one side of the gusset plate to the web of a primary member because of the relative out-of-plane flexibility of the member web.

### CONCLUSIONS

The following conclusions are drawn from the experimental testing and numerical modeling of both the full frame and the individual braces.

1. In reference to AISC *Seismic Provisions* acceptance criteria, testing of the full-scale, fully bolted buckling

restrained braced frame met all strength requirements and exceeded the required testing regimen of 2% drift associated with an assumed 1% design story drift.

2. Provisions of the AISC *Specification* and AISC *Seismic Provisions* are appropriate for fully bolted BRBF connections. The use of the uniform force method and the uniform force method—special case 2, “minimizing Shear in the Beam-to-Column Connection,” was shown to be appropriate for connection force distribution.
3. The frame design exhibits the ability to withstand multiple seismic events without fracture, brace or primary framing member instability or without brace-end connection failure.
4. The ability to easily replace the braces and connection components was demonstrated. Thus, the repairable advantage of the all-bolted connections was revealed.
5. Orienting columns such that the gusset plate is connected to the column web allows for rotation of the gusset connection under large drifts without noticeable damage to the primary beams and columns.
6. Orienting columns such that the gusset plate is connected to the column flange results in connection restraint against frame rotations that can cause damage to unstiffened primary beams and columns.
7. The methods used to develop a numerical model of the buckling restrained braces in SAP2000 were effective and could be easily adapted to different brace sizes for various systems. Utilization of the link properties in a full-frame model accurately predicted behavior of the system. Multilinear approximation was adequate to model the behavior of the BRB in the frame, but the Wen model provides a more accurate prediction including the nonlinear transition near yield.

### ACKNOWLEDGMENTS

The authors would like to recognize Puma Steel, AISC, Nucor Fastener and the University of Wyoming for funding, fabrication and material donations, without which this project would not have been possible.

### REFERENCES

- AISC (2005a), *Seismic Provisions for Structural Steel Buildings*, American Institute of Steel Construction, Chicago, IL.
- AISC (2005b), *Specification for Structural Steel Buildings*, American Institute of Steel Construction, Chicago, IL.

- AISC (2005c), *Steel Construction Manual*, 13th ed., American Institute of Steel Construction, Chicago, IL.
- ASCE (2007), "Seismic Rehabilitation of Existing Buildings," ASCE Standard ASCE/SEI 41-06, American Society of Civil Engineers, Reston, VA.
- FEMA (2003), "Recommended Provisions for Seismic Regulations for New Buildings and Other Structures," FEMA-450, Part 2: Commentary, Federal Emergency Management Association, Washington, DC.
- FEMA (2008), "HAZUS<sup>®</sup> MH Estimated Annualized Earthquake Losses for the United States," FEMA-366, Federal Emergency Management Association, Washington, DC.
- IBC (2006), *2006 International Building Code*, International Code Council.
- IBC (2009), *2009 International Building Code*, International Code Council.
- Lopez, W.A., Gwie, D. S., Lauck, T.W. and Saunders, C.M. (2004), "Structural Design and Experimental Verification of a Buckling-Restrained Braced Frame System," *Engineering Journal*, AISC, Fourth Quarter, pp. 177–186.
- McManus, P.M. and Puckett, J.A. (2011), "Repairable Seismic Moment Frames with Bolted WT Connections: Part I," *Engineering Journal*, AISC, Fourth Quarter, pp. 265–281.
- McManus, P.M., Puckett, J.A. and MacMahon, A. (2011), "Economic and Serviceable Seismic Systems, Phase II—All-Bolted Buckling Restrained Braced Frames," AISC Report, Department of Civil and Architectural Engineering, University of Wyoming, Laramie, WY.
- Romero, P., Reaveley, L., Miller, P.J. and Okahashi, T. (2007), "Full Scale Testing of WC Series Buckling-Restrained Braces," Department of Civil and Environmental Engineering, University of Utah, Salt Lake City, UT.
- Thornton, W.A. and Muir, L.S. (2009), "Design of Vertical Bracing Connections for High-Seismic Drift," *Modern Steel Construction*, AISC, March, pp. 61–64.

# Uncertainty in Life-Cycle Assessment Induced by Life-Cycle Inventory Data: The Case of Structural Steel

IORDANIS ZYGOMALAS and CHARALAMBOS BANIOPOULOS

---

## ABSTRACT

Life-cycle assessment (LCA) is currently widely used to quantify environmental impacts and thus support decision making within business sectors such as steel construction, which utilizes vast amounts of materials to deliver large-scale projects globally. Because the validity of LCA results greatly depends on the quality and appropriateness of the life cycle inventory (LCI) data referring to the environmental inputs and outputs associated with the examined subject, it is necessary to estimate the degree of uncertainty embedded in these data, which will inevitably be incorporated into the final LCA results. The purpose of this research is to examine the extent and the characteristics of uncertainty due to LCI data, based on findings for the case of commonly used structural steel components. Impact assessment results are calculated according to four relevant LCI databases and two assessment methods. The results are compared based on a detailed analysis of the impact caused for the production of the steel members. Major conclusions include the observation that data quality characteristics do not ensure the accuracy of the final LCA results because datasets referring to the same steel member type were found to lead to noticeable divergence. An overall lack of uniformity was observed within each of the mainly burdened impact indicators, while the influence of system boundaries was also examined. Issues concerning the collection of primary LCI data were raised, and it was also shown that different impact assessment methods provide different perspectives, which result in a more complete and factual approach.

**Keywords:** life-cycle assessment (LCA), life-cycle inventory (LCI), uncertainty, structural steel, steel structures.

---

## INTRODUCTION

Life-cycle assessment (LCA) has been introduced as a methodology to quantify the environmental impact associated with any given product. Based on the concept of the life cycle, it takes a very wide range of environmental information into account and has understandably come to be regarded as one of the most detailed and complete environmental impact assessment methods available.

However, during the course of its increasing application within almost every business sector, a few issues concerning its efficiency have arisen, perhaps the most critical of which being uncertainty—both the uncertainty embedded in the final results and, subsequently, the validity of the environmental impact calculated.

Because the application of LCA depends on the life-cycle inventory (LCI) data used to model a product's life cycle, the final result is directly affected by the quality and accuracy

of this environmental information. It is, however, acknowledged that obtaining and maintaining LCI datasets require a huge and constant effort (Simoes da Silva et al., 2007); it is, therefore, impossible to develop new data for each LCA conducted. The degree of influence of environmental data to the final results has become a subject of argument and, in some cases, has given reason to question the outcome of LCA. However, each sector—and even each LCA study carried out—is characterized by particular conditions and properties; as a result, in order to investigate uncertainty due to LCI data, it is necessary to examine its characteristics within a given scope.

One of the business sectors that not only utilizes vast amounts of materials and energy, but is also involved in adopting a strategy to incorporate sustainability into its product's design, is steel construction (Bragança, Mateus and Koukkari, 2007). The design and construction of steel projects such as high-rise buildings or heavy-traffic bridges require the application of sustainable development principles, and as a result, industry decision makers are increasingly using relevant decision-support tools such as LCA. It is within this particular sector that the current research analyzes uncertainty due to LCI data. Because structural steel members are associated with the greatest percentage of environmental impact caused by the construction of steel projects (Zygomalas, Efthymiou and Baniotopoulos, 2009), they are chosen as the reference point for this analysis. Prior to the description of the methodology and results of the

---

Iordanis Zygomalas, Dr.-Eng. Civil Engineer, Institute of Metal Structures, Department of Civil Engineering, Aristotle University of Thessaloniki, Thessaloniki, Greece (corresponding). E-mail: izygomal@civil.auth.gr

Charalambos Baniotopoulos, Dr.-Ing., Professor and Chair of Sustainable Energy Systems, School of Civil Engineering, University of Birmingham, Birmingham, UK. E-mail: ccb@civil.auth.gr

---

current research a brief presentation of the LCA methodology is given.

As a result of the global movement for sustainable development, sustainability has become the main agenda for the majority of practices in construction (Zygomalas et al., 2009). In order to incorporate the basic principles of sustainability into design and construction, it is first necessary to quantify all aspects of construction as far as their effects on the environment are concerned. By calculating the environmental impact caused by each construction process, the most environmentally damaging processes are identified, and it is then possible to work toward lowering this impact and, ultimately, optimizing the environmental performance of a project for the duration of its life and beyond its completion.

In order to document each and every construction process required for the delivery of a project, the concept of the life cycle has been introduced. For construction projects, the four main life cycle stages that can be identified are (1) raw material acquisition, (2) construction, (3) use/operation/maintenance and (4) end scenario/waste management (see Figure 1).

The calculation of the environmental impact across the whole life cycle of a project constitutes a new scientific field with new methods and new goals (Zygomalas et al., 2009). The methodology that has been developed for this purpose is life-cycle assessment (LCA). The application of LCA is to be conducted according to the relevant ISO (International Organization for Standardization) standards [ISO 14040 and ISO 14044 (ISO 2006a, 2006b, respectively)] and consists of four phases, as shown in Figure 2.

The first phase requires the definition of a series of theoretical parameters (such as the goal of the LCA, its scope, and so on), while at the second stage, environmental data (or LCI data) are documented for each process or material of the project's life cycle. These data are translated into environmental impact values at the third stage; finally, the results

obtained are interpreted at the fourth and final stage of the LCA.

## METHODOLOGY AND CALCULATION

### Overview

In order to examine uncertainty due to LCI data, a reference product is chosen for the analysis along with an appropriate functional unit referring to a specific quantity of the chosen product. After a thorough literature review, a number of LCI databases available containing relevant environmental data are identified, and the environmental impact for the defined product and quantity are calculated according to each LCI database. The impact assessment methods used are Eco-Indicator 99, IPCC Global Warming Potential (GWP) and TRACI. These methodologies are not only widely used on a global level, but also because they were developed for differing geographic regions. Eco-Indicator was developed mainly for Europe, GWP for global use and TRACI for the United States. The results obtained are compared in order to reach useful conclusions regarding uncertainty caused by LCI data, not only within the steel construction sector, but also as more general observations regarding LCA application.

### Reference Product and Functional Unit

The most commonly used structural steel members are hot-rolled sections such as wide-flange beams (European equivalent: IPE and HEA) and cold-formed hollow sections such as SHS (square hollow sections) and RHS (rectangular hollow sections). For the purpose of the current study, the production of hot-rolled structural steel sections is chosen from raw material acquisition to storage at the factory before shipment for use (cradle-to-gate). As far as the manufacturing process for these structural members is concerned, there are two main routes: the blast oxygen furnace (BOF) route, which produces primary steel utilizing raw materials, and the electric arc furnace (EAF) route, which produces steel of

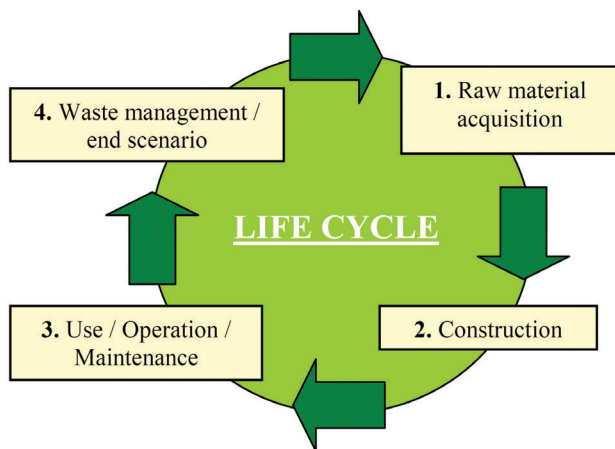


Fig. 1. The life cycle of a construction project.

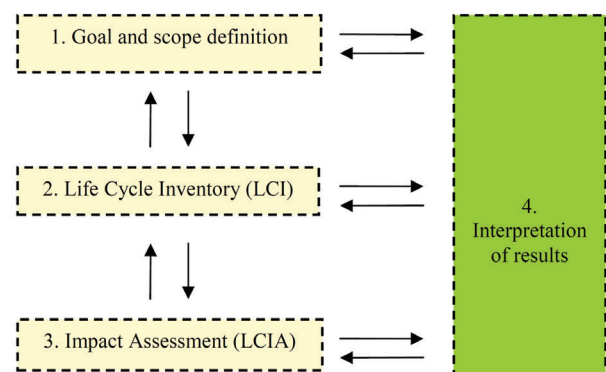


Fig. 2. Phases of life-cycle assessment (LCA).

equal properties by recycling iron and steel scrap. Although the blast furnace route is still being widely used globally (Worldsteel, 2009), it is the EAF that presents significant sustainable potential and is therefore regarded as more appropriate for the current analysis. It should be noted that the steelmaking route can differ significantly globally, with some European countries mainly utilizing the BOF route, while other countries such as the United States utilize only the EAF for the manufacturing of hot-rolled steel sections. The functional unit was subsequently defined as 2.2 lb (or 1 kg) of hot-rolled structural steel members manufactured via the EAF route.

### Selection of Available LCI Databases

The next step is to examine existing literature and determine the LCI databases available that contain verified data concerning hot-rolled structural steel members. As a result, the following LCI databases were selected.

#### *AUTH*

In 2009, the Institute of Metal Structures of the Aristotle University of Thessaloniki in Greece conducted a study to quantify environmental inputs and outputs concerning commonly used structural steel members, such as hot-rolled and cold-formed sections (Zygomalas et al., 2012). A number of detailed datasets are included in the database, based on the information provided by the leading steel member manufacturing company in Greece and completed, where necessary, by literature research.

The dataset for hot-rolled structural steel sections refers to the production of 2.2 lb (1 kg) of finished products via the EAF steelmaking route and their storage at the factory before shipment for use (cradle-to-gate). The main production stages documented and included in the development of this dataset are presented in Figure 3. Each production process was documented as described in the ISO 14040 and 14044 standards (ISO 2006a, 2006b), according to environmental inputs and outputs.

#### *Ecoinvent*

The Ecoinvent LCI database was initially developed in the late 1990s and contains more than 4000 datasets referring to products, services and processes; it was developed in Switzerland by the Swiss Centre for Life Cycle Inventories, which is also responsible for data updates (Classen et al., 2009). It refers to a mix of European technology, and the collection method used was a sampling procedure based on literature. A number of research centers in Switzerland and Germany were involved with the development and constant update of the database, while the data are intended for use mainly within the European region (IPPC, 2001).

The Ecoinvent database includes a dataset referring to the

manufacturing of steel with the EAF route, based on data from the year 2000 and according to the relevant ISO standards concerning LCA and LCI. The dataset also includes the transports of scrap metal and other input materials to the EAF and casting. Because this dataset refers to the manufacturing of steel up to the casting stage, it is necessary to add the rest of the processes required for the production of the hot-rolled structural steel members. These processes are the reheat furnace operation, the hot-rolling process and the transport of the finished products to storage rooms before they are sent out for use. The hot-rolling and transport processes are included in the Ecoinvent database and were therefore used in this case, while the reheat furnace process was used as found in the AUTH database.

#### *Canadian Raw Materials Database (CRMD)*

The CRMD was developed in collaboration with the Canadian business sector and government and aimed at providing life-cycle inventory data concerning several different products. Among these products are steel billets manufactured with the EAF route, as used for hot-rolling to produce the structural steel sections commonly used in steel construction projects. The functional unit used was 2.2 lb (1 kg) of finished product, and the data were provided by steel

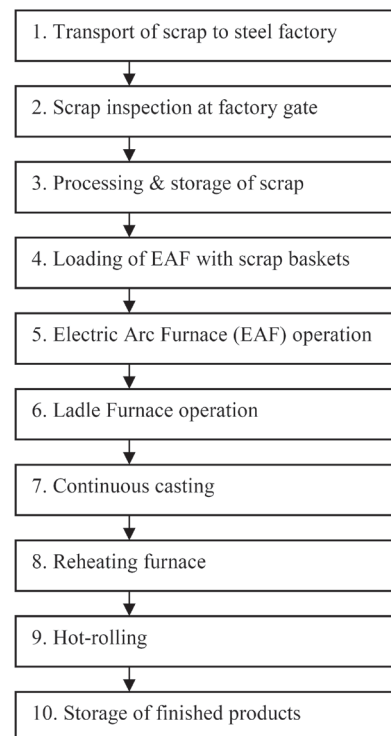


Fig. 3. Main processes for the production of 2.2 lb (1 kg) of hot-rolled structural steel members (EAF) taken into account for the development of the AUTH LCI database.

factories in Europe and North America because no steel sections are currently being manufactured in Canada. The primary data refer to the years 1994–1995, while secondary data were used as found in literature through 1990. These dates do present an issue concerning the current validity of the dataset; however, there is no recent update available.

In order for the data to be used in the current study, the data were completed with the remaining necessary processes for the production of the structural steel members, namely, the reheat furnace operation, hot-rolling and transport to storage rooms. These processes were used as found in the AUTH database.

### **Worldsteel**

The World Steel Association (Worldsteel, previously IISI) conducted an LCI study at a global scale, aiming at the quantification of raw materials, energy and environmental emissions associated with the production of the main finished products of the steel industry, including structural steel sections. A significant number of steel factories from different countries have provided the data, which cover all production stages from raw material acquisition to delivery of the finished products at the factory gate before sent for use (cradle-to-gate). The study was initially conducted in 1994–1995, and it was updated in 1999–2000 and then again in 2010. The data for the current analysis are used as published in the February 2010 update.

The Worldsteel datasets provide cradle-to-gate (from raw material extraction to the steel factory gate) data on all the major raw materials, energy usage, air and water emissions, and wastes for the steel products included in the study. Forty-three major data categories (flows) are included in the available datasets out of the 450 that were quantified. Environmental inputs and outputs were calculated for the production of 2.2 lb (1 kg) of steel products at the factory gate according to ISO 14040 standard (Worldsteel, 2005). In the case of structural steel sections, the data were provided by a number of steel factories from all over the world (with, however, very limited coverage of U.S. steel mills), some using the EAF steelmaking route, while others the blast furnace route. The data are, therefore, calculated as an average of both steelmaking routes.

It should also be noted that the data include an environmental credit corresponding to an 80% recycling rate, while in the United States, the current corresponding rate is about 98%. The rest of the selected databases do not incorporate any waste scenarios; therefore, their impact assessment results are expected to appear relatively increased. Because of the fundamental differences in system boundaries—namely, the inclusion of the blast furnace steelmaking route and the recycling scenario—it is not possible to directly compare the results based on this dataset to the ones calculated according to data from the other selected databases.

However, the dataset is included in the current research as a way to determine the influence of system boundary differentiation within LCI data on the results obtained.

## **RESULTS AND DISCUSSION**

### **Eco-Indicator Impact Assessment**

The Eco-Indicator 99 impact assessment method provides a detailed and complete presentation of the environmental impact associated with the system under examination and is, therefore, used within the scope of the current analysis. It is a damage-oriented approach, which is based on weighting results and calculating environmental impact according to a set of indicators. The methodology is mainly intended for LCA referring to the European region, and the unit used is the Eco-Indicator point (Pt), which was chosen in such a way that the value of 1 Pt is representative of one-thousandth of the annual environmental load of one average European inhabitant (The Netherlands Ministry of Housing, Spatial Planning and the Environment, 2000).

The impact assessment results for the production of 2.2 lb (1 kg) of hot-rolled structural steel members via the EAF steelmaking route are calculated according to the Eco-Indicator methodology (V2.06/Europe EI 99 E/E), for each of the four selected LCI databases, and are presented in Figure 4.

The first observation from the results is that the total environmental impact values are very close according to three of the four databases, ranging from 76.5 to 86.8 mPt (millipoint = 1/1000 Pt). As expected, the Worldsteel data lead to a relatively decreased value, which can be justified due to the inclusion of the 80% recycling rate. This differentiation, in combination with the fact that these data refer to both steelmaking routes and not only the EAF, does not allow for the direct comparison of the results from the four databases. However, it is clear that the degree of final result divergence (which can be obtained due to differences in data boundaries and corresponding technology) can be more than significant.

Furthermore, it should not be neglected that these results refer to 2.2 lb (1 kg) of structural steel members. Even the small value differences observed among the remaining three LCI databases can lead to noticeable value variation—considering that, within an LCA study concerning a steel structure, hundreds or thousands of tons of structural steel members are used.

The point at which even the three databases that lead to similar impact results vary is the burden of each environmental indicator. The respiratory inorganics and fossil fuels indicators, for example, although prominent within each database impact result, are burdened to varying degrees. Other indicators, such as ecotoxicity, are barely visible within all databases except Ecoinvent, where it accounts for a significant impact load. The same can be observed

in Figure 5, where impact assessment results are presented according to impact category, a more general environmental assessment model based on the grouping of the indicators.

Resources and human health accept the largest percentage of environmental impact according to all four LCI databases, yet at a varying degree. According to the three databases that do not include recycling scenarios, the resources category impact varies from 32.6 to 46.7 mPt, whereas the human health category varies from 27.9 to 39.9 mPt. Ecosystem quality is burdened significantly less, with values ranging from 4.1 to 17.4 mPt, according to the same three databases.

These values, calculated for each impact category, present noticeable divergence and can thus provide substantially different assessment conclusions. That is, although, as a total, most databases lead to similar impact values, the same is not the case for each individual category impact. These value differences can be interpreted as a general lack of data uniformity between the selected LCI databases. In order to investigate this in depth, it is necessary to calculate environmental impact results to a higher level of data detail. Within the Eco-Indicator methodology, this can be achieved with the impact indicators used. In Figure 6, the impact results for 2.2 lb (1 kg) of hot-rolled structural steel members are presented according to each impact indicator.

The first observation is that not all impact indicators are burdened and only a few are affected to a significant degree. Fossil fuels [which refers to the additional required energy for extraction due to low raw material quality (as high volumes of raw materials are extracted continuously, the quality of the remaining raw materials decreases and requires additional energy for further extraction)] are responsible for the greatest environmental impact according to all databases but one, followed by respiratory inorganics (which refers to effects on the human respiratory system caused by emissions of inorganic substances during the winter time).

As far as impact values within each indicator are concerned, there is an obvious lack of result uniformity. Within fossil fuels, the most heavily affected impact indicator, the impact value ranges significantly among the selected databases. The same can be observed for the respiratory inorganics indicator, with only the Ecoinvent and the AUTH databases providing similar values of 15.8 and 17.2 mPt, respectively. The ecotoxicity indicator (which refers to effects on the quality of the ecosystem due to the emission of ecotoxic substances to the air, water and soil) also presents an uneven value distribution because the Ecoinvent databases leads to a significantly increased impact value, compared to the other three, which lead to relatively negligible ones. Impact indicators that do present a relatively

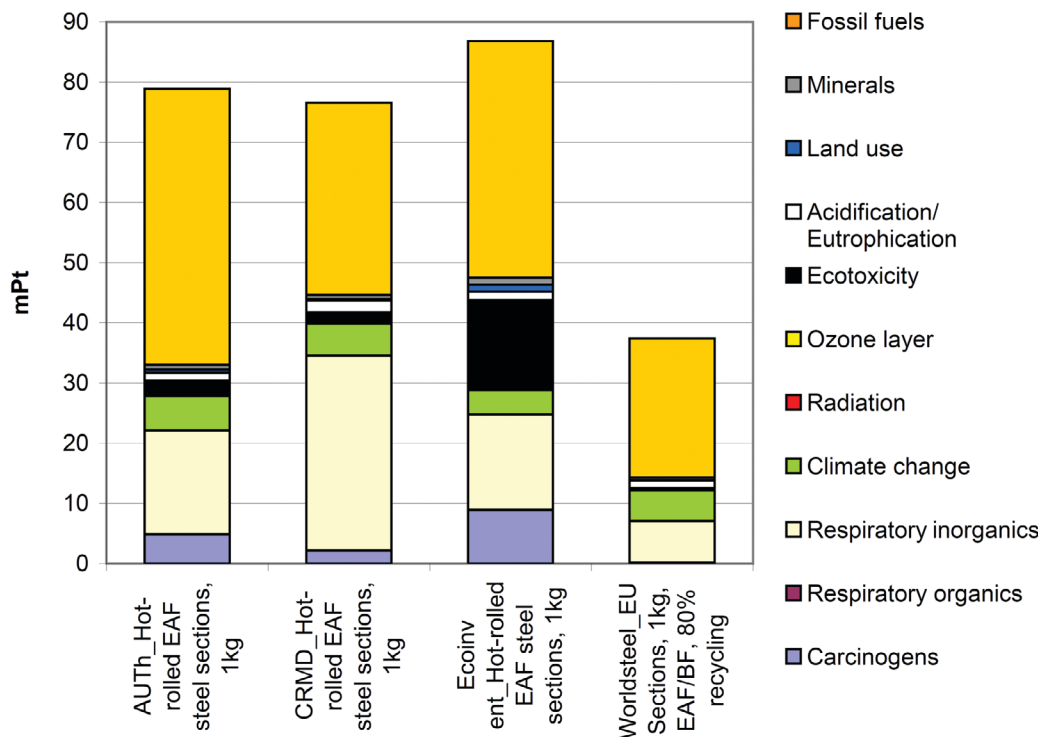


Fig. 4. Eco-Indicator 99 environmental impact results for the production of 2.2 lb (1 kg) of hot-rolled structural steel members (EAF), according to four LCI databases.

even value distribution, such as climate change and acidification/eutrophication, are associated with very low impacts and are, therefore, limited in terms of gravity and influence of the final result.

These observations lead to the conclusion that there is an overall lack of uniformity regarding the environmental impacts caused by the production of structural steel members. Although each database is based on data provided by manufacturers, there is significant divergence of results for environmental impact caused. Although this can partly be attributed to a number of reasons such as differences in geographic coverage, data collection time period and technology level, different processes or data sampling methodologies, and different electrical grids of the age of the data, it should not be neglected that the production process for hot-rolled structural steel members via the EAF steelmaking route consists of the same stages and, therefore, does not present major variations or utilizes fundamentally different machinery or manufacturing processes. Thus, it can be expected that similar LCA studies on the same steel product or project, but based on data from different LCI databases, can lead to varying final impact results. In order to provide an indicative estimate of this result variation, impact result divergence was calculated as a percentage of the average value for each of the mainly burdened indicators and the total impact. These percentages are presented in Table 1 for each of the four selected LCI databases.

As can be observed, there are very few cases in which divergence percentages can be considered within acceptable limits. The divergence percentage reaches almost 80%

within the respiratory inorganics indicator and 205.2% within ecotoxicity. These value differences are directly associated with the quality and accuracy of LCI data, and although expected, they are certainly a clear indication of the extent of uncertainty embedded in LCI data, which is inevitably transferred to final LCA results.

In order to examine the source of this uncertainty, it is necessary to examine the processes responsible for the environmental impacts caused for each indicator. For this purpose, the situation within the mainly burdened impact indicators is analyzed further.

### Fossil Fuels

The fossil fuels impact indicator accepts the greatest environmental impact caused for the production of the structural steel members, as was shown in Figure 6. In Figure 7, this impact is presented for each of the four selected LCI databases, according to the processes that cause it. As can be observed, the impact is almost completely caused by three processes. These processes all refer to energy-related raw materials consumed during the production of the steel members, namely, oil, coal and natural gas.

The impact caused by the consumption of oil does not vary significantly across the three databases that do not include recycling scenarios, ranging from 4.6 to 7.6 mPt. For natural gas, the impact caused is again relatively lower according to the Worldsteel database; however, due to the inclusion of recycling within the data, this difference cannot be regarded indicative of uncertainty. According to the rest of the databases, the natural gas-related impact attains

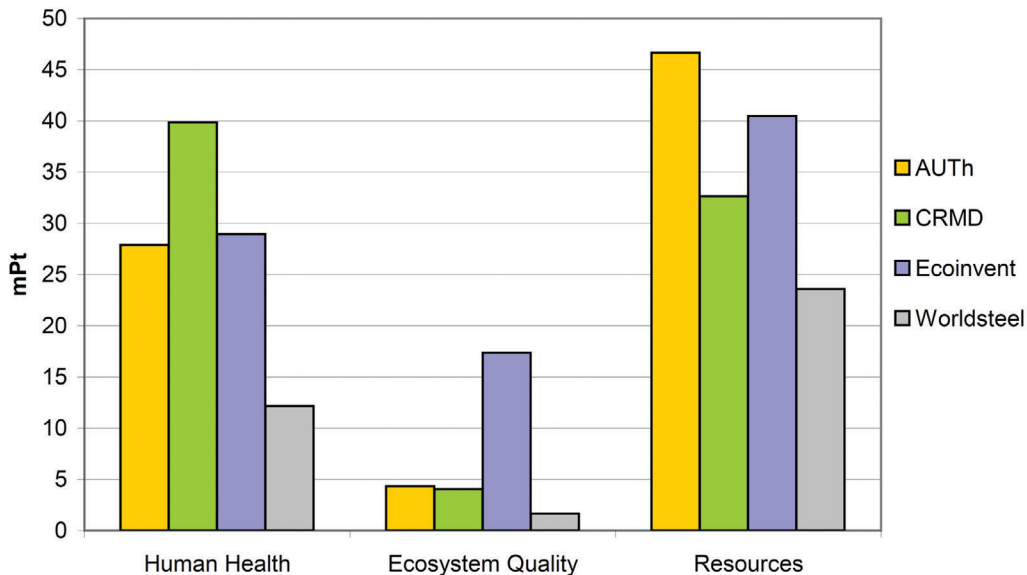


Fig. 5. Eco-Indicator 99 environmental impact results for the production of 2.2 lb (1 kg) of hot-rolled structural steel members (EAF), according to four LCI databases, per impact category.

Impact Indicator	Average Impact, (Pt)	AUTh Divergence, %	CRMD Divergence, %	Ecoinvent Divergence, %	Worldsteel Divergence, %
Total impact	0.068	16.0	12.6	27.7	46.5
Fossil fuels	0.033	38.6	3.7	18.5	34.0
Respiratory inorganics	0.018	4.6	78.7	12.6	61.6
Ecotoxicity	0.005	49.6	62.9	205.2	92.6
Carcinogens	0.004	20.9	46.3	122.1	96.7
Climate change	0.005	13.6	5.8	19.6	0.2

values from 16.8 to 22.3 mPt, a quite noticeable value range. With coal, the consumption of which is directly associated to the consumption of electrical energy, the situation is even more complex. Only two of the four databases present similar results at 10.3 and 10 mPt, while the remaining two lead to greater values of 14.7 and 19.8 mPt.

These differences in values of the impact caused derive from calculations based on the environmental data contained in each database and can thus be interpreted as corresponding variations of LCI data. It is, therefore, clear that even fundamental environmental information such as the amount of energy required for the production of the steel members presents variations depending on the database in which it is found. Further analysis of the production processes included in the AUTh database reveals that the

greatest amount of electrical energy is consumed during the operation of the EAF, the hot-rolling process and the ladle furnace stage. Accordingly, natural gas energy and oil are mainly consumed at the EAF, hot-rolling and reheat furnace stages. In order to minimize uncertainty embedded in LCI data within steel related LCA and in regard to fossil fuels, it is necessary to examine these processes thoroughly and determine the exact energy requirements. It should be noted that this observation also applies to the other mainly burdened impact indicators, such as respiratory inorganics.

#### *Respiratory Inorganics*

The respiratory inorganics indicator is the second most burdened indicator for the production of hot-rolled structural

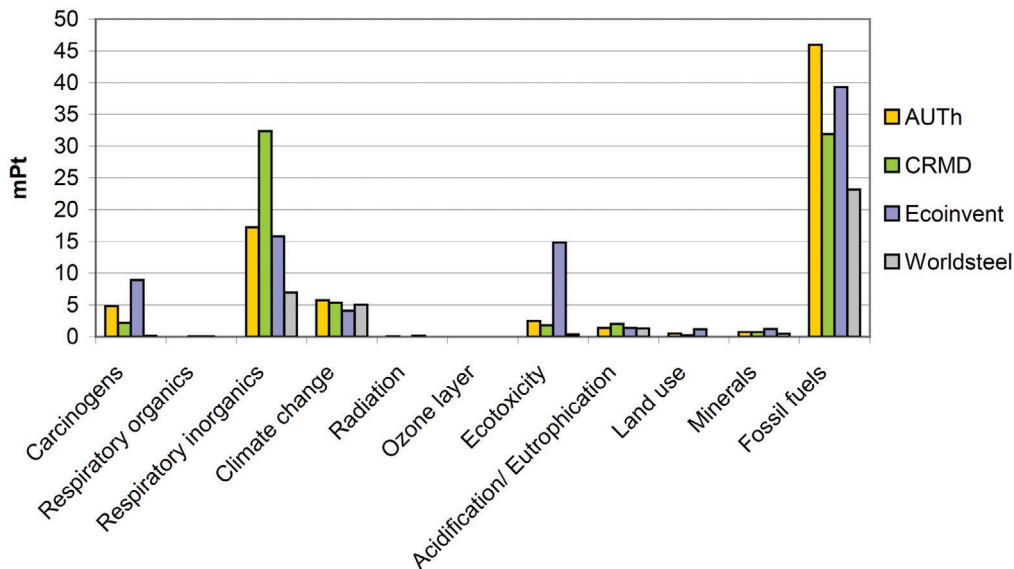


Fig. 6. Impact results for the production of 2.2 lb (1 kg) of hot-rolled structural steel members (EAF), according to four LCI databases, per impact indicator.

steel members via the EAF steelmaking route. Figure 8 shows the corresponding impacts caused according to the four selected databases, including the main substance emissions that cause them.

The first observation is the increased total impact calculated according to one of the four databases. Although the Ecoinvent and AUTH databases lead to similar results, these values are close to half of the impact according to CRMD. In such cases, it is not possible to determine which result should be used, and the 50% difference is quite significant. The impact caused by the emission of sulfur oxides to the air ranges from 1 to 3.8 mPt according to two databases, while it is negligible according to the other two. Furthermore, the emission of sulfur dioxide to the air also presents noticeable variation, from 1 to 4.2 mPt. This substance emission is a result of the consumption of electrical energy and is, therefore, directly affected by the amount taken into account during the calculation of the LCI data. Thus, this type of energy is again identified as critical to the validity of the steel-related LCI data.

The value of the impact caused by the emission of particulates to the air also presents significant divergence (from 1.3 to 22.5 mPt), although it is very similar according to two databases (9.8 and 10 mPt). Further analysis of the AUTH database production processes reveals that the greatest percentage of particulates emitted to the air is caused by the consumption of electrical energy for the production of the structural steel members. The environmental impact caused by the emission of nitrogen oxides to the air is the only value that does not present significant divergence among the four databases, ranging from 3 to 4.8 mPt. As an overall

observation, there is a lack of uniformity with regard to the impacts calculated. This can be attributed to data differentiation and can lead to similar result divergence within steel-related LCA.

### IPCC Global Warming Potential (GWP) Impact Assessment

In order to acquire an additional perspective on the environmental impact of the production of hot-rolled structural steel members, its assessment was calculated according to another widely used methodology, the IPCC Global Warming Potential (GWP) 2007. This methodology was developed by the Intergovernmental Panel on Climate Change (IPCC, 2007), a global organization aiming at providing a clear, scientific view on the current state of climate change and its potential consequences. It is based on the calculation of a single index that refers to the quantity of carbon dioxide equivalent emissions to the air in kilograms of carbon dioxide (kg CO<sub>2</sub> eq). For the purpose of the current study, the GWP index was calculated for the production of 2.2 lb (1 kg) of hot-rolled structural steel members, according to the four selected LCI databases, and for a 20-, 100- and 500-year time horizon. The results are presented in Figure 9.

The examination of the impact results according to the IPCC GWP 2007 methodology presents a slightly different assessment, compared to Eco-Indicator. The first observation is that the impact according to the Worldsteel database is not the lowest of the four, even though it is the only dataset that includes a recycling scenario. All four impact values present a more even distribution, ranging, for example, from

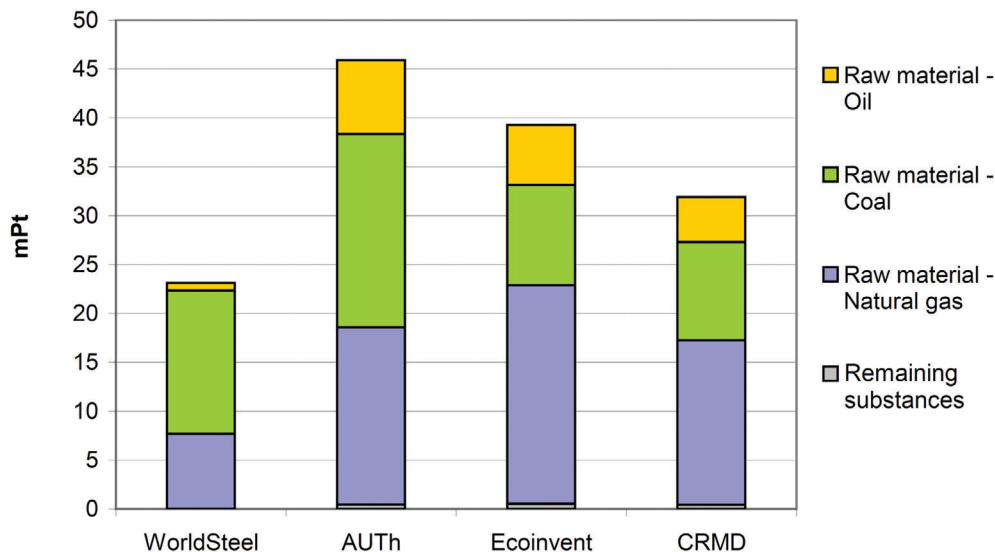


Fig. 7. Fossil fuels indicator impact for the production of 2.2 lb (1 kg) of hot-rolled structural steel members (EAF), according to four LCI databases.

0.996 to 1.405 kg CO<sub>2</sub> eq. for the 100-year time horizon. The range of values for the 20- and 500-year time horizons remain similar. In general terms, a more uniform depiction of the environmental impact caused by the production of 2.2 lb (1 kg) of structural steel members is presented.

It is, therefore, highlighted that within the scope of LCI and LCA studies, impact assessment results can be calculated with more than one assessment methodology, each based on certain assumptions and criteria. Several impact assessment methods focus on a particular aspect or category of

environmental impacts, such as the IPCC GWP 2007, which examines global warming and climate change. Although other methodologies, such as the Eco-Indicator, aim at providing a more complete approach to the assessment of environmental impacts, it should be noted that they are based on specific assumptions regarding impact assessment as well. It is advisable, then, to calculate environmental impacts according to more than one methodology in order to gain a wider, more complete and more factual perspective. Particularly in the case of comparative studies, the calculation of

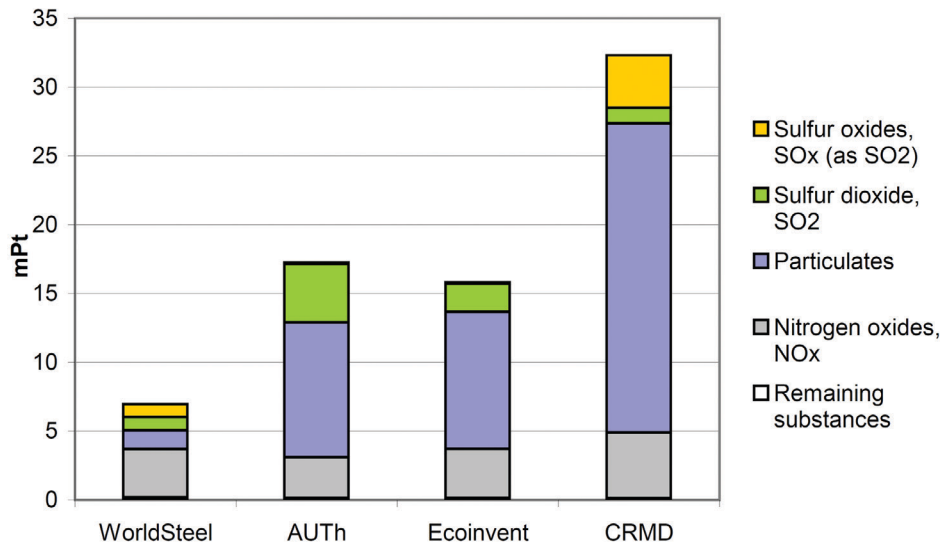


Fig. 8. Respiratory inorganics indicator impact for the production of 2.2 lb (1 kg) of hot-rolled structural steel members (EAF), according to four LCI databases.

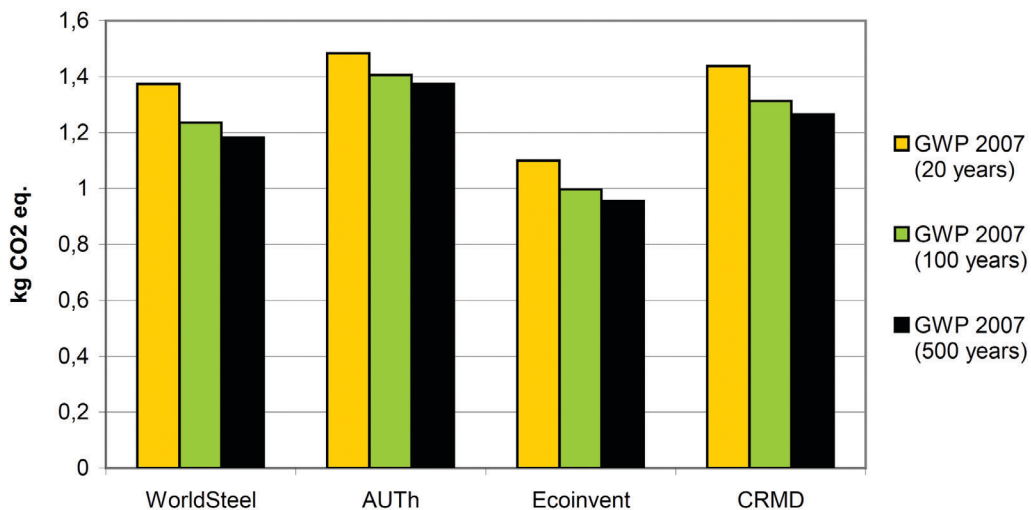


Fig. 9. IPCC GWP 2007 impact assessment for the production of 2.2 lb (1 kg) of hot-rolled structural steel members (EAF), according to four LCI databases.

Impact Category	Unit	AUTH	CRMD	Ecoinvent	Worldsteel
Ozone depletion	kg CFC-11 eq.	9.0872E-08	4.89151E-08	1.0269E-07	0
Global warming	kg CO <sub>2</sub> eq.	1.406224548	1.312803155	0.988808454	1.23522998
Smog	kg O <sub>3</sub> eq.	0.043009061	0.06858607	0.050892542	0.051060138
Acidification	mol H+ eq.	0.290464931	0.357480433	0.189167198	0.178937872
Eutrophication	kg N eq.	0.016775008	0.004248367	0.004377911	0.000110648
Carcinogenics	CTUh	3.66154E-07	2.49415E-07	3.46166E-06	1.38632E-09
Noncarcinogenics	CTUh	3.19333E-07	1.10754E-07	2.92674E-06	7.29306E-08
Respiratory effects	kg PM <sub>10</sub> eq.	0.001953061	0.000805941	0.00162357	0.000206099
Ecotoxicity	CTUe	4.76130729	2.801574071	35.14301133	0.007596337

impact assessment results according to more than one methodology is necessary, as was shown by the current analysis of the production of structural steel members.

### TRACI Impact Assessment

TRACI (Tool for the Reduction and Assessment of Chemical and other environmental Impacts) is another widely used impact assessment methodology that was developed by the U.S. Environmental Protection Agency specifically for the United States with the use of input parameters that are consistent with U.S. locations. Environmental impact assessment results for the four selected LCI databases are presented in Table 2.

As can be observed, the results obtained according to the TRACI methodology present noticeable differences in most impact categories. In ecotoxicity, for example, the Ecoinvent database leads to a very high result compared to the rest of the databases, while the same can be observed for the AUTH database in the eutrophication impact category. On the other hand, only the smog and acidification impact categories present an accepted range of values.

### The Effect of the Market on LCI Data

At this point, a significant issue concerning the source of LCI data arises. For the collection of primary LCI data, it is businesses involved with the product, system or service under study that are asked to provide detailed information concerning the environmental impact of the production processes they are currently applying. It is necessary, however, to consider the conditions under which today's businesses operate before putting the data they provide to use as the basis of decision-making methodologies and tools. It is true that within every major business sector where large-scale projects and clients are involved—with the steel industry being no exception—there is extreme competitiveness among the participants for not only maintaining a strategic

market position but also for broadening it. Every business that is interested in its future survival and prosperity is trying to adapt to the changing market conditions in order to gain more clients.

These changing market conditions have lately been greatly influenced by the global movement for sustainable development, with European and global organizations oriented toward achieving it through legislation adaptation and the promotion of more environmentally friendly policies. It is therefore quite common, within large-scale projects such as steel constructions, to investigate material and component suppliers from the point of view of their product's environmental impact. As a result, it is not unreasonable to require verification of the environmental data supplied by any business whose turnover and subsequent net profit are coming to depend on these data. The only efficient verification process of data provided by businesses is thorough examination. The degree, however, to which data can be verified, remains questionable. As an alternative, data and measurements conducted by independent organizations and according to specific guidelines would certainly provide a more dependable reference, corresponding to the actual environmental impact caused.

### CONCLUSIONS

At the outset of each LCA study, one of the critical tasks that have to be carried out is finding the appropriate LCI data. Even in cases that facilitate the collection of primary data directly from manufacturers, the verification of the obtained data is required, while the use of secondary data as found in existing LCI databases is inevitable. As was shown with the analysis of structural steel members, there are a number of available LCI databases that contain data concerning the same products, processes or systems. The selection of the most appropriate data usually depends on a number of data quality factors, including geographic coverage, technology

level and collection time period. It should not, however, be based solely on the examination of these factors and in no case should it be taken for granted that the validity of the final LCA result is ensured by the fact that a specific existing dataset matches the data quality requirements of the study. Because it is not possible to determine the most appropriate data based only on the examination of the data's quality characteristics, the extent of uncertainty embedded should be taken into account before the interpretation of relevant LCA results.

LCI datasets referring to the same product or system, even with very minor differences in terms of data quality, can lead to noticeable divergence of the final LCA result. Impact assessment results for the production of structural steel members showed significant value variation among different LCI databases when calculated for each of the mainly burdened impact indicators. An overall lack of environmental impact result uniformity was observed, in spite of the fact that all selected LCI databases are based on data provided by manufacturers. This could be attributed to data quality differentiations—such as differences in geographic coverage, data collection time period, technology level, data sampling methodologies or the age of the data—yet only partly, because the production process for hot-rolled structural steel members via the EAF steelmaking route does not present major variations or utilize fundamentally different machinery. Additional reasons include different manufacturing processes and different electrical grids.

It was estimated that, within certain indicators, the relevant impact calculated presented divergence of up to almost 80%, and even 205% at one instance, with regard to the average value among the selected databases. This variation is directly associated with the quality and accuracy of the data; although expected to a certain level, it is a clear indication of the extent of uncertainty embedded in LCA and, inevitably, transferred to the final LCA results. Thus, it should be expected that LCA studies that differ only in the source of LCI data can lead to varying impact assessment results. Furthermore, issues such as electrical grid differences, different production processes or methodology differences also increase the level of uncertainty embedded in LCI data.

The detailed analysis of the calculated impacts of the production of hot-rolled structural steel members for the most heavily burdened impact indicator—which was found to be fossil fuels—showed that even fundamental environmental information such as the amount of consumed electrical energy presents variations depending on the database in which it is found. As was shown, it is the amount of electrical energy that causes the largest percentage of environmental burden, and as a result, it can be assumed that the largest percentage of the divergence of impact assessment results between the examined databases can be attributed to

the differences in electrical grid mixes documented in each database.

The influence of system boundaries was also shown by the calculation of impact assessment results based on a dataset that includes a recycling rate, as opposed to the rest of the selected datasets that do not include end-of-life scenarios. As expected, a significant difference between the corresponding calculated impacts was observed, the extent of which highlights the importance of examining the characteristics of LCI data thoroughly, before incorporating it into an LCA study.

An issue concerning the collection of data was also raised. Primary LCI data are provided by businesses that operate within sectors, such as the steel industry, where market conditions have and are constantly becoming even more competitive. In order to consolidate their current market position and also attempt to broaden their standing, these businesses are now called to become competitive in terms of sustainability of the services or products offered. Large-scale clients and projects require materials and products with low environmental impact, in line with the orientation of European and global organizations toward legislation adaptation and the promotion of more environmentally friendly policies. As a result, it is advisable to thoroughly examine the data provided by any business whose turnover and subsequent net profit are coming to depend on such data to a continuously increasing degree. Alternatively, LCI data collected by independent third-party organizations and according to widely acknowledged guidelines [such as Product Category Rules (PCRs) and Environmental Product Declarations (EPDs)] would certainly provide a more dependable reference, corresponding to actual environmental impacts caused.

It was also highlighted that within the scope of LCI and LCA studies, it is necessary to calculate impact assessment results according to more than one assessment methodologies. Although the use of a methodology capable of providing results across a wide range of impact categories provides a multilevel depiction of the environmental impact caused, it should not be neglected that even this type of methodology is based on specific assumptions regarding impact assessment. In order to gain a wider, more complete and more factual perspective, it is suggested that impact assessment results be calculated with methods that focus on particular aspects or categories of environmental impacts as well.

## REFERENCES

- Bragança, L., Mateus, R. and Koukkari H. (2007), "Perspectives of Building Sustainability Assessment," *Portugal SB07—Sustainable Construction, Materials and Practices*, L. Bragança et al., eds., IOS Press, Amsterdam, The Netherlands, pp. 356–365.

- Classen, M., Althaus, H.J., Blaser, S., Tuchschnid, M., Jungbluth, N., Doka, G., Faist Emmenegger, M. and Scharnhorst, W. (2009), *Life Cycle Inventories of Metals*, Final report, Ecoinvent data v2.1, No 10, EMPA, Dübendorf, Switzerland.
- IPCC (2007), *The Physical Science Basis, Contribution of Working Group I to the Fourth Assessment*, Report of the Intergovernmental Panel on Climate Change (IPCC), S. Solomon et al., eds., Cambridge University Press, Cambridge, United Kingdom.
- IPPC (2001), *Best Available Techniques Reference Document on the Production of Iron and Steel*, European Integrated Pollution Prevention and Control (IPPC) Bureau, European Commission, Brussels, Belgium.
- ISO (2006a), *ISO 14040:2006 Environmental Management—Life Cycle Assessment—Principles and Framework*, International Organization for Standardization, Geneva, Switzerland.
- ISO (2006b), *ISO 14044:2006 Environmental Management—Life Cycle Assessment—Requirements and Guidelines*, International Organization for Standardization, Geneva, Switzerland.
- Simoès da Silva, L., Grecea, D., Krigsvoll, G., Gervásio, H., Blok, R. and Aktuglu, Y. (2007), “LCA Databases (EPD vs Generic Data),” *Proceedings of the First Workshop of COST Action C25—Sustainability of Constructions: Integrated Approach to Life-time Structural Engineering*, L. Bragança et al., eds., September 13–15, 2007, Lisbon, Portugal, pp 0.13–0.22.
- The Netherlands Ministry of Housing, Spatial Planning and the Environment (2000), *Eco-Indicator 99, Manual for Designers: A Damage Oriented Method for Life Cycle Impact Assessment*, Amsterdam, The Netherlands.
- Worldsteel (2005), *Worldwide LCI Database for Steel Industry Products—Methodology Report*, World Steel Association, Brussels, Belgium.
- Worldsteel (2009), *Steel Statistical Yearbook 2008*, Worldsteel Committee on Economic Studies, World Steel Association, Brussels, Belgium.
- Zygomalas, I., Efthymiou, E. and Baniotopoulos, C.C. (2009), “On the Development of a Sustainable Design Framework for Steel Structures,” *Transactions of FAMENA*, Vol. 33, No. 2, pp. 23–34.
- Zygomalas, I., Efthymiou, E., Baniotopoulos, C. and Blok, R. (2012), “A Newly Developed Life Cycle Inventory (LCI) Database for Commonly Used Structural Steel Components,” *Structure and Infrastructure Engineering*, Taylor & Francis Group, Vol. 8, Issue 12, pp. 1173–1181.

# Current Steel Structures Research

No. 33

REIDAR BJORHOVDE

## INTRODUCTION

This issue of “Current Steel Structures Research” for the *Engineering Journal* focuses on a selection of research projects of one major American university. The descriptions will not discuss all of the current projects at the school—there are simply too many. But selected studies provide a representative picture of the research work, and demonstrate the importance of the school to the United States and indeed to the efforts of industry and the profession worldwide.

The university and its many researchers and graduate students are very well known in the world of steel construction: Virginia Polytechnic Institute and State University. Commonly known today as Virginia Tech, over the years the school has significantly expanded its graduate program offerings. The size of the civil engineering faculty in general—and especially the structural engineering group—has become a critical part of one of the leading institutions in the United States. The studies that are presented here reflect elements of the projects as well as other long-time efforts of a primary U.S. advanced academic institution. As has been typical of American, European and worldwide engineering research projects for years, many of the projects are multi-year, and a number are also multipartner efforts. This calls for very careful planning, cooperation and implementation of needs and applications, including the education of graduate students and advanced researchers. The outcomes of the projects focus on industry needs and implementation in design standards.

The Virginia Tech researchers have been active for many years, as evidenced by their leading roles in research and development in the United States, but they have also been frequent participants in the work of other countries and regions. Large numbers of high-quality technical papers and conference presentations have been published, contributing to a collection of studies that continues to offer solutions to complex problems for designers as well as fabricators and erectors.

References are provided throughout the paper, whenever such are available in the public domain. However, much

of the work is still in progress, and in some cases reports or publications have not yet been prepared for public dissemination.

## SOME CURRENT RESEARCH WORK AT VIRGINIA TECH

Virginia Tech has been active in steel structures research for a number of years, and research as well as education and professional service thrive at the university. With the growth of the number of faculty members and students focused on structural steel, the Via Department of Civil and Environmental Engineering is recognized as one of the leading programs in the field. There are currently six faculty members and one emeritus faculty member who are actively involved in steel research, education, specification development and outreach. Three of these are past recipients of the T.R. Higgins Award, five serve on AISC task committees, and three serve on the AISC Committee on Specifications.

Steel-related research and education were not always part of the focus of the civil engineering program at Virginia Tech. Prior to 1987, one faculty member in the department was responsible for all structural steel instruction, and there was no structural engineering laboratory. In 1987, Professors Thomas M. Murray and W. Samuel Easterling were hired and charged with developing an experimental structural engineering program. This started with the design and construction of a structural engineering laboratory. The initial 12,000-ft<sup>2</sup> laboratory opened in 1990. Since that time, expansion of the facility has increased the size to more than 25,000 ft<sup>2</sup>. In 2009, the laboratory was named the Thomas M. Murray Structural Engineering Laboratory, in recognition of Professor Murray’s signal efforts to establish the facility and the overall program.

The Structural Engineering and Materials group has grown to a total of 11 faculty members, with seven professors focusing on steel research: Finley Charney, W. Samuel Easterling, Matthew Eatherton, Roberto Leon, Cris Moen and William Wright. Thomas Murray (emeritus) continues to be active in several areas. Some of the ongoing research is described in the following sections, in alphabetical order of the faculty. The primary interest areas of the individual professors are:

- Charney: Earthquake engineering; steel frame analysis and behavior.
- Easterling: Steel–concrete composite floor systems.

---

Reidar BJORHOVDE, Dr.-Ing., Ph.D., P.E., Research Editor of the *AISC Engineering Journal*, Tucson, AZ. E-mail: rbj@bjorhovde.com

---

- Eatherton: Steel frame structures; earthquake engineering.
- Leon: Steel and composite structures; earthquake engineering.
- Moen: Cold-formed steel structures; structural stability.
- Murray: Vibrations of steel-framed floors; steel connections.
- Wright: Fatigue and fracture of steel bridges.

Research support is provided by a number of organizations, both private and governmental, including the American Steel Construction Institute (AISC), the American Iron and Steel Institute (AISI), the Federal Highway Administration (FHWA), the National Cooperative Highway Research Program (NCHRP), the National Institute of Standards and Technology (NIST), the National Science Foundation (NSF), Nucor Corporation, the Metal Building Manufacturers Association (MBMA), the Steel Deck Institute (SDI), the Steel Structures Technology Center (SSTC) and Virginia Tech.

Professor W. Samuel Easterling is the Department Head of Civil Engineering at Virginia Tech. Over the years, he has conducted a great many significant research projects in composite construction, cold-formed structures and metal building systems. As the chief of a large academic department, his time available for teaching and research has become restricted over the past several years, but he continues to be very active in various projects and is a prominent participant in the research and development activities of AISC, AISI, ASCE, MBMA and SDI.

### **Selected Projects of Professor Finley Charney**

*Improved Structural Systems for Performance Based Earthquake Engineering:* Funded by NIST, this project aims to develop new or improved existing systems that inherently satisfy seismic performance requirements at multiple limit states. Further, the computed performance of the new systems must be based on realistic models, including gravity framing. To improve the reliability of the predicted behavior, a variety of uncertainties in modeling and computational procedures are included in the analysis. A preliminary study that evaluated the performance of a hybrid energy-dissipating device that performs like a viscoelastic damper at low levels of deformation and transforms into a metallic yielding device (a buckling restrained brace) at higher levels of deformation provided the basis for the project (Marshall and Charney, 2011).

*Assessment of Gravity Framing Contributions to System Behavior:* During the Northridge earthquake in 1994, many steel structures exhibited failure of primary moment-resisting connections, but the structures did not collapse

because the gravity system framing acted as a backup partially restrained frame system. Thus, to provide an accurate assessment of the collapse performance of new systems developed under the NIST project, it is essential that the gravity system be included in the analysis. The first phase of the study is complete, using special steel moment frame archetypes that were analyzed as part of the ATC 76 project. The gravity system was not included in the ATC 76 analysis.

In the current study, the original ATC 76 archetypes of two-, four- and eight-story frames without consideration of the gravity system have been reanalyzed. Additional analysis was performed using a variety of assumptions related to the flexural capacity of the gravity connections, the location of gravity column splices and methodologies for including yielding in the gravity columns. The beam-to-column connections in the gravity system were modeled using the recommendations of ASCE 41-06 (ASCE, 2007). The main lateral load-resisting system was modeled as was done in ATC 76.

A series of pushover curves for the four-story system with elastic gravity columns and nonstaggered splices is shown in Figure 1. The GS suffix in the legend (e.g., 35GS) indicates the percent of the flexural capacity of the gravity beam that was assumed to be developed at the connection. It is noted that the gravity columns, acting alone (0GS), have a minor influence on the frame response, as seen when compared to the line curve below the 0GS curve. The latter applies to the structure modeled without the gravity system. It is expected that the 35GS system is realistic in terms of the types of practical gravity systems, and for this system, the pushover behavior is considerably improved. The project has also provided analyses of probabilities of collapse for various ground motions, taking into account connection strengths, column modeling and column splice modeling.

*Development of Collapse-Prevention Systems:* In the central and eastern United States, the level of ground shaking for serviceability events (50% probability of being exceeded in 50 years) is very low compared with the expected shaking for the more rare maximum considered event (2% in 50 years). In contrast, ground shaking for serviceability on the West Coast is very significant. In Charleston, South Carolina, for example, the serviceability shaking is negligible and damage is highly unlikely. This is compared with some locations in California, where the serviceability event can produce ground motions as high as 30% of the design level event, resulting in significant damage to nonstructural components and to inelastic deformation in the main lateral load-resisting system.

The preceding observation has led to the concept of developing “collapse prevention” systems in the central and eastern United States, for which the *only* design limit state to be considered is collapse. The design of the main structure is for gravity plus wind only, and seismic collapse safety is

provided by auxiliary systems that are benign under low-level shaking but engage and prevent collapse under the extremely rare design events.

Several schemes for collapse prevention in steel structures are being examined, including slack cables and slack linkages. These systems would engage only after a set interstory drift is attained. The cable or linkage becoming taut, plus the residual strength of the main lateral load resisting system, provide ultimate resistance of the system. Preliminary results from this research are shown in Figure 2, where response history traces are shown of the roof drift of a four-story steel moment frame with and without a slack linkage collapse prevention system. The linkage is designed to engage at 2% interstory drift. The result is a stable response, although there is significant residual deformation after the event, but this is more desirable than the collapse that occurs without the linkage. Traditional design of the structure would require significant increases in strength and stiffness, which leads to larger seismic forces and larger structural components—hence, additional cost.

*Hybrid Frame Systems:* Funded by AISC, this project expands on previous efforts to develop a new, hybrid moment-resisting steel frame (Charney and Atlayan, 2011). The goal of the study is to develop an improved type of seismic lateral force-resisting system that will perform better than traditional systems under various ground motion intensities. The key concept is to provide early yielding in some elements of the structure and to delay it in the other elements, as illustrated in Figure 3. The energy dissipation due to early yielding provides vibration control and reduces

the likelihood of resonant buildup. The delayed yielding increases post-yield stiffness, which reduces the residual deformations and reduces the likelihood of dynamic instability under high ground motion intensities.

Hybrid behavior can be achieved using various strategies, including mixed materials and mixed systems. In a hybrid material strategy, the hybrid behavior shown in Figure 3 can be achieved through the combination of a low yield point (LYP) steel, which may have a yield strength of 14.5 ksi, and high performance steel (HPS), which has a yield strength of 70 to 100 ksi. The hybrid multicore buckling restrained brace (BRB) shown in Figure 4 is an example of the mixed material strategy. Similarly, LYP steel can be used in moment frame connections where early yielding is desired, and high-strength reinforcement can be added to other connections in the moment frame to delay yielding (Atlayan and Charney, 2012a, 2012b). An example of the mixed-system strategy is the hybrid moment frame where three different types of connections (e.g. special moment frame, intermediate moment frame and ordinary moment frame) can be combined in a single hybrid moment frame (Charney and Atlayan, 2011). In this system, the special connections are designed to yield first, followed by the intermediate connections and then the ordinary connections.

The hybrid BRB part of the research work has been completed. The performance generally improves with the level of hybridity. It has also been found that the improvement in response at lower-level ground motions is somewhat higher than for higher-level motions, which enhances the serviceability behavior of the system. This is the main benefit of allowing minor yielding at lower-level ground motions.

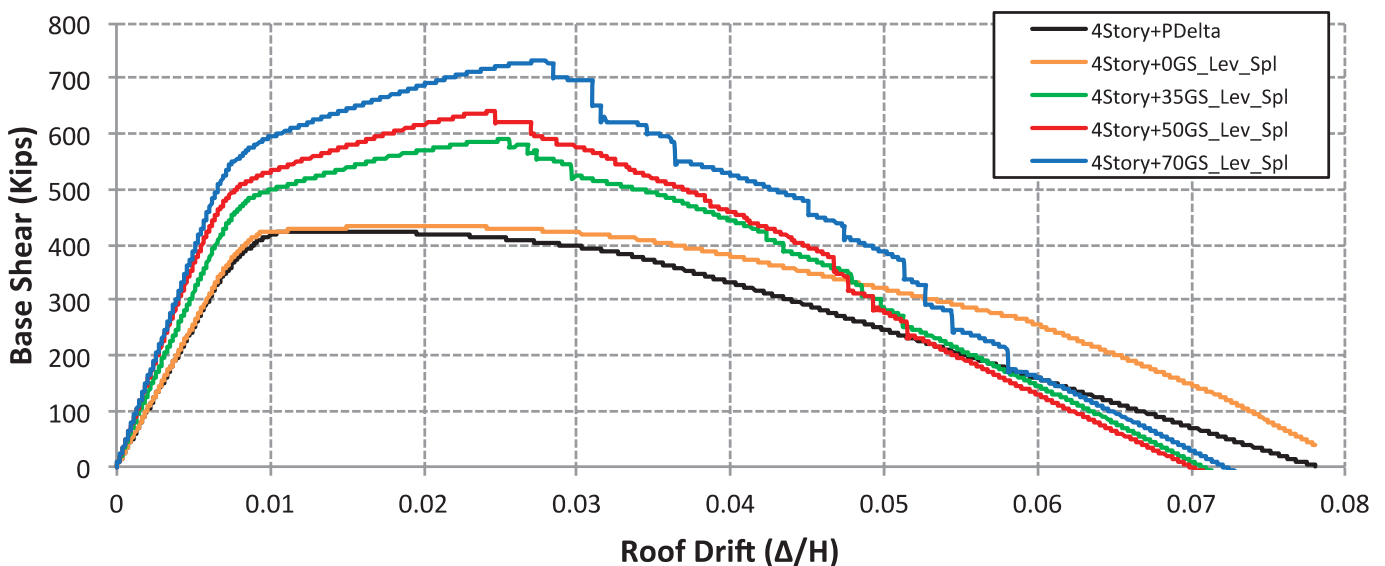


Fig. 1. Pushover curves for four-story frame with various gravity connection capacities (figure courtesy of Professor Finley Charney).

### Selected Projects of Professor Matthew Eatherton

*Effect of Defects on the Seismic Behavior of Steel Moment Connections:* Steel moment frames in seismic regions depend on large inelastic strains in the beam-to-column connections to dissipate seismic energy. For that reason, the ends of the beams in a moment frame are defined as protected zones, and many types of attachments are prohibited. Examples of unauthorized attachments in the protected zone are commonplace. However, there are almost no data available on how moment frames that have fasteners, defects or repaired defects in the connection region will behave during an earthquake. Physical testing is critical to determine whether connections with these types of conditions will provide adequate seismic performance.

Such a testing program is currently under way at Virginia Tech. Twelve full-scale connection tests are being performed on W24×62 and W36×150 beams with and without reduced beam sections (RBS). Figure 5 shows a specimen with a powder-actuated fastener that has sustained significant inelastic deformations without fracture. To further evaluate the low cycle fatigue fracture potential of these types of connections, a large coupon test program will be conducted

in coming year. The testing will include control specimens with no defects, powder-actuated fasteners, self-drilling screws, tack welds and specimens repaired using welding or grinding.

*Super-High-Tension Bolts:* Super-high-tension bolts were developed in Japan and are currently being used in construction in that country. The specified minimum tensile strength is 200 ksi, as compared to 150 ksi for ASTM A490 bolts (and the European grade 10.9). There is a desire to make super-high-tension bolts available for use in the United States to facilitate more compact connections using fewer bolts. However, to use super-high-tension bolts in the United States, it is necessary to develop installation procedures that are similar to current U.S. practice, as described in the Research Council on Structural Connections (RCSC) specifications. Japanese bolt installation procedures are generally more restrictive than U.S. procedures in that the torque at the snug-tight condition and the subsequent angle of nut turn are controlled even for twist-off type bolts.

The current project aims to develop suitable installation procedures for twist-off super-high-tension bolts. More than 300 pretension tests are being conducted, using various bolt

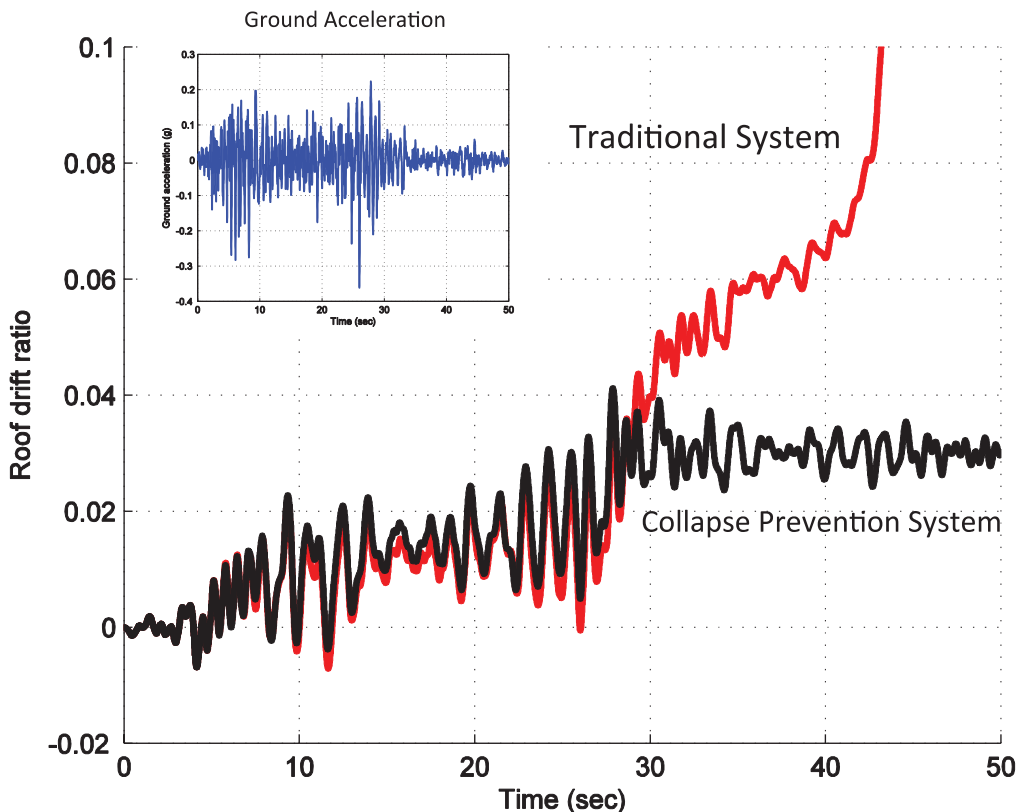


Fig. 2. Computed responses of traditional and collapse-prevention system (figure courtesy of Professor Finley Charney).

diameters, bolt lengths, temperature, number of threads in the grip, variations in lubrication from as-received to rusted or relubricated, and bolt hole geometry. The pretension tests use an instrumented Skidmore-Wilhelm machine to record bolt tension during the installation, including for the snug-tight condition, twist-off of the spline and, in some cases, tightening past yield with a hydraulic wrench. The nut angle of turn is also recorded at key times during each test. It is anticipated that recommendations will be made for appropriate installation procedures.

*Ring-Shaped Steel Plate Shear Walls:* The ring-shaped steel plate shear wall (RS-SPSW) builds on the advantages of conventional, solid steel plate shear walls but improves seismic performance, reduces demands on boundary elements and allows simple shear beam-to-column connections. The wall consists of an SPSW in which the web plate is cut with a pattern of holes, leaving ring-shaped portions of steel connected by diagonal links. The ring shape resists out-of-plane buckling through the mechanics of how a circular ring deforms into an ellipse. Tests and finite element analyses

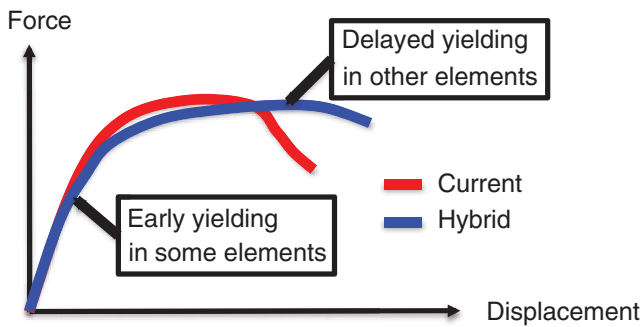


Fig. 3. Effect of hybrid detailing on pushover response (figure courtesy of Professor Finley Charney).

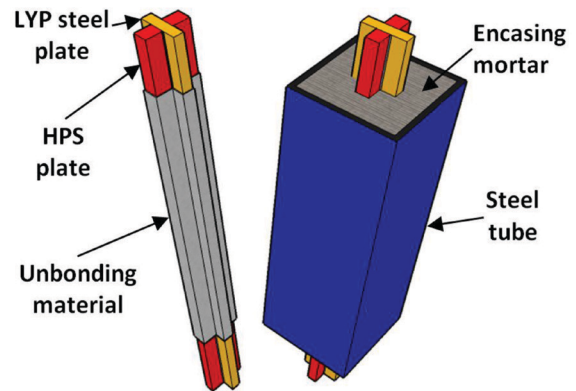


Fig. 4. Hybrid buckling restrained brace (figure courtesy of Professor Finley Charney).



Fig. 5. Deformed protected zone with intermittent powder-actuated fasteners in the flange (photograph courtesy of Professor Matthew Eatherton).

have shown that the compression diagonal of the ring will shorten a similar amount as the tension diagonal elongates. Essentially, the slack is removed in the direction perpendicular to the tension field, thus resisting the tendency for the plate to buckle. Because of the unique features of the ring's mode of distortion, the load-deformation response of the resulting RS-SPSW system can exhibit full hysteretic behavior. Improved energy dissipation and stiffness make the moment connections that are required for conventional steel plate shear walls unnecessary. Furthermore, through the introduction of more design variables associated with the geometry of the rings, it is possible to tune the strength, stiffness and ductility of the RS-SPSW system.

Parametric finite element modeling has been performed to identify key variables and quantify their effect on system behavioral characteristics (Maurya, 2012). Tests on panels that are approximately 40 in. by 40 in. (see Figure 6) have validated the RS-SPSW concept, and full-scale panel tests are planned for next year. Further computational studies will be conducted to examine the behavior of the RS-SPSW buildings and determine appropriate design procedures.

*Self-Centering Beams for Resilient Earthquake Resistance:*  
A self-contained self-centering beam (SC-beam) has been

developed that provides self-centering seismic behavior with enhanced constructability (Darling, 2012). The SC-beam consists of either a beam or a truss with concentric tubes for the bottom chord. The tubes of the bottom chord are precompressed with post-tensioning strands and connected to the top chord and columns to produce restoring forces regardless of whether the SC-beam is racked to the right or left.

Preliminary analyses show that the system offers several advantages as compared with other self-centering systems. Thus, the SC-beam can be shop fabricated and erected with conventional field techniques. Post-tensioning in the field and fit-up of bearing surfaces is not needed. Preliminary designs required approximately the same amount of steel as the comparison special moment-resisting frame. There will likely be a cost premium because of fabrication needs (Darling and Eatherton, 2012). Finally, the strength, stiffness and ductility can be independently tuned. Frame layout in a floor plan is not constrained by special detailing, as is currently required for SC moment frames that experience floor expansion.

*Seismic Moment Connections for Deep Beams with Slender Webs:* Typical built-up sections for pre-engineered metal

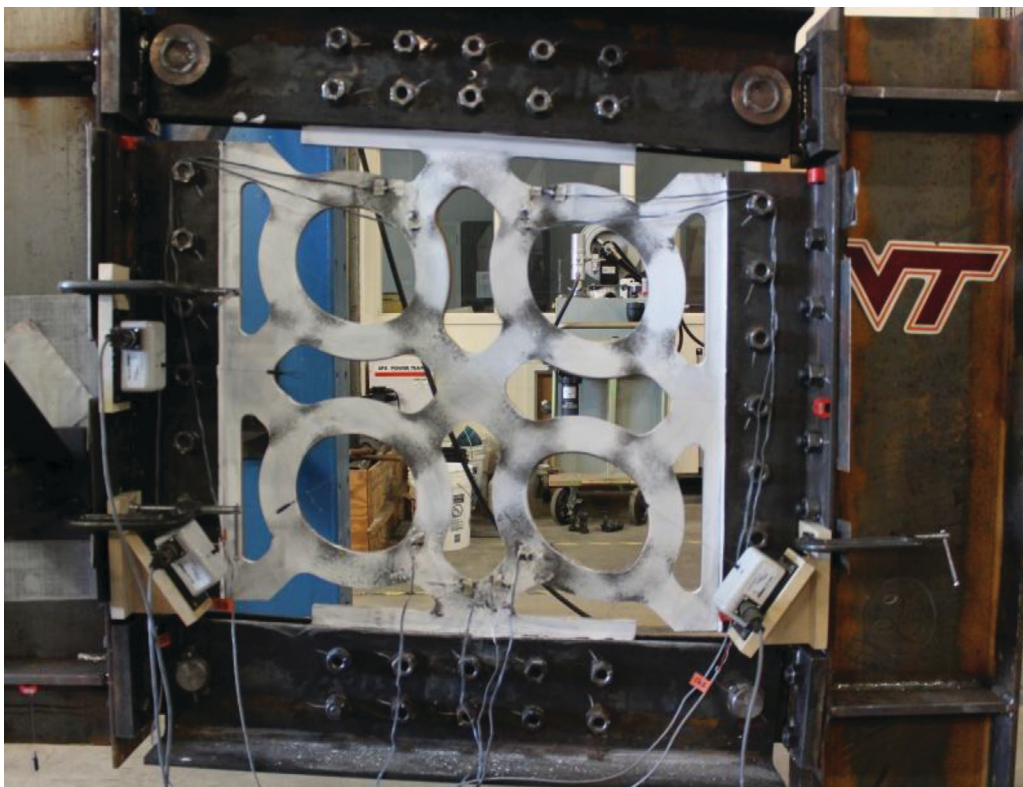


*Fig. 6. RS-SPSW test specimen subjected to large drift angle with negligible buckling (photo courtesy of Professor Matthew Eatherton).*

buildings have thinner webs than what is used for wide-flange shapes. The web slenderness for deep built-up members can be considerably larger than the limits for highly ductile members or moderately ductile members, as specified in the AISC *Seismic Provisions* (AISC, 2010). However, previous tests suggest that with proper detailing, these members may be able to develop adequate cyclic performance (Ryan, 1999).

Research is now being conducted on connections for deep built-up members with slender webs to improve their seismic performance. Several configurations have been evaluated, using finite element analysis and full-scale tests of 48-in. built-up sections. Figure 7 illustrates the behavior of an unstiffened slender-web beam, undergoing buckling of web and flanges. The web provides little rotational restraint to the flanges, which therefore buckle when subjected to relatively small story drift. Possible schemes for stiffening the web have been identified; these will be further studied for practical implementation.

#### ***Selected Projects of Professor Roberto Leon***

For many years a professor at Georgia Tech in Atlanta, Georgia, Dr. Leon recently joined the faculty at Virginia Tech, where he is continuing his research in the areas of steel and composite structures with emphasis on seismic design. He recently completed a large experimental program on the behavior of concrete-filled tube (CFT) composite columns. The project included testing the longest and most slender specimens ever tested under different combinations of axial and biaxial flexural loads, and included the use of high-strength concrete ( $f'_c > 12$  ksi). Columns with equivalent length to diameter ( $kL/d$ ) ratios of  $> 100$  were tested. The results are being used to validate and improve current AISC composite column design provisions. The experiments also shed light on the influence of wet concrete forces on the tubes, local buckling and plastic hinge length

Dr. Leon is continuing work on composite systems in the area of seismic performance system factors and through studies on connections to composite columns. The connections study emphasizes the development of innovative through-bolted connections to rectangular columns that utilize combinations of shape memory alloy (SMA) rods for recentering and conventional steel rods for energy dissipation. Further, detailed analytical models, physical tests and design provisions for connections to composite columns utilizing through, internal or external diaphragms are examined. This second type of connection is very common in Asia but not in the United States due to the perceived complexity of fabrication. This project aims at developing economic connections to CFT columns for use in low-rise construction (fewer than 10 stories) in North America.

Additional work focuses on the development of a robust brace in which (1) the need for energy dissipation does

not lead to residual deformations and (2) the reuse of the recentering components and easy replacement of the energy dissipating components damaged in an event are easily achievable. This device uses conventional buckling-restrained struts to dissipate energy and superelastic shape memory alloy (SMA) wires to recenter the structure (see Figure 8). These hybrid braces could reduce permanent drift considerably. They are assembled from easily replaceable damageable elements.

Dr. Leon continues to examine the validity of the equations that are used to predict the deflection of composite beams, the influence of long-term effects (creep and shrinkage) on composite columns performance, the applicability for design of plastic section analysis to unsymmetrical composite sections and the effects of composite diaphragm action on 3D building analysis. The study on floor diaphragms includes determination of appropriate values of stiffness and strength to be used in analysis, the effects of openings in the floor slab and any preexisting slab cracking, as well as the modeling of connections to chord and collectors and interactions between in-plane and out-of-plane forces at the local level.

#### ***Selected Projects of Professor Cristopher Moen***

*Steel Beam Deflections and Stresses during Lifting:* The behavior of steel beams during lifting is often challenging for engineers and contractors, and a new analysis approach is now available (Plaut, Moen and Cojocar, 2012). The equation-based approach assumes that the beams are horizontally curved, doubly symmetric, prismatic and linearly elastic and are suspended at two symmetric locations. The two cables lifting the beams may be vertical or inclined symmetrically. Weak-axis and strong-axis deflections, roll angle and cross-sectional twist, internal forces, bending and twisting moments, and longitudinal stresses can be calculated using the newly derived analytical solutions (Plaut and Moen, 2012) implemented as a freely available spreadsheet at [www.moen.cee.vt.edu/](http://www.moen.cee.vt.edu/). Lifting locations along a steel beam that minimize displacements and stresses can also be identified.

*Capacity Prediction of Open-Web Steel Joists Partially Braced by a Standing Seam Roof:* A new strength prediction approach has been developed for open web steel joists partially braced by a standing seam roof (Moen, Cronin and Fehr, 2012). The approach uses the AISC column curve to calculate the top chord flexural buckling capacity and to determine the elastic buckling load, including standing seam roof bracing stiffness. Recently derived buckling load equations are presented that account for the lateral stiffness provided by the roof and the parabolically varying axial load from a uniform vertical pressure along the span. A new hybrid experimental-computational protocol is introduced

for approximating standing seam roof lateral stiffness for systems without and with intermediate bridging. Figure 9 illustrates the roof system with trusses and the standing seam roof.

*Limit State Design of Metal Building Wall and Roof Systems:* A multiyear project aims at developing and validating an equation-based strength prediction framework for simple- and continuous-span metal building wall and roof systems subjected to gravity loads or wind uplift. The intent is to provide a procedure that can be used in lieu of the current empirical test-based approaches. The limit state checks include girt or purlin flexural capacity, panel capacity and panel connection strength. The connection strength is an addition to the current method. The connection limit state

was incorporated on the basis of suction load tests with wall girt rotation and fastener failures (Fisher, 1996; Gao and Moen, 2012, 2013).

The limit state design procedure is based on the AISI direct strength method (AISI, 2012). In the past, the restraints of the system could only be determined by tests, but now hand solutions are available for through-fastened metal panels (Gao and Moen, 2012). Significant advances have been made in this very complex area, and work is continuing to extend the procedures to continuous girt and purlin spans, subjected to uplift and suction, and to derive screw demand equations for the connection strength check.

*Strength Prediction of Steel Columns and Beams with Holes:* The extension of the direct strength method to columns and



*Fig. 7. Full-scale test of 48-in. slender web beam with end-plate moment connection (photograph courtesy of Professor Matthew Eatherton).*

beams with holes was recently approved for inclusion in the Specification for Cold-Formed Steel Structural Members (AISI, 2012). The method is based on simplified elastic buckling solutions—including local, distortional and global buckling—and takes into account discrete holes of any size, shape and spacing (Moen and Schafer, 2009, 2010). The simplified elastic buckling prediction methods were derived for cold-formed steel members, but they are also applicable to hot-rolled steel members. Finally, the method has been modified to address the strength and behavior of columns with periodic perforations, of the type found in the columns of rack structures (Smith and Moen, 2013).

**Selected Projects of Professor William Wright**

*Highway Bridge Fire Hazard Assessment:* Fires involving highway bridge structures are relatively rare, but the consequences can be significant when they occur. In extreme cases, the fire can result in a bridge collapse, but the typical case involves some degree of serviceability impairment. When fires do occur, there is an immediate need to assess the safety of the structure and its potential re-opening. Longer-term decisions also have to be made concerning subtle damage that can reduce the service life of the structure. The goal of the project is to develop a guide for fire damage evaluation specific to bridge structures. As a starting point, the research team developed a database that details bridge fires that were found through a thorough literature search and through communications with state departments of transportation (DOTs).

A survey of the available fire data in the United States shows that most fires involving bridges do not cause damage. For typical steel and concrete bridges, the bridge itself is not a combustible fuel source. The predominant cause of fire exposure is burning vehicles on or underneath the structure. Wildfires, stored combustible materials, utility pipelines and construction operations have also been documented. Focusing on vehicle fires, the data show that most are minor events that do not cause significant damage to bridges. There have been three reported cases of complete bridge collapse due to fire, all involving ignition of fuel-carrying vehicles at a critical location underneath the bridge. Approximately 25 cases have been found where the bridges were either totally or partially incapacitated for carrying traffic. That compares to approximately 500 events per year involving collisions on bridges involving fire.

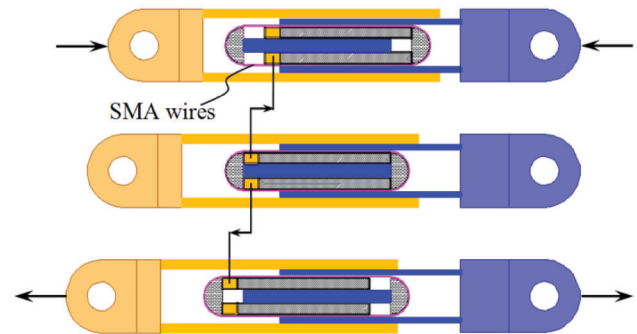


Fig. 8. Behavior and schematic view of a robust brace (figure courtesy of Professor Roberto Leon).

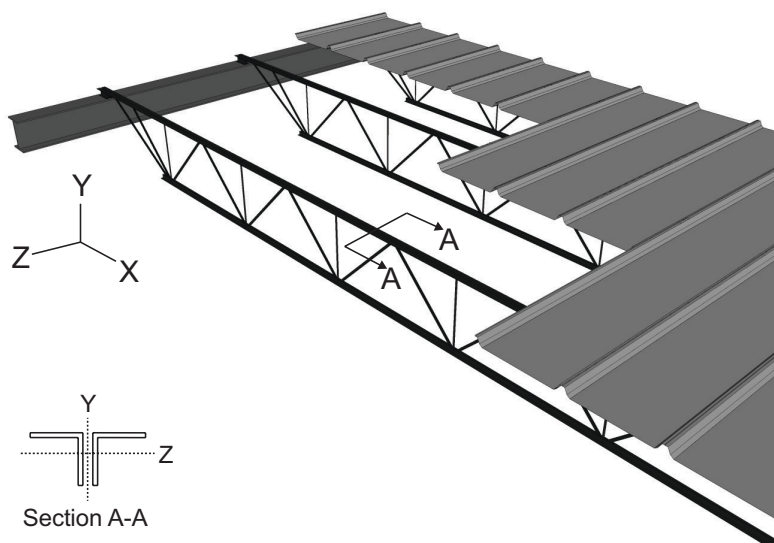


Fig. 9. Structural system with trusses and standing seam roof (figure courtesy of Professor Cristopher Moen).

One goal of this study is to understand the specific situations that cause damage. This is being accomplished by performing a series of finite element fire simulations involving a typical grade separation structure. The variables being investigated include vehicle fire intensity, fire position and vertical clearance over the fire source. A fire case study involving a grade separation structure on I-65 in Birmingham, Alabama, was selected as the basis for developing the simulation methodology. A collision involving a fuel truck caused a severe fire close to one of the bridge piers. Figure 10 shows the charred pavement and indicates the fire location and the resulting deflection of the superstructure.

A methodology for simulating fire events on bridge structures has been developed. The fire dynamics simulation (FDS) software developed by NIST was utilized to generate the heat flux applied to the bridge. Fires can be generated with different footprints and fuel content to simulate the range of vehicles that may be involved in fires. The bridge geometry with cavities between the girders underneath the bridge creates a boundary condition that greatly affects the longitudinal and transverse flame spread under the structure. The heat fluxes generated in FDS are then applied to a finite element thermal analysis model developed in ABAQUS. The model generates a temperature–time history for all elements in the bridge. The final step applies these temperatures to a structural analysis model to determine the time-dependent structural response of the bridge. Because

steel properties change at increasing temperatures, the non-linear material model accounts for the changes in the stress-strain curve at elevated temperatures. Steel creep also has a significant effect on the response, depending on temperature and fire event duration.

The modeling methodology has been calibrated against several significant structural system tests that have been performed on building floor structures. The next step was to model the fire event shown in Figure 10, and it was possible to predict the actual deflections. A parametric study was then conducted to understand the effect of fire size (vehicle and contents type), fire location and clearance under the bridge.

*Fracture Critical System Analysis:* Current design and inspection practices for highway bridges require nonredundant tension members to be classified as *fracture critical* (FC). Fracture critical members are defined as those whose failure may reasonably be expected to cause collapse. Once designated, FC members must be fabricated from materials with a higher Charpy V-Notch (CVN), including higher standards for welding and weld inspection. FC members must also be subjected to higher levels of in-service inspection as mandated by the National Bridge Inspection Standards. This requires a bi-annual, hands-on inspection of every fracture critical member that is more rigorous than the general inspection protocol for all bridges. The intent of the



Fig. 10. Fuel tanker fire below an overpass on I-65 in Birmingham, Alabama (photograph courtesy of Professor William Wright).

FC designation is to reduce the probability of defects that can lead to fatigue cracks and to provide a higher probability of detecting fatigue cracks before they grow to critical size for fracture.

History has shown that fabrication quality is beneficial to reduce fatigue vulnerability of structures. However, much of the effort expended to perform fracture critical in-service inspections has had questionable success in preventing fracture. The cost of hands-on FC inspection is significant and should only be utilized when there is a clear benefit to bridge safety. Therefore, this project is developing guidelines for using refined analysis to take advantage of 3D system capacity in determining which members may cause collapse.

The inspection adds significant maintenance costs to structures with FC members. The current approach of classifying bridge members as fracture critical is largely based on simple analysis assumptions such as girder-line analysis and 2D pin-connected truss models. These methods are very conservative because they ignore the 3D system performance of the structure.

Research is under way to understand the system strength of damaged structures. Fracture events create a sharp discontinuity in members that significantly alters the load path assumed by the bridge designers. However, observation of girder-type bridges that experience fracture of one girder indicates that significant alternate load paths exist. There has never been a system collapse of a girder-type bridge due to fracture, even when one girder in a two-girder system is completely fractured. The structures typically do not experience large deflections in the damaged condition, demonstrating that alternate load paths exist.

The study is developing highly detailed finite element simulations of several bridges that have experienced brittle fracture of a main load-carrying member. As a prime example, the Hoan Bridge on I-794 in Milwaukee, Wisconsin, shown in Figure 11, experienced brittle fracture in two of the three girders that support the end span of a continuous plate girder structure. The bridge did not collapse, despite the approximate 4-ft vertical deflection above the fracture location. This is a very severe test of system capacity because the fractures occurred in an end span and the girders were noncomposite with the concrete deck. Simplified analysis approaches indicate that collapse would have been expected with this level of damage, yet the system strength was sufficient to prevent collapse. Using the documented condition of the Hoan Bridge as a verification benchmark, this study has developed a highly detailed, nonlinear model of the damaged structure, as shown in Figure 12.

As a first step, the model is being used to understand the load paths that prevented collapse of the bridge. Loss of two main load-carrying members caused shedding of loads to the concrete deck, floor beams and other secondary members that were never considered to be part of the load path of

the structure. The capacity of the secondary members and their connections must be determined to validate the system capacity. A major goal of the project is to establish procedures to validate system-modeling results to ensure that any members carrying load in the model have the integrity to actually carry loads in the structure.

*Design and Fabrication Standards to Eliminate Fracture Critical Concerns for Steel Members Traditionally Classified as Fracture Critical:* This project is a research collaboration between Purdue University (Professor Robert Connor) and Virginia Tech (Professor Wright). The aim is to develop improved requirements for steel toughness that provide a quantifiable measure of fracture resistance. Brittle fracture became a major concern following the collapse of the Silver Bridge in Point Pleasant, West Virginia. There have been dozens of cases where structures are seriously damaged following brittle fracture of a main load-carrying member. A review of these cases reveals that there are three general causes of brittle fracture:

- Fatigue cracks grow to a critical size that allows brittle fracture to initiate under live load.
- High constraint details or local brittle zones allow brittle fracture to initiate under live load without any preexisting fatigue.
- Vehicle impact events cause a dynamic shock load to steel members.

Of the three, only the fatigue cracks are addressed by the American Association of State Highway and Transportation Officials (AASHTO) Fracture Control Plan (FCP) that was developed in 1978. The FCP places a strong emphasis on preventing fatigue cracks through fabrication quality control and in-service inspection. CVN toughness requirements are established for bridge steels that help prevent brittle fracture initiation from small fatigue cracks. The intent of the FCP is to either prevent fatigue cracks or to detect them through inspection before they reach critical size. Large fatigue cracks, constraint conditions and impact events can still cause brittle fracture initiation for structures meeting the requirements of the FCP. In addition, the toughness requirements in the FCP do not provide any appreciable crack arrest capability once fracture initiates. Therefore, when brittle fracture is initiated, it typically does not arrest in members or portions of members under tension.

The use of high-performance steel (HPS) grades in the ASTM A709 Specification for Bridge Steels is a major advance for fracture control. These grades can be produced with CVN values that far exceed those provided by conventional structural steels. The property enhancement leads to a much higher level of fracture initiation resistance from fatigue cracks and constraint details under live loads. More importantly, it also offers a significant capacity for crack

arrest that can limit the propagation of damage if fracture does initiate. Given the volume and scale of steel bridge fabrication, it is unlikely that 100% quality control and 100% inspection reliability can be achieved. Crack arrest resistance provides a significant approach to limit damage in the rare cases where a critical defect is not found. Once the

fracture propagates from the local defect initiation site, it runs into tougher material and arrests. This prevents sudden total member loss that has been the main concern from the fracture limit state.

The work at Virginia Tech focuses on a series of small specimen fracture tests to establish the fracture initiation



Fig. 11. Two of three girders with full-depth fractures in the Hoan Bridge in Milwaukee, Wisconsin (photograph courtesy of Professor William Wright).

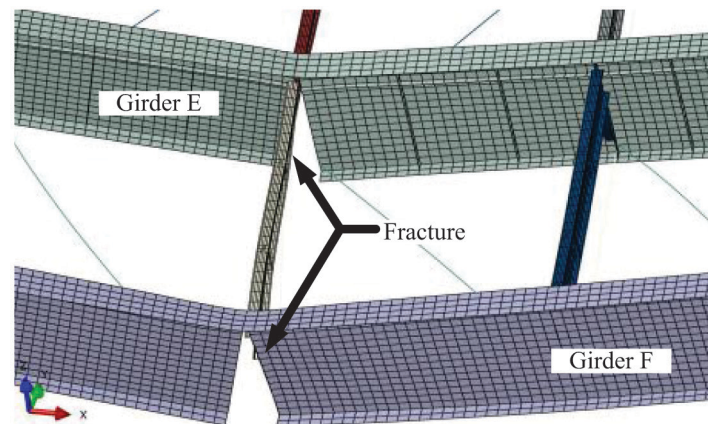


Fig. 12. Nonlinear finite element model to study the system capacity of the Hoan Bridge (figure courtesy of Professor William Wright).

resistance and crack arrest resistance of HPS and conventional bridge steels. While the CVN test is used for quality control in steel production, the test results cannot be directly used to predict fracture resistance. A more elaborate version of this test using precracked CVN specimens is being used to better quantify fracture resistance. This allows the establishment of a master curve for fracture resistance as a function of material temperature. Once the performance is established, correlations are developed to set material testing requirements based on the conventional CVN testing procedures.

In coordination with the work at Virginia Tech, the researchers at Purdue University will perform a series of full-scale fracture tests of bridge members. This will ensure that the small specimen test results translate into realistic performance criteria of actual bridge members. The final product will be a new supplemental material toughness specification (FC-Plus) that provides enhanced fracture initiation resistance and crack arrest resistance. The intent is that these criteria can be specified by designers for certain low-redundancy members in order to improve system reliability. This may eliminate the need for special FC inspection for bridge types such as two-girder systems.

#### ACKNOWLEDGMENTS

Professors W. Samuel Easterling, Finley Charney, Matthew Eatherton, Roberto Leon, Cris Moen and William Wright have provided significant assistance in the development of this paper. Their efforts are very sincerely appreciated.

#### REFERENCES

- AISC (2010), *Seismic Provisions for Structural Steel Buildings*, ANSI/AISC 341-10, American Institute of Steel Construction, Chicago, IL.
- AISI (2012), *North American Specification for the Design of Cold-Formed Steel Structural Members*, ANSI/AISI S100-2012, American Iron and Steel Institute, Washington, DC.
- ASCE (2007), *Seismic Rehabilitation of Existing Buildings*, ASCE/SEI 41-06, American Society of Civil Engineers, Reston, VA.
- Atlayan, O. and Charney, F.A. (2012a), "Hybrid Buckling Restrained Braced Frames," *Proceedings, Conference on Behavior of Steel Structures in Seismic Areas*, Santiago, Chile, January 9–11.
- Atlayan, O. and Charney, F.A. (2012b), "Hybrid Steel Frames," *Proceedings, 15th World Conference on Earthquake Engineering*, Lisbon, Portugal.
- Charney, F.A. and Atlayan, O. (2011), "Hybrid Moment-Resisting Steel Frames," *Engineering Journal*, AISC, Volume 48, No. 3, pp. 169–182.
- Darling, S.C. (2012), "Seismic Response of Short Period Structures and the Development of a Self-Centering Truss Moment Frame with Energy-Dissipating Elements for Improved Performance," M.S. Thesis, Virginia Tech, Blacksburg, VA.
- Darling, S. and Eatherton, M. (2012), "Computational Study on Self-Centering Truss Moment Frames with Replaceable Energy-Dissipating Elements," *Proceedings, Conference on Behavior of Steel Structures in Seismic Areas*, Santiago, Chile, January 9–11.
- Fisher, J. M., (1996), "Uplift Capacity of Simple Span Cee and Zee Members with Through-Fastened Roof Panels," Report MBMA 95-01, Metal Building Manufacturers Association, Cleveland, OH.
- Gao, T. and Moen, C.D. (2012), "Predicting Rotational Restraint Provided to Wall Girts and Roof Purlins by Through-Fastened Metal Panels," *Thin-Walled Structures*, Vol. 61, pp. 145–153.
- Gao, T. and Moen, C.D. (2013), "Flexural Strength Experiments on Exterior Metal Building Wall Assemblies with Rigid Insulation," *Journal of Constructional Steel Research*, Vol. 81, pp. 104–113.
- Marshall, J.D. and Charney, F.A. (2011), "Seismic Response of Steel Frame Structures with Hybrid Passive Control Systems," *Earthquake Engineering and Structural Dynamics*, Vol. 41, pp. 715–733.
- Maurya, A. (2012), "Computational Simulation and Analytical Development of Buckling Resistant Steel Plate Shear Wall (BR-SPSW)," M.S. Thesis, Virginia Tech, Blacksburg, VA.
- Moen, C.D., Cronin, L. and Fehr, R. (2012), "Capacity Prediction of Open-Web Steel Joists Partially Braced by a Standing Seam Roof," *Proceedings of the 2012 Annual Technical Session and Meeting*, Structural Stability Research Council, Grapevine, TX.
- Moen, C.D. and Schafer, B.W. (2009), "Elastic Buckling of Cold-Formed Steel Columns and Beams with Holes," *Engineering Structures*, Vol. 31, No. 12, pp. 2812–2824.
- Moen, C.D. and Schafer, B.W. (2010), "Direct Strength Method for the Design of Cold-Formed Steel Columns with Holes," *Journal of Structural Engineering*, ASCE, Vol. 137, No. 5, pp. 559–570.
- Plaut, R.H., Moen, C.D. and Cojocar, R. (2012), "Beam Deflections and Stresses during Lifting," *Engineering Journal*, AISC, Vol. 49, No. 4, pp. 187–194.
- Plaut, R.H. and Moen, C.D. (2012), "Analysis of Elastic, Doubly Symmetric, Horizontally Curved Beams during Lifting," *Journal of Structural Engineering*, in press.

Ryan, J.C. (1999), "Evaluation of Extended End-Plate Moment Connections Under Seismic Loading," M.S. Thesis, Virginia Tech, Blacksburg, VA.

Smith, F.H., and Moen, C.D. (2013), "Elastic Buckling Prediction of Cold-Formed Steel Columns with Periodic Perforations," *Proceedings of the Annual Stability Conference*, Structural Stability Research Council, St. Louis, MO.

## GUIDE FOR AUTHORS

**SCOPE:** The ENGINEERING JOURNAL is dedicated to the improvement and advancement of steel construction. Its pages are open to all who wish to report on new developments or techniques in steel design, research, the design and/or construction of new projects, steel fabrication methods, or new products of significance to the uses of steel in construction. Only original papers should be submitted.

**GENERAL:** Papers intended for publication may be submitted by mail to the Editor, Keith Grubb, ENGINEERING JOURNAL, AMERICAN INSTITUTE OF STEEL CONSTRUCTION, One East Wacker Drive, Suite 700, Chicago, IL, 60601, or by email to [grubb@aisc.org](mailto:grubb@aisc.org).

The articles published in the *Engineering Journal* undergo peer review before publication for (1) originality of contribution; (2) technical value to the steel construction community; (3) proper credit to others working in the same area; (4) prior publication of the material; and (5) justification of the conclusion based on the report.

All papers within the scope outlined above will be reviewed by engineers selected from among AISC, industry, design firms, and universities. The standard review process includes outside review by an average of three reviewers, who are experts in their respective technical area, and volunteers in the program. Papers not accepted will not be returned to the author. Published papers become the property of the American Institute of Steel Construction and are protected by appropriate copyrights. No proofs will be sent to authors. Each author receives three copies of the issue in which his contribution appears.

**MANUSCRIPT PREPARATION:** Manuscripts must be provided in Microsoft Word format. Include a PDF with your submittal. View our complete author guidelines at [www.aisc.org/ej](http://www.aisc.org/ej).